

# Design and Noise Acceptability of Future Supersonic Transport Aircraft

MSc. Thesis

J.I. Nijse



Cover image: British Airways Concorde G-BOAC by Eduard Marmet,  
[https://commons.wikimedia.org/wiki/File:British\\_Airways\\_Concorde\\_G-BOAC\\_02.jpg](https://commons.wikimedia.org/wiki/File:British_Airways_Concorde_G-BOAC_02.jpg).  
CC BY-SA 3.0 (<https://creativecommons.org/licenses/by-sa/3.0>)

# Design and Noise Acceptability of Future Supersonic Transport Aircraft

## MSc. Thesis

by

J.I. Nijssse

to obtain the degree of Master of Science

at the Delft University of Technology,

to be defended publicly on Friday December 18, 2020 at 10:30 AM.

Student number: 4218124  
Project duration: May 2018 – December 2020  
Thesis committee: Prof.dr.ir. L.L.M. Veldhuis, TU Delft, committee chair  
Ir. J.A. Melkert, TU Delft, supervisor  
Dr.ir. M. Snellen, TU Delft

An electronic version of this thesis is available at <http://repository.tudelft.nl/>.



# Contents

<b>Contents</b>	<b>iii</b>
<b>Summary</b>	<b>vii</b>
<b>List of Figures</b>	<b>ix</b>
<b>List of Tables</b>	<b>xi</b>
<b>Abbreviations</b>	<b>xiii</b>
<b>Lift of Symbols</b>	<b>xv</b>
<b>1 Introduction</b>	<b>1</b>
1.1 Market analysis . . . . .	1
1.2 Characteristics of supersonic flight . . . . .	2
1.3 Research goal . . . . .	2
1.4 Report structure . . . . .	3
<b>2 The design program</b>	<b>5</b>
2.1 Aircraft design . . . . .	5
2.2 Program building . . . . .	6
2.3 Program layout . . . . .	6
<b>3 Aircraft weight and design point</b>	<b>9</b>
3.1 Initial MTOW estimation . . . . .	9
3.2 Design point calculation . . . . .	10
3.2.1 Stall speed . . . . .	10
3.2.2 Takeoff distance . . . . .	10
3.2.3 Landing distance . . . . .	11
3.2.4 Climb performance . . . . .	11
3.2.5 Cruise speed . . . . .	12
3.2.6 Correction factors . . . . .	12
3.2.7 Results . . . . .	13
3.2.8 Verification and validation . . . . .	14
<b>4 Engine design</b>	<b>17</b>
4.1 Engine design method . . . . .	17
4.1.1 Cycle calculation . . . . .	18
4.1.2 Design steps . . . . .	22
4.1.3 Engine size calculations . . . . .	23
4.2 Engine off-design calculation . . . . .	25
<b>5 Geometric design</b>	<b>27</b>
5.1 Fuselage design . . . . .	27
5.1.1 Nose and tail section . . . . .	27
5.1.2 Cabin . . . . .	28
5.2 Wing design . . . . .	31

5.2.1	Planform shape . . . . .	31
5.2.2	Subsonic leading edge . . . . .	33
5.3	Empennage design . . . . .	34
5.4	Fuel tanks . . . . .	34
<b>6</b>	<b>Aerodynamics and Class II weight estimation</b>	<b>37</b>
6.1	Lift analysis . . . . .	37
6.2	Drag analysis . . . . .	39
6.2.1	Subsonic drag . . . . .	39
6.2.2	Supersonic drag . . . . .	40
6.3	Class II weight estimation . . . . .	41
6.3.1	V-n diagrams . . . . .	41
6.3.2	Weight estimation . . . . .	42
6.3.3	Calibration . . . . .	42
6.3.4	Technological developments . . . . .	42
<b>7</b>	<b>Exploring the design space</b>	<b>43</b>
7.1	Full program validation . . . . .	43
7.2	Design space exploration . . . . .	44
7.2.1	Parameter selection . . . . .	45
7.2.2	Parameter variations . . . . .	45
7.3	Aircraft designs . . . . .	55
<b>8</b>	<b>Low-speed noise analysis</b>	<b>57</b>
8.1	Noise regulations . . . . .	57
8.2	Noise modelling . . . . .	59
8.2.1	Fully analytical methods . . . . .	59
8.2.2	CFD combined with acoustic analogy . . . . .	59
8.2.3	Fully numerical methods . . . . .	59
8.2.4	Semi-empirical methods . . . . .	59
8.2.5	Method applicability . . . . .	59
8.3	Low-speed noise estimation method . . . . .	61
8.3.1	Aircraft noise sources . . . . .	61
8.3.2	Supersonic aircraft noise . . . . .	62
8.3.3	Noise reduction measures . . . . .	63
8.3.4	Noise prediction . . . . .	65
<b>9</b>	<b>Supersonic noise prediction</b>	<b>69</b>
9.1	Sonic boom background . . . . .	69
9.2	Sonic boom prediction . . . . .	71
9.3	Prediction results . . . . .	75
9.3.1	Method comparison . . . . .	75
9.3.2	Acceptability of boom loudness . . . . .	80
<b>10</b>	<b>Conclusion</b>	<b>83</b>
<b>11</b>	<b>Recommendations</b>	<b>85</b>
	<b>Bibliography</b>	<b>87</b>
<b>A</b>	<b>Validation data for design point method</b>	<b>93</b>
<b>B</b>	<b>Support data for engine method</b>	<b>95</b>
B.1	Validation data for engine design . . . . .	95
B.2	Station numbering . . . . .	98
B.2.1	Primary station numbering . . . . .	98
B.2.2	Secondary station numbering . . . . .	98

---

<b>C Geometric data</b>	<b>101</b>
C.1 Aircraft configuration	101
C.2 Supersonic aircraft length and slenderness	104
<b>D Program inputs</b>	<b>105</b>
D.1 Main inputs	105
D.1.1 Run parameters	105
D.1.2 Key design parameters	105
D.1.3 Performance first guess parameters	106
D.1.4 Airport constraints	106
D.1.5 Maximum lift coefficients first guess	107
D.1.6 Climate parameters	107
D.2 Secondary inputs	108
D.2.1 Run parameters	108
D.2.2 Passenger data	108
D.2.3 Class I inputs	109
D.2.4 Aerodynamics inputs	109
D.2.5 Airfoil inputs	110
D.2.6 Class II inputs	110
D.2.7 Geometry inputs	111
D.2.8 Engine inputs	111
D.3 Parameter selection for sensitivity analysis	112
<b>E Sonic boom and aircraft shaping</b>	<b>115</b>



# Summary

Despite the COVID-19 outbreak, civil aviation is expected to grow in the long term. As part of this growth, companies are designing a new generation of supersonic aircraft. Concorde proved that flying supersonically results in high fuel burn, loud noise around airports and a loud sonic boom below the flight path. Therefore, it may be the case that this new generation of supersonic aircraft is unacceptable for the public. Due to a request of the International Civil Aviation Organization (ICAO) Committee on Aviation Environmental Protection (CAEP) two theses were created: one focussing on the acceptability of the emissions of supersonic aircraft and this one focussing on the acceptability of their produced noise.

To investigate the noise production a design program has been created first. Using Python, various modules were combined into a single program for the design and analysis. This program consists of an iterative phase, containing a Class I weight estimation, design point calculation, engine design, geometry design, aerodynamics and a Class II weight analysis. When a design solution converges, the non-iterative phase is started which performs the noise and climate analyses and produces the output files.

The Class I weight estimation predicts the takeoff mass based on the design mission profile and a predicted fuel usage. Based on this takeoff mass estimate the design point for wing loading and thrust loading is calculated. A set of constraints is then created to limit the wing size and thrust based on parameters like runway distance required and climb performance. This results in an optimal wing area and thrust for the given takeoff mass. Comparing the calculated design point to data from a set of real and conceptual aircraft resulted in a reasonable accuracy.

The selected engine type is a low-bypass turbofan. To model the engine a cycle calculation method is used. This method evaluates every component in a zero-dimensional analysis where its temperature, pressure and mass flow rate are calculated. By using predefined component efficiencies and optimising the fuel flow rate for the required thrust, a suitable engine design is created. Its size and mass are estimated by using statistics. For all mission phases the engine off-design performance is calculated.

Following this, the fuselage and wings are designed. The fuselage is a cylinder with the nose and tail sections defined as Von Kármán shapes. To ensure the wave drag is low the fuselage has a high slenderness ratio. The wing design is based on a trade-off between five planforms. The result of this trade-off is a cranked arrow wing with a subsonic leading edge and an inboard trailing edge sweep angle of  $90^\circ$ . The empennage design is based on statistical relations. The fuel tanks are placed in the wings and tailcone. If necessary, additional fuel tanks can be placed inside the fuselage.

With the exterior of the aircraft known, the generated lift and drag are evaluated with the aerodynamics evaluation. The lift analysis is performed separately for subsonic and supersonic flight. The drag analysis is split into lift-dependent and lift-independent drag for both subsonic and supersonic flight. After these analyses V-n diagram for manoeuvring a Class II weight estimation is performed.

Because the program has changed since the publication of the first thesis a new validation was performed. It was found that the differences from the real data still were less than 10%. The deviations of the operational empty weight (OEW) are closer to those of the maximum takeoff weight (MTOW) than before the changes.

A parameter variation analysis was performed to get more insight in the program behaviour and to check the validity of the model. The parameters that had the highest influence on the design were identified and evaluated. It was found to be possible to linearise the influence of parameters like number of passengers and design mission range on the takeoff mass. For the cruise Mach number, stall speed and leading edge sweep angle optimum values were found. Based on these outcomes five aircraft were designed with a passenger capacity of 18 to 250. With these aircraft the noise analysis will be performed.

The noise analysis was split into two parts: a low-speed analysis for airport community noise and a sonic boom analysis. Other contributions to noise received on ground were not considered since these two categories are the largest noise events of supersonic aircraft. The best way to predict the low-speed noise of conceptual aircraft was found to be using semi-empirical methods. Unfortunately, none of these methods were accessible, so a different way of predicting supersonic aircraft noise had to be found.

The basis for supersonic aircraft noise is not different from subsonic aircraft noise. Landing gear, flaps and the engine are the main contributors to noise during takeoff and landing. It was found that only a few of the changes between subsonic and supersonic aircraft contribute noticeably to the noise reception on ground. These are the increased landing gear length, lower engine bypass ratio and higher approach speed. There are no specific features on supersonic aircraft that have a lower noise output compared to subsonic aircraft. Therefore supersonic aircraft will generate more noise than subsonic aircraft during takeoff and landing.

While the noise generated by aircraft reduced over the past 50 years, this is a trend that applies to both supersonic and subsonic aircraft. At the introduction of Concorde it had a higher cumulated noise measured according to International Civil Aviation Organization (ICAO) standards than any subsonic aircraft. The noise reduction that was achieved in subsonic aircraft can mainly be attributed to an increased engine bypass ratio, which is not possible for supersonic aircraft. An option would be to deviate from takeoff and landing procedures with reduced thrust or a different climb profile. However, this is currently not allowed.

The Federal Aviation Administration (FAA) proposed a new noise limit for supersonic aircraft, allowing them to produce 3.5 EPNdB louder cumulated noise compared to current regulations and the option to deviate from approach and departure profiles. This may be just enough to meet the regulations, but any margin to the regulation limit will not be as large as with subsonic aircraft. Finally, a noise prediction for an improved Concorde was performed, resulting in a cumulated noise 12 EPNdB louder than the 2021 regulations for subsonic aircraft. A similar margin is expected for smaller supersonic aircraft.

The sonic boom noise is estimated by two methods: one method assuming a non-optimised shape resulting in a loud boom, the second method assuming a theoretical optimum for boom reduction. Older aircraft like the F-5E fighter jet and Concorde matched well with the prediction for non-optimised shape while low-boom business jet designs matched well with the theoretical optimum method. The difference between the two methods was up to 68%, indicating the possible reduction of sonic boom loudness. This boom reduction however comes with a penalty of increased drag, fuel burn and weight.

The definition of sonic boom loudness acceptability decreased over the past years. Additionally, the preferred metric changed from overpressure to loudness. However, this made it impossible to predict the sonic boom acceptability of simple conceptual aircraft designs. If the current technology demonstrators like the Boom XB-1 and the NASA X-59 prove to produce a low boom, low-boom business jets will also be possible. But especially with multiple overflights the noise limit for sonic booms will be low.

In conclusion, a low-fidelity supersonic aircraft design program was successfully created and was shown to produce valid aircraft designs. However, it is unlikely that these aircraft can meet subsonic airport noise regulations. If the sonic boom can be reduced to acceptable levels it is unsure whether the added drag and weight will allow for a cost-effective operation. Therefore it is unlikely for near future supersonic aircraft to be acceptable in terms of noise.

# List of Figures

1.1	Expected demand for supersonic aircraft, based on passenger percentage switching from subsonic to supersonic flights, assuming restricted supersonic overland flight . . . .	2
2.1	Flow chart of the design program . . . . .	7
3.1	Design mission profile . . . . .	9
3.2	Example design point diagram for four-engine Mach 1.6 aircraft . . . . .	13
3.3	Calculated design point vs. real design point for various supersonic aircraft and the Airbus A320 . . . . .	15
4.1	Propulsive efficiency variation with flight speed and Mach number at 60,000 ft ISA for various engine types . . . . .	18
4.2	Noise levels of various engine types . . . . .	18
4.3	Single-stage versus three-stage compression . . . . .	19
4.4	Relation between engine thrust and length . . . . .	23
4.5	Relation between mass flow rate and fan diameter . . . . .	24
4.6	Relation between mass flow rate and engine diameter . . . . .	24
4.7	Relation between engine thrust and mass . . . . .	25
5.1	Example aircraft drawing with fuselage sections shown . . . . .	27
5.2	Buildup of total drag coefficient for a cone-cylinder configuration at M=2 as a function of thickness ratio . . . . .	28
5.3	Slenderness ratio for various supersonic aircraft, compared to Mach number . . . . .	29
5.4	Aircraft length plotted against number of passengers . . . . .	30
5.5	Fuselage slenderness ratio and seats abreast plotted against number of passengers . . . . .	30
5.6	Variable-sweep wing planform . . . . .	31
5.7	Oblique wing planform . . . . .	31
5.8	Delta wing planform . . . . .	32
5.9	Ogive wing planform . . . . .	32
5.10	Cranked arrow wing planform . . . . .	32
5.11	Example wing and horizontal stabiliser with fuselage section shown . . . . .	33
5.12	Example horizontal tail . . . . .	34
5.13	Fuel tank layout . . . . .	35
6.1	Example lift curve slope variation with Mach number . . . . .	39
6.2	Supersonic lift/drag methods applied to the NLR aircraft design . . . . .	40
6.3	Example V-n diagram . . . . .	41
7.1	Takeoff mass variation with number of passengers . . . . .	46
7.2	Takeoff mass variation with design mission range . . . . .	47
7.3	Fuel mass fraction variation with mission range . . . . .	48
7.4	Takeoff mass variation with cruise Mach number . . . . .	48
7.5	Normalised takeoff mass variation with cruise Mach number . . . . .	49
7.6	Takeoff mass variation with passenger number for 2 and 4 engines . . . . .	50
7.7	Takeoff mass variation with mission range for a 100-seat aircraft with 2 or 4 engines . . . . .	50
7.8	Takeoff mass variation with clean stall speed . . . . .	51

7.9	Takeoff mass variation with nosecone slenderness . . . . .	51
7.10	Takeoff mass variation with tailcone slenderness . . . . .	51
7.11	Takeoff mass variation with various nosecone and tailcone slenderness ratios for a 50-seat aircraft . . . . .	52
7.12	Takeoff mass variation with wing aspect ratio . . . . .	53
7.13	Takeoff mass variation with wing leading edge sweep angle at M=1.6 . . . . .	53
7.14	Takeoff mass variation with combustion chamber efficiency . . . . .	54
7.15	Takeoff mass variation with supersonic sfc scaling factor . . . . .	54
8.1	Reference noise measurement points . . . . .	58
8.2	Annex 16 chapter 14 limit noise values for the different reference points . . . . .	58
8.3	Cumulative noise limits for the various Annex 16 chapters . . . . .	58
8.4	Existing noise estimation methodologies and tools with their applications . . . . .	60
8.5	Jet aircraft noise levels at entry into service until 1990 . . . . .	61
8.6	Noise generating airframe components . . . . .	61
8.7	Relative power levels of aircraft noise sources at takeoff and approach for a typical 2000-2010 widebody aircraft with high BPR engines . . . . .	62
8.8	Approach noise breakdown for long range and short range aircraft . . . . .	63
8.9	EPNL vs. bypass ratio for a 40,000 lb (178 kN) sea-level thrust engine . . . . .	64
8.10	Development of ICAO noise limits over time . . . . .	64
9.1	Sonic boom pressure wave propagation . . . . .	70
9.2	F-16 cockpit canopy . . . . .	70
9.3	XB-1 blended cockpit . . . . .	70
9.4	X-59 blended cockpit . . . . .	70
9.5	Various sonic boom signatures . . . . .	71
9.6	F-5 SSBD in flight . . . . .	72
9.7	Experimental data and prediction for sonic boom signature for various aircraft types . . . . .	73
9.8	sonic boom signature for F-5E and F-5 SSBD . . . . .	73
9.9	Non-optimised boom overpressure during cruise . . . . .	75
9.10	Effective area distribution for the SSBJ . . . . .	76
9.11	Theoretical minimum boom overpressure during cruise overlaid on the Carlson method results . . . . .	77
9.12	Relative effective area (maximum = 1) vs. relative distance from nose of SSBJ and SST50 . . . . .	77
9.13	Overpressure variation with altitude . . . . .	78
9.14	Overpressure variation with Mach number . . . . .	78
9.15	Overpressure variation with cruise mass . . . . .	78
9.16	Overpressure variation with aircraft length . . . . .	78
9.17	Minimum boom strength variation with number of passengers . . . . .	78
9.18	Acoustic rays forming a focus boom during transonic acceleration . . . . .	79
9.19	Limit boom overpressure suggested by the U.S. Environmental Protection Agency . . . . .	80
B.1	Maximum TIT trend with certification year . . . . .	96
B.2	Station numbering for mixed and unmixed turbofan . . . . .	98
B.3	Station numbering for turbofan . . . . .	99
E.1	Internal arrangements of low-boom and high-boom designs . . . . .	116
E.2	Effective area distribution for low-boom and high-boom SSBJ designs . . . . .	116

# List of Tables

3.1	Overview of climb gradient requirements in CS-25 . . . . .	11
3.2	Characteristics of aircraft chosen for validation of the design point method . . . . .	14
3.3	Validation results for the design point calculation method . . . . .	14
4.1	Key values for the ideal gas used in the program . . . . .	20
4.2	Input parameters for the engine module . . . . .	22
4.3	SFC data for various aircraft during subsonic and supersonic cruise. Imperial units are used for the sfc since they are the most widely used . . . . .	26
5.1	Passenger distribution over the classes . . . . .	29
5.2	Seat dimensions for various classes . . . . .	29
6.1	Polhamus method lift coefficient for $M=0.25$ compared to source data . . . . .	38
6.2	Digital DATCOM lift coefficient for $M=0.95$ compared to source data . . . . .	38
7.1	Aircraft take-off mass comparison for program validation . . . . .	43
7.2	Aircraft empty mass comparison for program validation . . . . .	44
7.3	OEW and fuel mass data for passenger variation . . . . .	46
7.4	Linear fit for relation between mission range and takeoff mass . . . . .	47
7.5	OEW and fuel mass data for range variation of 100 seat aircraft . . . . .	47
7.6	Relative variation with mission range of takeoff, operational empty and maximum fuel mass . . . . .	48
7.7	Engine data compared for 2-engine and 4-engine option . . . . .	50
7.8	Selection of aircraft design requirements . . . . .	55
7.9	Selection of aircraft design outputs . . . . .	55
8.1	Noise levels of subsonic jet aircraft and Concorde compared to regulatory values . . . . .	65
8.2	Boeing 747-200B cumulative noise margin relative to Chapter 3 limits for various engine variants . . . . .	66
8.3	Fokker 28 and Fokker 100 cumulative noise margin relative to Chapter 3 limits for various aircraft and engine variants . . . . .	66
8.4	Airbus A320 cumulative noise margin relative to Chapter 3 limits for various aircraft and engine variants . . . . .	67
9.1	Boom prediction methods compared to the real overpressure . . . . .	74
9.2	Sonic boom noise phenomena . . . . .	80
A.1	Validation data for design point calculation . . . . .	93
B.1	Component efficiencies and pressure ratios . . . . .	95
B.2	Engine data for validation of efficiency numbers . . . . .	96
B.3	Thrust validation data . . . . .	97
C.1	Seat dimensions and number of galleys, lavatories and closets . . . . .	101
C.2	Number of galleys, lavatories and closets related to number of passengers . . . . .	103
C.3	Various data from several supersonic aircraft . . . . .	104

---

D.1	Main input run parameters . . . . .	105
D.2	Main input design parameters . . . . .	106
D.3	First guesses for performance parameters . . . . .	106
D.4	Airport constraint inputs . . . . .	106
D.5	First guess for maximum lift coefficients . . . . .	107
D.6	Parameters for climate analysis . . . . .	107
D.7	Secondary run inputs . . . . .	108
D.8	Passenger input data . . . . .	108
D.9	Inputs for class I weight estimation . . . . .	109
D.10	Inputs for aerodynamics module . . . . .	109
D.11	Airfoil data . . . . .	110
D.12	Inputs for class II weight estimation . . . . .	110
D.13	Inputs for geometry module . . . . .	111
D.14	Inputs for engine module . . . . .	111
D.15	Results of 20% change in input value on takeoff mass . . . . .	112

# Abbreviations

**AEO** all engines operating

**ANOPP** Aircraft NOise Prediction Program

**BPR** bypass ratio

**CAEP** Committee on Aviation Environmental Protection

**CFD** Computational Fluid Dynamics

**EASA** European Union Aviation Safety Agency

**EPNL** Effective Perceived Noise Level

**FAA** Federal Aviation Administration

**FLOPS** FLight OPTimization System

**FPR** fan pressure ratio

**GSP** Gas turbine Simulation Program

**ICAO** International Civil Aviation Organization

**ISA** International Standard Atmosphere

**KBE** knowledge-based engineering

**MAC** mean aerodynamic chord

**MFTF** mixed-flow turbofan

**MLW** maximum landing weight

**MTOW** maximum takeoff weight

**NASA** National Aeronautics and Space Administration

**NLR** Nederlands Lucht- en Ruimtevaartcentrum (Netherlands Aerospace Centre)

**OEI** one engine inoperative

**OEW** operational empty weight

**OFW** oblique flying wing

**OPR** overall pressure ratio

**PNL** Perceived Noise Level

**psf** pound per square foot

**SAE** Society of Automotive Engineers

**sfc** specific fuel consumption

**SPL** sound pressure level

**SSBD** Shaped Sonic Boom Demonstration

**SSBJ** supersonic business jet

**SST** supersonic transport aircraft

**SUAVE** Stanford University's Aeronautical Vehicle Environment

**TF** turbofan

**TIT** turbine inlet temperature

**VNRS** Variable Noise Reduction System

# List of Symbols

## Roman symbols

$A$	aspect ratio	-
$A_{capture}$	capture area	$m^2$
$A_e$	effective cross-sectional area	$m^2$
$A_8$	nozzle area	$m^2$
$a$	sound speed	m/s
$a$	atmospheric advance ratio	-
$b$	span	m
$C_{Di}$	induced drag coefficient	-
$C_{D0}$	zero-lift drag coefficient	-
$C_L$	lift coefficient	-
$C_{L\alpha}$	lift curve slope	-
$c$	chord length	m
$c_p$	constant pressure specific heat capacity	$J\ kg^{-1}\ K^{-1}$
$c_v$	constant volume specific heat capacity	$J\ kg^{-1}\ K^{-1}$
$CGR$	climb gradient	-
$D$	diameter	m
$e$	Oswald efficiency factor	-
$F$	fuselage lift factor	-
$F(x)$	Whitham F-factor	-
$f_{loss,M}$	ram recovery factor	-
$g$	gravitational acceleration	-
$H$	atmospheric scale height	m
$h$	altitude	m
$K$	drag due to lift factor	-
$K_p$	Polhamus potential-flow contribution coefficient	-
$K_p$	atmospheric propagation factor for overpressure	-
$K_R$	ground reflection factor	-
$K_S$	shape factor	-
$K_t$	atmospheric propagation factor for duration	-
$K_v$	Polhamus vortex contribution coefficient	-
$k$	relation between $M$ , $\beta$ and $\gamma$	-
$L$	length	m
$l_h$	tail arm	m
$L/D$	lift-to-drag ratio	-
$l/d$	slenderness ratio	-
$LHV$	fuel lower heating value	J
$\dot{m}$	mass flow rate	kg/s
$M$	Mach number	-
$n$	load factor	-
$n_{eng}$	number of engines	-
$P$ or $p$	pressure	Pa
$p_{so}$	flat-top overpressure	psf
$\Delta p$	overpressure	psf
$q$	dynamic pressure	$N/m^2$
$R$	specific gas constant	$J\ kg^{-1}\ K^{-1}$
$S$	area	$m^2$
$s$	entropy (in engine design)	$J\ K^{-1}$
$s$	distance	m

$T$	Temperature	K
$T/W$	thrust loading	-
$\Delta t$	signature duration	s
$V$	velocity	m/s
$V_A$	approach speed	m/s
$V_S$	stall speed	m/s
$V_{vt}$	vertical tail volume coefficient	-
$W$	work	J
$W$	mass	kg
$\bar{W}$	relation between aircraft conditions and mass	-
$W/S$	wing loading	N/m <sup>2</sup>
$x$	distance from nose in longitudinal direction	m

**Greek symbols**

$\alpha$	angle of attack	°
$\beta$	$\sqrt{1 - M^2}$	-
$\gamma$	specific heat ratio	-
$\Delta$	difference	-
$\eta$	efficiency	-
$\Lambda$	sweep angle	°
$\mu$	Mach angle	°
$\Pi$	pressure ratio	-
$\rho$	density	kg/m <sup>3</sup>
$\tau$	temperature ratio	-
$\tau_{corr,p}$	thrust correction for pressure	-
$\tau_{corr,\rho}$	thrust correction for density	-

**Subscripts**

<i>air</i>	pure air
<i>amb</i>	ambient
<i>appr</i>	approach
<i>calc</i>	calculated value
<i>cc</i>	combustion chamber
<i>choked</i>	choked nozzle
<i>comp</i>	compressor
<i>core</i>	engine core
<i>cr</i>	cruise
<i>crit</i>	critical
<i>e</i>	effective
<i>eq</i>	equivalent
<i>engine</i>	complete engine
<i>f</i>	fuel
<i>fan</i>	fan
<i>g</i>	ground
<i>gas</i>	air/fuel mixture
<i>h</i>	altitude
<i>inlet</i>	engine inlet
<i>is</i>	isentropic
<i>l or land</i>	landing
<i>lg</i>	landing gear
<i>LE</i>	leading edge
<i>max</i>	maximum
<i>mech</i>	mechanical
<i>noz</i>	nozzle
<i>OE</i>	operating empty
<i>poly</i>	polytropic

---

<i>ref</i>	reference
<i>s</i>	stall
<i>sub</i>	subsonic
<i>sup</i>	supersonic
<i>unchoked</i>	unchoked nozzle
<i>TO</i>	takeoff
<i>turb</i>	turbine
<i>v</i>	ambient
<i>vt</i>	vertical tail
<i>w</i>	wing
0	sea-level
0, $x$	total quantity at engine station $x$
0,5 $c$	at half-chord
11km	at 11 km altitude



# Introduction

The outbreak of the COVID-19 virus put a halt to the growth expectations of civil aviation. Before the outbreak, civil aviation was expected to grow for the coming decades. Therefore people are looking for new ways of flying. Examples of this in the past are the Airbus A380, the largest passenger aircraft built and Concorde, the best known supersonic airliner.

Concorde flew for the first time in 1969. While it was thought to be the start of a supersonic revolution, the aircraft were removed from service in 2003 which immediately meant the end of supersonic civil aviation. This did not come as a completely unexpected move as passenger numbers were decreasing and maintenance costs rose. Additionally, people considered the take-off noise of Concorde to be excessive [1]. However, at the time Concorde was designed noise regulations were not enforced yet.

In a time where noise regulations become more and more strict, it is important for aircraft designers to take these regulations into account from the very start of the design process. Especially for new aircraft variants it is important to be prepared to meet noise regulations as they may face a ban from certain airports if they can not be given a noise certificate.

## 1.1. Market analysis

Although there have only been a few supersonic transport aircraft in commercial service, it seems that a new generation of supersonic aircraft is coming soon. At least three companies are currently actively working on creating an actual supersonic transport aircraft (SST) and/or demonstrator. The National Aeronautics and Space Administration (NASA) is working on the X-59 QueSST, which is a demonstrator aircraft for a shape that reduces the sonic boom<sup>1</sup>. Boom Supersonic is constructing a 1/3 scale demonstrator aircraft before building a full-scale airliner for 55-75 passengers. And Aerion is developing a supersonic business jet (SSBJ) jet for 12-18 passengers.

These developments have created the desire to know more about the environmental impact of supersonic aircraft. While generally not much scientific data is available about these aircraft and the only information can be get from media reports, this does indicate that there have been developments in supersonic aviation research that apparently justify the development of new supersonic aircraft. Market studies also suggest that there is a market for supersonic aircraft, but the larger the aircraft, the smaller the expected market share (Figure 1.1). Aircraft with more than 100 passengers will be very unlikely to become profitable due to their fuel use and size. Aircraft like business jets with less than 25 passengers have the highest chance to be profitable for both manufacturers and airlines [2, 3].

However, as can be seen in the media, the new commercial supersonic aircraft manufacturers do have to defend themselves for supporting an aircraft design that may be less favourable for the general public

<sup>1</sup>Banke, J. NASA's Supersonic X-59 QueSST Coming Together at Famed Factory. NASA, 9 October 2019 (last updated 15 October 2019). <https://www.nasa.gov/aero/nasa-supersonic-x59-quesst-coming-together-at-famed-factory>. Accessed 27 November 2019

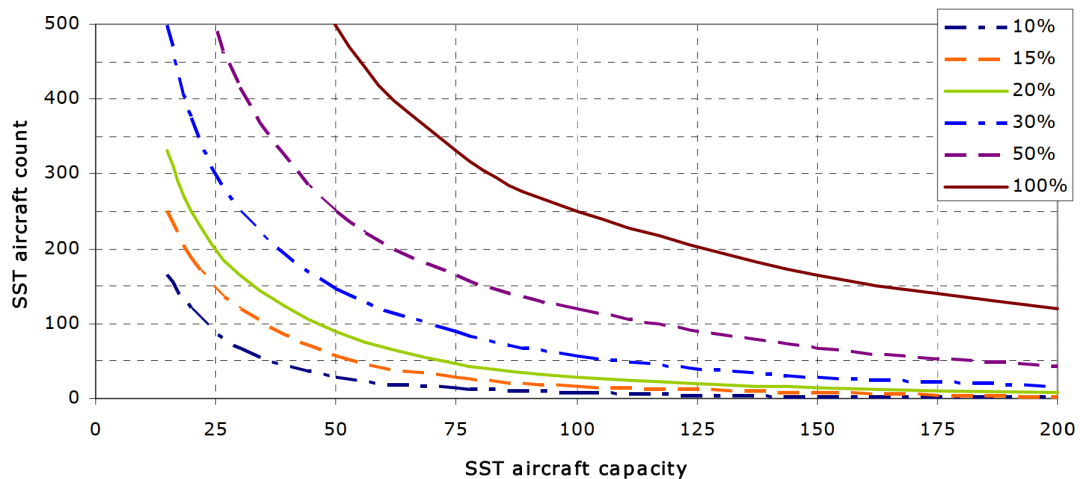


Figure 1.1: Expected demand for supersonic aircraft, based on passenger percentage switching from subsonic to supersonic flights, assuming restricted supersonic overland flight [2]

due to noise and emissions<sup>2</sup>. Although current regulations do suggest subsonic noise rules have to be applied to supersonic aircraft it is unknown whether they can be met by this new generation of supersonic aircraft. Specific supersonic rules may give more room for a viable supersonic aircraft<sup>3</sup>.

## 1.2. Characteristics of supersonic flight

The ultimate reason for flying supersonically is the time gained. While the take-off and cruise phases of SSTs are similar to those of subsonic aircraft, a Mach 2 SST flies more than twice the speed of a subsonic aircraft. Especially at longer distances this makes a major difference. Additionally, supersonic aircraft will more likely fly at higher altitudes, which reduces the probability of encountering turbulence and allows for a more direct route since the airspace at higher flight levels is less crowded.

The higher speed of supersonic aircraft also is the big downside of flying this fast. Since drag rises faster with increasing speed, flying supersonically will require more than double the fuel of a subsonic flight on the same route.

Another problem that shows up for supersonic aircraft is noise. However noise reducing technologies applied to subsonic aircraft will also be applied to supersonic aircraft, they produce more airframe and engine noise due to their higher speed. A noise problem specific to supersonic aircraft is the sonic boom generation. Supersonic flight causes a strong shock wave in front of the aircraft. When this shock wave travels to the ground, it is perceived as a boom. This phenomenon led to a ban on civil supersonic aircraft flying over land areas [4].

## 1.3. Research goal

The previous sections show that it is essential to know more about the environmental characteristics of supersonic aircraft before they can enter commercial service again. Since Concorde and the Tu-144 were built before noise regulations were enforced and before emission regulations existed, there are no practical examples of the application of supersonic noise and emissions regulations. New studies based on data that are as actual as possible may give better insight in the theoretical environmental characteristics of supersonic aircraft and may or may not indicate that supersonic aircraft are not desirable at all due to their noise and emissions. Therefore the ICAO Committee on Aviation Environmental Protection (CAEP) has requested to investigate the acceptability of supersonic aircraft by estimating the production of noise and emissions for these aircraft. Based on this request, two theses have been written up to this date: one on emissions [5] and this one on noise. For this thesis, the

<sup>2</sup>Frost, N. This is the worst time to be excited about supersonic flight. *Quartz*, 16 October 2019. <https://qz.com/1728390/supersonic-flight-may-be-back-but-the-environment-isnt-ready-for-it/>. Accessed 27 November 2019

<sup>3</sup>Hadhazy, A. Supersonic's not-so-super emissions. *Aerospace America*, October 2019. <https://aerospaceamerica.aiaa.org/features/supersonics-not-so-super-emissions/>. Accessed 27 November 2019

following research objective was defined:

*Estimate the noise produced by future supersonic aircraft entering service in the 2020-2025 timeframe by creating a low-fidelity SST design tool and applying existing noise models to generated aircraft designs and comparing this to the noise produced by subsonic aircraft.*

Together, these two theses aim to investigate the airport noise, sonic boom and cruise flight noise and the emissions and climate effects of supersonic aircraft. In order to be able to do this in a quantitative manner, a design program has been created which allows for a comparison between various aircraft designs. Since this is a broad topic not all design areas are investigated in detail.

The main research goal for this thesis is split into two parts:

- Build a design program for the design of supersonic airliners
- Perform a noise analysis for multiple flight phases and aircraft sizes

These two tasks can be further split into subtasks for creating calculation modules for the design point, engine and fuselage, as well as the application of noise estimation methods to this aircraft.

## 1.4. Report structure

As described in the previous section, the result of the first part of this thesis is a computer program for producing supersonic aircraft designs. A general description of this program will be given in Chapter 2. The next step is to estimate the 'design point' for wing loading and thrust loading, which will be shown in Chapter 3. Chapter 4 will explain the propulsion module of the design program. The geometric calculations and layout of the aircraft will be explained in Chapter 5. As a final step, the aerodynamics and the class II weight estimation are summarised in Chapter 6. To investigate the validity of the program, a validation and parameter variation were performed as described in Chapter 7. This chapter also briefly mentions the set of supersonic aircraft that were created using the program.

The second part of this thesis is the noise analysis of the supersonic aircraft. The methodology and results for the airport community noise prediction can be found in Chapter 8. The sonic boom prediction is explained in Chapter 9 with its results. Finally, the conclusions from this research can be found in Chapter 10 and Chapter 11 will provide some recommendations for further research, including improvements to the design program and improvements to the accuracy of the noise analysis.



# 2

## The design program

Since so many disciplines come together in aircraft design, it is essential to know conflicting requirements as early as possible. Therefore, new aircraft designs start as rough concepts where only key parameters are defined. Throughout the design process many variables can still change while details are filled in.

To explain the way in which the design program was created, Section 2.1 will show the steps in which aircraft design usually takes place and will relate this to the design program. Some decisions related to building the program are stated in Section 2.2. After this, the layout of the design program will be shown in Section 2.3.

### 2.1. Aircraft design

Conceptual aircraft design is one of the major steps in designing a complete aircraft. Usually aircraft design is divided into the following three main categories [6, 7].

1. **Conceptual design:** This is the initial stage of the design process where many different concepts are evaluated. These concepts are based on primary requirements set up earlier, usually based on market surveys. During this stage, the aircraft specifications are mainly defined in terms of performance, like payload, weight, thrust and range. This is also the stage where creativity plays an important role. At the end of this stage, the designer should be able to make a drawing of the aircraft, so the wing shape and position and engine positions should be known as well. However the structure and control system are not a factor in conceptual design, they should be taken into account in the design decisions. The output of the conceptual design should be an aircraft that not only meets the requirements, but one that is for sure to be the best to meet the requirements.
2. **Preliminary design:** During this stage the design will be developed further. This is the phase where wind tunnel testing and CFD and FEM analyses will take place. No major changes will be made to the design, except when the more detailed aerodynamic or stability analyses require configuration changes. At the end of this phase the aircraft configuration will be frozen, so that the detailed design can start.
3. **Detailed design:** The detailed design will focus on smaller items, up to rivets and bolts and make the design ready for production. At the end of this stage, everything about the aircraft is documented and production tools are built. Then production and flight testing of the aircraft can be started.

The next steps for an airline manufacturer would be production, flight testing and certification, after which the aircraft is ready to be delivered to customers. However, this sequence is purely theoretical. Certification of the aircraft needs to be included in the design process from the very beginning of the project. Production of the aircraft has to be thought of already during the conceptual design.

Since the goal of this thesis is to provide a noise production estimation for various supersonic aircraft

designs, the design will only take place on a conceptual level. This means that the aircraft will be designed based on generic top-level requirements and that the designs will not be detailed. Therefore, the noise results may be inaccurate, but allows trends among various designs to be visible.

Conceptual design can be detailed further into milestones, as listed below [7, 8].

1. Requirements setting and analysis
2. Initial weight estimation
3. Key performance parameters
4. Aircraft configuration
5. More detailed weight estimation
6. Performance analysis
7. Optimization

Since the request is to find out whether supersonic aircraft will be acceptable, the optimization part will not be included in this thesis. One reason for this is the limited amount of time, another reason is that once a theoretical basis for acceptance or non-acceptance can be established, there is no need for an optimised design, since the acceptability can be reasoned through arguments found in the design process.

## 2.2. Program building

After the decision on the necessary design steps was made, decisions had to be made about how the various aircraft would be designed. Since the design task would be very large, it was decided to work on the problem with two students.

Since multiple aircraft would have to be designed following the same general rules, it was decided that using a knowledge-based engineering (KBE)-like software tool would be the best option. Designing manually would result in fewer aircraft designs and any calculations made would have to be simplified, resulting in lower accuracy. In TU Delft there already is a conceptual design program for subsonic aircraft, called Initiator [9]. However, due to the major differences between designing subsonic and supersonic aircraft this program could not be used for the goals of this project.

Another option for creating conceptual aircraft designs is using programs like Stanford University's Aeronautical Vehicle Environment (SUAVE) [10, 11]. SUAVE is an open-source program for the analysis of conventional and unconventional aircraft designs, which includes supersonic aircraft. This would make it one of the few programs already available that are suitable for designing or analysing supersonic aircraft. Downsides of this program are that it has a number of features that are considered to be too detailed for a preliminary design and that it is quite complex to operate, which would require a lot of time to fully understand.

For this reason the decision was taken to write a new program specifically made for the preliminary design of supersonic aircraft. Since both students have most of their programming done in Python, it was decided that Python 2 would be used as programming language. KBE will be used as a basis for the program.

The reason for choosing a KBE tool was that it seemed to offer the best possibilities given the timeframe and the knowledge of the students. The idea behind KBE is establishing knowledge models for design engineering. This allows for more automation, a more transparent design process and better re-use of knowledge. Therefore, KBE is ideal for this project, since many similar designs will have to be produced based on the same set of design rules. Another advantage of applying KBE is that it allows for multiple separate calculation tools to be combined in a single program.

## 2.3. Program layout

The program is built up in a modular way. The main program calls other programs which load the input variables, perform calculations for the various aircraft modules or prepare the output. The structure of the program is shown in Figure 2.1. Since the programming had to be done by two students, the different modules were chosen so that they could be created independently of the other modules and could be combined at a later stage. As can be seen in the image the program is divided into two

parts: the iterative part, where the design calculations will take place, and the non-iterative part, where the design is fixed and the performance of the designed aircraft will be calculated. Each module will be shortly described below. The detailed explanation of each module can be found in the following chapters and in the thesis by Den Boer [5].

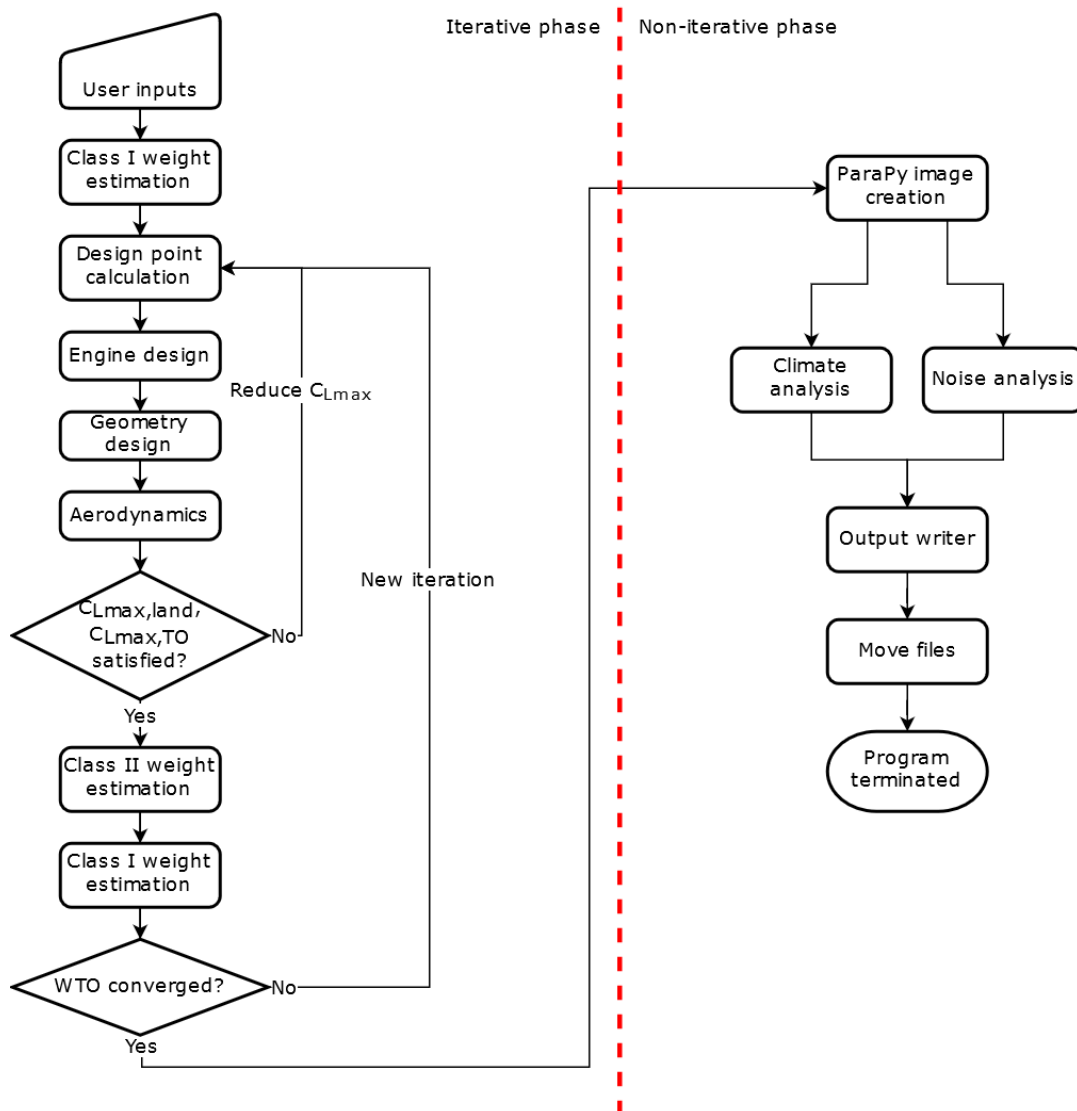


Figure 2.1: Flow chart of the design program. Adapted from [5]

### Inputs

Before running the program the design requirements should be known. The program will use them as a starting point for the design calculations, aside with some other parameters that influence the design. More information about the program itself and the inputs and outputs can be found in Appendix A of Den Boer [5].

### Class I weight estimation

The first step in the design is the initial weight estimation. In this step a first estimate is made for the maximum takeoff weight (MTOW), fuel weight and operational empty weight (OEW). When this step is executed for the first time, it will be based on many estimated numbers. After an iteration it will be based on calculated values during the design process. A summary of this module can be found in Section 3.1 and the more detailed explanation is given by Den Boer [5].

**Design point calculation**

When the design MTOW is defined, the desired performance can be calculated using the performance requirements. By using the requirements as constraints on the wing loading and thrust loading a design point can be chosen, which will be the basis of the following calculations. This module will be explained thoroughly in Chapter 3.

**Engine design**

Using the thrust loading resulting from the design point calculation and the desired number of engines, the required thrust per engine can be calculated. This is then used as a guide for a more detailed performance calculation of the engine, where the air flow inside the engine will be considered too. For more information about this module, please refer to Chapter 4.

**Geometry design**

The geometry design starts at the wing loading that resulted from the design point calculation. Using initial estimates and mission requirements, this can be used to create the entire outside geometry of the aircraft. This will be explained in Chapter 5.

**Aerodynamics**

When the geometry is designed, the aerodynamics module calculates and estimates the lift and drag of the various aircraft parts at both low speed and cruise speed. This is explained shortly in Chapter 6 with reference to Den Boer [5].

**Lift coefficient check**

After the aerodynamics module there is a check to verify that the high lift coefficient required for landing can be met. Since a supersonic aircraft is optimised for supersonic speed, generating sufficient lift at low speeds may be impossible with a certain high-lift device setup. If it is found that this is indeed impossible, the required lift coefficients are reduced and the calculations will start again from the design point calculation.

**Class II weight estimation**

After the above design steps, a more detailed weight estimation can be executed. While the Class I weight estimation uses mostly statistical data from other aircraft, the Class II weight estimation uses component weights which can be estimated much more accurately. This is also explained in Chapter 6.

**MTOW convergence check**

This is the step where the iteration is defined. Here the difference between two successive Class I weight estimations will be compared. If the difference is below a certain margin, the iteration will be stopped. Otherwise, it will continue with the new weights.

**ParaPy image generation**

When the aircraft design is finished, a model of it will be generated using ParaPy which is then used for the generation of some images from various viewing angles.

**Climate analysis**

This module covers the main research questions of the first thesis and evaluates the aircraft with respect to environmental regulations. Additionally the effect of a fleet of supersonic aircraft on global temperature change is indicated by this module. Den Boer explains the working of this module [5].

**Noise analysis**

This module will help answer some of the research questions of this thesis. The noise production of the aircraft will be evaluated at various flight phases and comparisons will be made to subsonic aircraft. More details are given in Chapter 8 and 9.

**Output writer and termination**

Here many relevant parameters and graphs concerning the final design will be combined in a single document and saved for the user.

Additionally, the package contains many additional programs and databases that were created during the validation process of the various modules. These are considered useful so that future users can easily make adjustments based on new data and validate the new results.

## Aircraft weight and design point

Now the outline of the design program has been explained in the previous chapter, the actual contents of the program will be described starting from this chapter. The first steps for designing this aircraft is making an initial estimation of the MTOW. This will be explained shortly in section 3.1. Following that, a so-called design point can be set, based on requirements for thrust and wing area. The calculation steps leading to the design point and the validation of the results will be shown in section 3.2.

### 3.1. Initial MTOW estimation

The initial estimation for the MTOW is done using a class I method, dividing the takeoff weight into payload weight, OEW and fuel weight. The payload weight is calculated using the number of passengers and assuming the average weight for a passenger with luggage. The operating empty weight was then calculated based on a statistical relation found between the takeoff weight and operating empty weight for similar supersonic aircraft.

For the fuel weight calculation, a mission profile was set up first, as shown in Figure 3.1. The profile looks much like that of an average subsonic passenger aircraft, except for the transonic and supersonic segments. With the now defined mission profile, fuel fractions can be estimated for each flight segment. A separation was made between segments that have a short duration and cruise segments. Short segments can be reasonably approximated by a single number for different missions. However, since the cruise distance is a very important factor in fuel usage, the fuel fractions for the cruise segments depend on the cruise distance. This is done using the Breguet range equation.

The product of these fuel fractions is the mission fuel fraction, which can then be converted to the ratio between fuel weight and takeoff weight.

Combining these three weight or weight ratio estimations then results in an estimate for the MTOW. For a full description of the MTOW estimation, please refer to Den Boer [5].

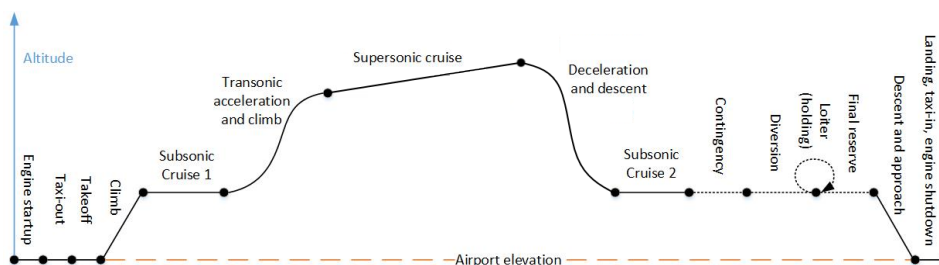


Figure 3.1: Design mission profile. Adapted from [5]

## 3.2. Design point calculation

Now a first estimate for the MTOW is defined, the next step is choosing some key design parameters for the geometry and performance: wing area and takeoff thrust. This is done using a wing loading / thrust loading diagram. Based on certain performance requirements, limits can be set for the wing loading and thrust loading. Combining these limits yields an optimum for both wing loading and thrust loading, which then results in a design wing area and takeoff thrust.

The basis for the applied requirements was found in European Union Aviation Safety Agency (EASA) and Federal Aviation Administration (FAA) regulations. All regulators require certain performance goals to be met, mainly for climb gradients. These can be combined with calculations for takeoff and landing distance, cruise performance and other flight segments which can then be used to calculate the required wing loading or thrust loading. As there are little differences between the various regulators, regulations cited here will be the EASA CS-25 [12] which are the certification specifications for large aircraft.

For the calculation of the performance limits related to the regulations, methods from various sources were considered and evaluated. In the end it was decided to mostly stick to the methods suggested by Roskam [8]. Reasons for this were ease of use, the number of known and unknown variables and whether equations could be used in combination with methods and correction factors created by the authors. More about this will be shown in section 3.2.6.

### 3.2.1. Stall speed

The first performance requirement is the stall speed. Although the CS-25 regulations do not set a hard limit, it is useful to set a stall speed at an early stage of the design and relate it to the maximum lift coefficients. The stall speed in landing configuration can be related to the allowed approach speed and the runway distance required. The highest wing loading required that can be met with a certain stall speed can be described with equation 3.1:

$$\frac{W}{S} = \frac{1}{2} \rho V_s^2 C_{L_{max}} \quad (3.1)$$

where  $\frac{W}{S}$  is the wing loading in  $N/m^2$ ,  $\rho$  is the air density in  $kg/m^3$  at the chosen altitude,  $V_s$  is the stall speed in  $m/s$  and  $C_{L_{max}}$  is the maximum lift coefficient for the selected configuration.

Two stall speeds are considered in the program. The clean stall speed, which directly depends on a user input for the stall speed, and the landing stall speed. For this, the clean stall speed is converted to the stall speed at the landing altitude of the mission airport. The maximum wing loading during landing is then calculated using the landing stall speed and  $C_{L_{max}}$  in landing configuration.

From the landing stall speed the desired approach speed is estimated by multiplying the stall speed with a factor of 1.3 [8]. This factor is based on the CS-25 regulations, where the reference approach speed is taken as 1.23-1.3 times the reference stall speed [12].

### 3.2.2. Takeoff distance

The takeoff distance is defined in CS 25.113 as the distance between the start of the takeoff path and the point where the aircraft reaches 11 m (35 ft) above the runway surface [12]. To calculate the requirement for wing loading and thrust loading, a method described by Torenbeek is used [13] which uses equation 3.2. With this equation the minimum thrust loading for a given wing loading is calculated for the required takeoff distance.

$$\frac{T}{W} = 1.1 \cdot \sqrt{\frac{n_{eng}}{(n_{eng} - 1)} \cdot \frac{1}{A \cdot \rho \cdot g \cdot s_{TO}} \cdot \frac{W}{S}} \quad (3.2)$$

In this equation,  $\frac{T}{W}$  is the dimensionless thrust loading,  $n_{eng}$  is the number of engines,  $A$  is the wing aspect ratio,  $\rho$  is the standard atmosphere air density at the airport altitude,  $g$  is the gravitational acceleration and  $s_{TO}$  is the takeoff distance in m.

### 3.2.3. Landing distance

CS 25.125 defines the landing distance as the "distance necessary to land and to come to a complete stop from a point 15 m (50 ft) above the landing surface" [12]. The landing distance requirement used here is based on a relation between runway length and approach speed defined by Roskam [8]. It can be found below in equation 3.3, where  $s_{land}$  is the landing distance in feet and  $V_{appr}$  is the approach speed in knots.

$$s_{land} = 0.3 \cdot V_{appr}^2 \quad (3.3)$$

Following this the landing stall speed can be determined, assuming again that the approach speed is 1.3 times the stall speed. With the stall speed known, the maximum wing loading can be calculated.

### 3.2.4. Climb performance

In CS 25.111 the minimal climb performance is described for various climb segments. CS-25 also defines the climb performance for various flight segments. For every segment a minimum climb gradient is required, depending on the number of engines of the aircraft.

Based on the required climb gradient and estimated velocity the L/D-ratio can be calculated. This can then be used for the calculation of the minimum thrust loading. Table 3.1 shows an overview of the different climb segments with the corresponding required climb gradients. The definition of the climb segments is described below.

- Initial climb, one engine inoperative (OEI) (CS 25.111)
- Transition segment climb, OEI (CS 25.121a)
- Second segment climb, OEI (CS 25.121b)
- En-route climb, OEI (CS 25.121c)
- Landing climb, all engines operating (AEO) (CS 25.119)
- Approach climb, OEI (CS 25.121d)

Table 3.1: Overview of climb gradient requirements in CS-25

	minimum climb gradient [%]			speed factor relative to $V_s$	flaps setting	landing gear
	$n_{eng} = 2$	$n_{eng} = 3$	$n_{eng} = 4$			
CS 25.111	1.2	1.5	1.7	1.2	takeoff	no
CS 25.121a	0	0.3	0.5	1.1-1.2	takeoff	yes
CS 25.121b	2.4	2.7	3.0	1.2	takeoff	no
CS 25.121c	1.2	1.5	1.7	1.2	clean	no
CS 25.119	3.2	3.2	3.2	1.3	landing	yes
CS 25.121d	2.1	2.4	2.7	1.5	approach	sometimes

Based on these data the lift-to-drag ratio can be calculated, which is then used for the thrust loading calculations in equation 3.4 (for AEO climb) and equation 3.5 (for OEI climb).

$$\frac{T}{W} = \frac{1}{L/D} + CGR \quad (3.4)$$

$$\frac{T}{W} = \frac{n_{eng}}{n_{eng} - 1} \cdot \left( \frac{1}{L/D} + CGR \right) \quad (3.5)$$

where  $CGR$  is the climb gradient fraction (specified as percentage in Table 3.1) and  $L/D$  is the lift-to-drag ratio.

### 3.2.5. Cruise speed

Another requirement that needs to be satisfied is the cruise speed requirement. At cruise altitude there should be enough thrust to overcome the drag. For jet aircraft this is expressed by equation 3.6:

$$\frac{T}{W} = \frac{C_{D_0} \cdot q}{\frac{W}{S}} + \frac{W}{S} \cdot \frac{K}{q} \quad (3.6)$$

where  $C_{D_0}$  is the zero-lift drag coefficient and  $q$  is the dynamic pressure in  $N/m^2$  with  $q = \frac{1}{2}\rho V^2$ .  $K$  is the 'drag-due-to-lift factor' and for subsonic flight can be expressed as equation 3.7:

$$K_{sub} = \frac{1}{\pi A e} \quad (3.7)$$

where  $e$  is the Oswald efficiency factor which relates the wing drag to that of an ideal wing with an elliptical chord distribution and an elliptical lift distribution. Due to the relationship with elliptic lift distribution this method is only suitable for subsonic flight. At supersonic speeds this factor directly depends on the Mach number and therefore varies per flight condition, opposed to the subsonic  $K$ .

The first time the design point is calculated in the program, the aerodynamics module has not been run yet. Therefore,  $K_{sup}$  is estimated by equation 3.8 [14]:

$$K_{sup} = \frac{A(M^2 - 1)}{4A\sqrt{M^2 - 1} - 2} \cos \Lambda_{LE} \quad (3.8)$$

with  $\Lambda_{LE}$  being the leading edge sweep angle. Since this equation is only meant as a quick estimation of  $K_{sup}$ , a more elaborate calculation method is included in the aerodynamics module, as explained by Den Boer [5]. This method results in  $K_{sup}$  depending on  $C_L$  (which in turn depends on  $M$ ) in equation 3.9:

$$K_{sup} = \frac{dC_{D_i}}{d(C_L^2)} \quad (3.9)$$

where  $C_{D_i}$  is the induced drag coefficient.

### 3.2.6. Correction factors

Since all limits mentioned above should be compared to each other, some factors need to be applied in order to set all weights and thrusts at sea level takeoff standard. These factors will be explained below.

#### Weight correction

The weight correction was applied for all limits that were required at an aircraft weight different from the takeoff weight. This includes the landing and approach climbs and cruise segments. The factor was applied by calculating the maximum weight at the beginning of the segment: maximum landing weight (MLW) for the landing and approach phases, and the estimated weight at beginning of subsonic and supersonic cruise for both cruise phases.

#### Thrust correction

Furthermore it is known that thrust varies with altitude and flight speed. The altitude variation is known to be related to density and bypass ratio. With increasing altitude, density decreases and so does thrust. This effect can be calculated using equation 3.10.

$$\tau_{corr,\rho} = \left( \frac{\rho_{11km}}{\rho_0} \right)^{0.7} \cdot \frac{\rho_h}{\rho_{11km}} \quad (3.10)$$

In this equation,  $\tau_{corr,\rho}$  is the thrust ratio for density correction and  $\rho$  is the air density at the altitude specified in its subscript.

Since the atmospheric properties in the region below 11 km altitude are different from those in the layer above 11 km, they are treated differently in the above equation. If the flight altitude is below 11 km, only the first part of the equation will be considered, with  $\rho_{11km}$  substituted by  $\rho_h$ . The factor 0.7 is there to include the bypass ratio effect [15].

To account for the flight speed, a pressure effect is also considered (equation 3.11). This describes the ram compression at the engine inlet based on the Mach number.

$$\tau_{corr,P} = \left( 1 + \eta_{inlet} \cdot \frac{\gamma_{air} - 1}{2} \cdot M^2 \right)^{\frac{\gamma_{air}}{\gamma_{air}-1}} \tag{3.11}$$

Here  $\eta_{inlet}$  is the inlet efficiency factor and  $\gamma_{air}$  is the specific heat ratio of air.

These two factors need to be multiplied and applied to the calculated thrust loading, resulting in the static sea level thrust loading.

### 3.2.7. Results

Using all constraints mentioned above, a single diagram can be created showing all requirements in one graph as shown in Figure 3.2. With these constraints a region can be found which results in a viable design. The minimum thrust loading and the minimum and maximum wing loading are defined with the requirements, so the area between these constraints indicates the design space. The design point for jet-powered aircraft is located in the bottom right corner of the design space, allowing for a wing that is as small as possible and an engine with the lowest possible thrust, which both help to keep the weight as small as possible.

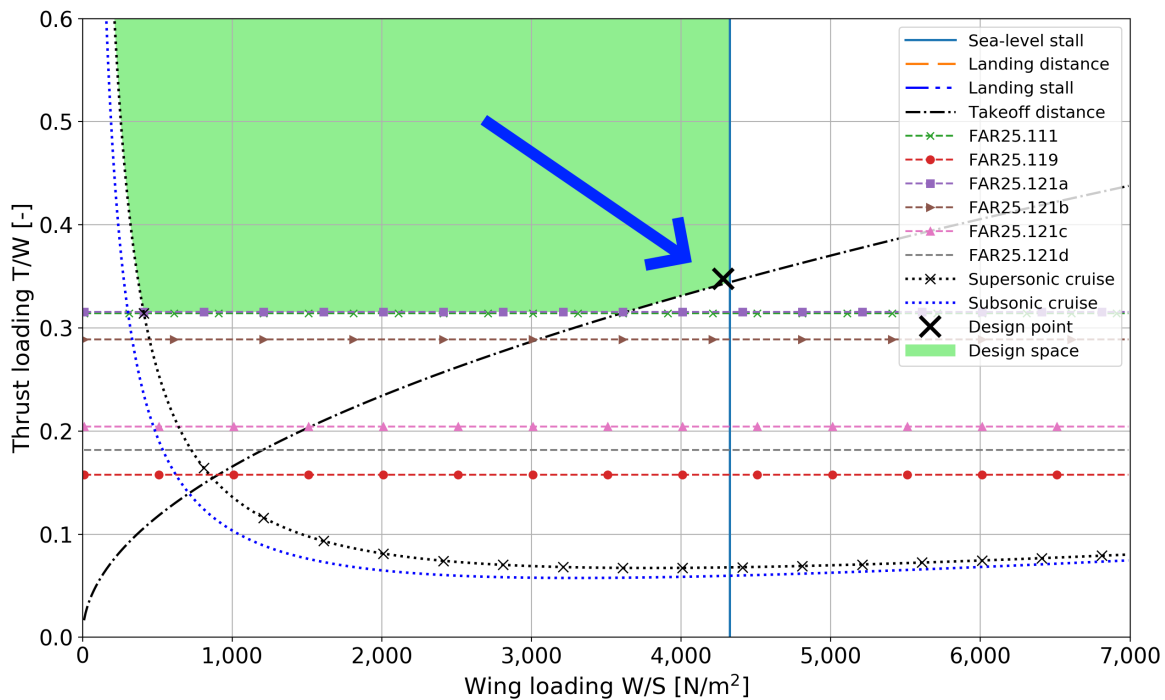


Figure 3.2: Example design point diagram for four-engine Mach 1.6 aircraft

Sometimes the indication of 'bottom right corner' is trivial like in Figure 3.2, where the takeoff distance constraint is a more limiting constraint than the intersection between the horizontal and vertical lines. However here a 'top right' point can be identified which has a larger thrust and smaller wing, and a 'bottom left' point with less thrust and a larger wing.

If this happens the slope between both optional design points is calculated. Based on this number either the 'top right' or 'bottom left' point is chosen. This either means high wing loading (a smaller wing) combined with higher thrust, or low wing loading (a larger wing) combined with lower thrust. In case of a steep slope the bottom left point is better since the large increase in required thrust can not be offset with the smaller wing area and therefore the takeoff weight will increase. The opposite is also true: a shallow slope will result in a better performance from the top right point. The critical slope

gradient was determined through experiments where both possible design points were evaluated for various slopes.

### 3.2.8. Verification and validation

The requirements mentioned earlier were not the only requirements considered for this research. Also parameters like ceiling and turn rate and newer methods based on Roskam's method were considered to be used for the design point calculation. However, some methods produced unverifiable results and others were considered too strict for supersonic aircraft. All methods found were first evaluated with theoretical data of concept studies. If a method's results could not be verified using this data, it was not used.

To validate the entire design point calculation method, only two aircraft could potentially be used that really flew, namely Concorde and the Tupolev Tu-144. The Tu-144 had too little data available, so only Concorde could be used for validation with a real aircraft. Additionally, four supersonic conceptual design studies were found that had enough data available to make a reasonable validation. Finally, a subsonic aircraft (Airbus A320) was added for additional validation of the subsonic methods with a real aircraft. Table 3.2 shows the aircraft used for the validation and some characteristics.

Table 3.2: Characteristics of aircraft chosen for validation of the design point method

	$M_{cr}$	$n_{pax}$	$W_{TO}$ [kg]	$n_{eng}$	$W/S$ [N/m <sup>2</sup> ]	$T/W$ [-]
Concorde	2.02	88-100	185,065	4	5,056	0.31
NLR	1.6	250	340,000	4	4,276	0.35
HELESA	1.6	18	43,100	2	4,365	0.45
SC-13	1.3	128	140,160	2	4,932	0.58
SSXJET	2.2	8	34,360	2	3,907	0.37
A320-232	0.89	180	78,000	2	6,252	0.31

While the data even for the conceptual design studies was fairly complete, not all data required for the design point calculations could be found. Therefore, a number of assumptions had to be made, especially for the Oswald efficiency factor, lift and drag. More about the data used for validation and the additional assumptions is written in Appendix A. These assumptions will be validated in Chapter 7.

The design point calculation method was applied to the datasets of each aircraft as if they were the output from the earlier methods in the program. The sea-level stall speed is omitted in this validation, since source data was not available and it is not a real requirement for these aircraft. The resulting wing loading and thrust loading are shown in Figure 3.3 and in Table 3.3.

Table 3.3: Validation results for the design point calculation method

Aircraft	$W/S_{ref}$	$W/S_{calc}$	Delta [%]	$T/W_{ref}$	$T/W_{calc}$	Delta [%]
Concorde	5,096	5,068	0.55	0.36	0.37	-3.32
NLR	4,241	4,276	-0.82	0.27	0.35	-23.63
HELESA	4,764	4,365	9.12	0.40	0.45	-11.88
SC-13	4,870	4,932	-1.25	0.43	0.58	-26.91
SSXJET	3,611	3,907	-7.59	0.46	0.37	25.10
A320-232	6,367	6,252	1.84	0.27	0.31	-11.30

The results show quite some variation between the calculated design points and the reference design points. As can be seen, the wing loading is always less than 10% off the real value, which is considered accurate for this early design stage. The thrust loading has more variation, though the calculations for the real aircraft are more accurate than the concept studies, which may indicate that their input data is more realistic and therefore more accurate.

The landing stall speed requirement always is the constraint for wing loading. Therefore the model is very sensitive for  $V_{app}$  since the value appears squared in equation 3.1.

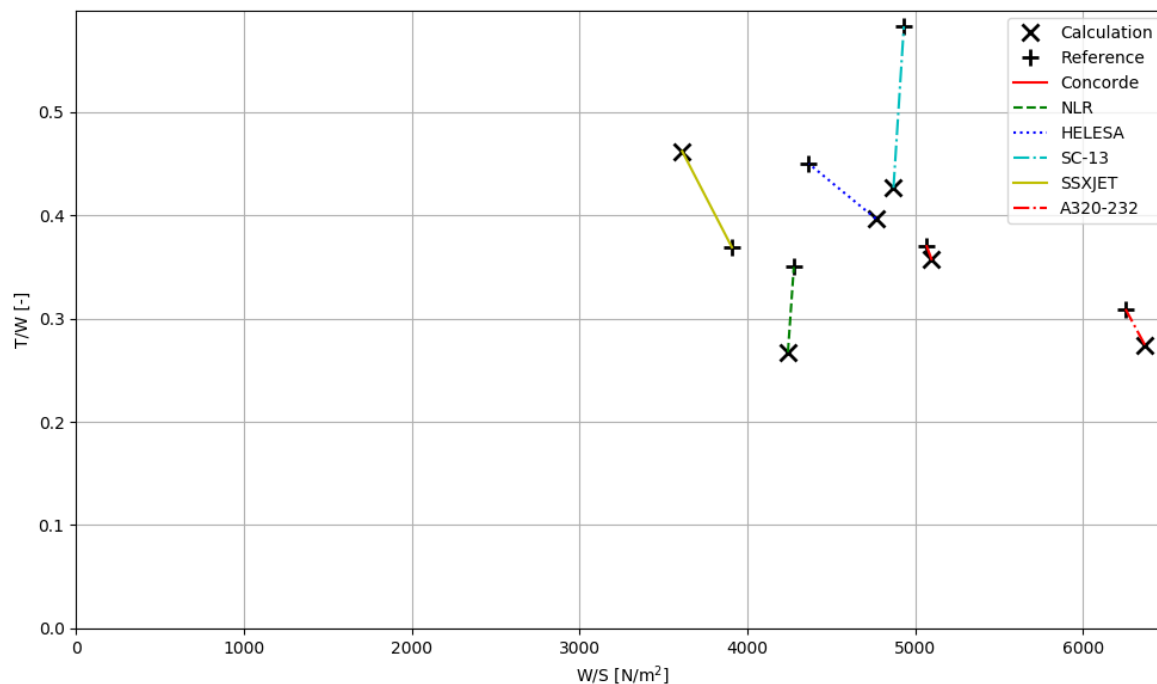


Figure 3.3: Calculated design point vs. real design point for various supersonic aircraft and the Airbus A320

The thrust loading usually is constrained by the takeoff distance. Although the method used here is much more accurate than other methods evaluated, it still is not optimal, as the differences for most aircraft are more than 10%.

The differences for the HELESA aircraft can be explained by the large margins the designers applied with respect to constraining requirements. If the same margins as this design program would be applied to those constraints, the design point would be close to a wing loading of 4,800 N/m<sup>2</sup> and a thrust loading of 0.4, which is much closer to the calculated result.

The low calculated thrust loading of the SC-13 may be explained by the very high design thrust of this aircraft. This may be much more than really required, since the authors claim the aircraft's T/W at MLW is 0.97, which is a lot higher than average.

Despite these issues, this proves a design point can be accurately calculated given the correct inputs.



# 4

## Engine design

When the design point is set, the engine parameters can be calculated. Although it may seem unusual to design the engine before the aircraft geometry, the methods used treat the engine independently of the aircraft, while the geometry does depend on the engine parameters. Therefore, it was decided to perform the engine calculations before the geometric calculations.

This chapter will first evaluate the steps taken to come up with a design for the engine and the calculation method of the engine module (Section 4.1). Using the design parameters, the off-design calculations will be treated in Section 4.2.

### 4.1. Engine design method

The primary goal of this engine design method is to calculate the fuel use of the engine at its design point and during various points in flight. A design method was set up that does not go into much detail, but tries to calculate as much data as possible with as few assumptions as possible. The reason for this is that such a method allows for the generation of realistic data in an early design stage when detailed analyses are not yet available.

The general engine type was selected based on estimated noise and fuel use. Turbojets have a reasonable efficiency during high speed flight, but generate much noise and have a high fuel burn. Turbofans have much better subsonic performance and efficiency, but engines with a high bypass ratio are unsuitable for supersonic flight due to their large frontal area [16]. Figure 4.1 shows the propulsive efficiencies of various engine types. It can be seen that the efficiency of turbofans is higher than turbojets, even at low bypass ratios. But the higher efficiency of high bypass ratio (BPR) engines is offset by the increase in drag and size, which plays a far greater role at supersonic speeds.

Early supersonic fighter jets had pure turbojet engines, some with afterburners, but they indeed generated much noise. Especially afterburners contribute highly to take-off noise due to the high flow velocity. Jet noise approximately scales with the eighth power of the jet velocity [18]. This also is the reason why high bypass turbofan engines became popular. The slower the flow velocity is, the less noise will be generated by the engine (Figure 4.2). Modern supersonic fighter jets usually have turbofans, but with a very low bypass ratio, but noise is less of an issue for military aircraft than for civil aircraft.

Therefore, a non-afterburning low-bypass turbofan engine was selected for the aircraft. This allows for reasonable performance, fuel efficiency and noise, both at subsonic and supersonic speeds.

Many handbooks and methods are available to describe steps for designing an engine. Examples of this are the book by Mattingly et al. [19] and the book by Walsh and Fletcher [20]. Although these books contain useful information, they will not be used entirely because the goal of this method is to keep the design as simple as possible with room to easily change parameters or configurations without changing the entire design method. Since the final goal is evaluation rather than design, the engine should be described with more data than just the main performance parameters like thrust, size and fuel usage, but without the need of knowing detailed flow parameters throughout the engine.

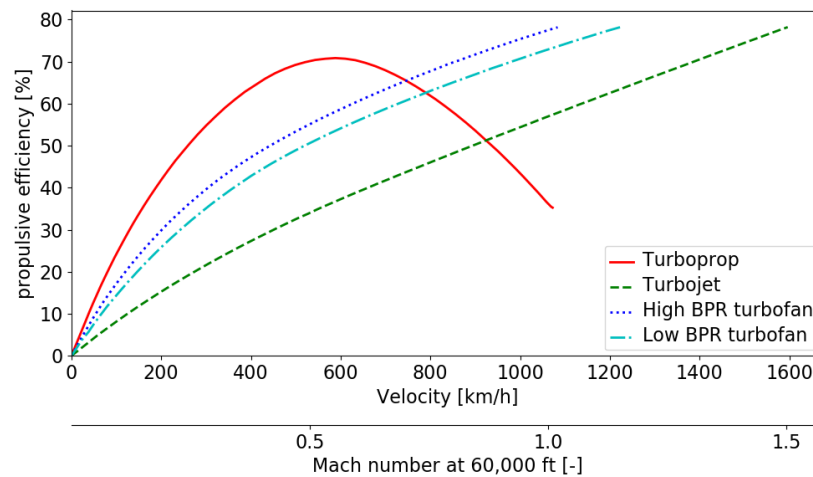


Figure 4.1: Propulsive efficiency variation with flight speed and Mach number at 60,000 ft ISA for various engine types. Adapted from [17]

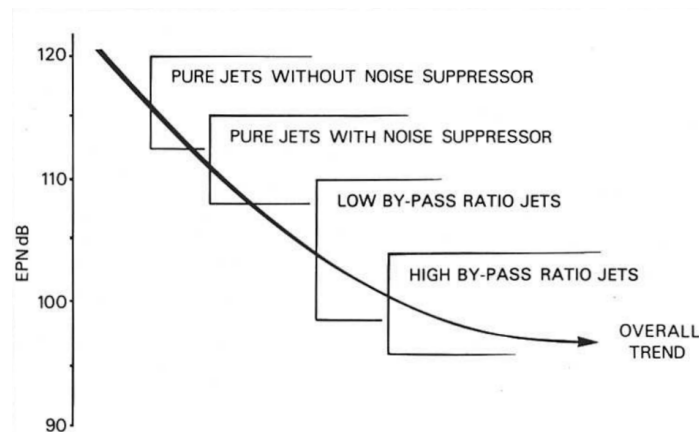


Figure 4.2: Noise levels of various engine types [17]

For this reason the main engine components will be treated as black boxes in a zero-dimensional analysis. This does not take into account flow aerodynamics, but rather the flow properties before and after a component based on thermodynamic analyses. For this reason an analysis method using station calculations is used in the program. This then results in known flow parameters before and after every component, finally giving the design thrust for a given set of design inputs.

Section 4.1.1 will explain the cycle calculations. After that, section 4.1.2 will show the steps taken to come up with a feasible engine design for any selected aircraft. Finally, section 4.1.3 will show the geometric calculations of the engine.

#### 4.1.1. Cycle calculation

This paragraph explains the cycle calculations for each engine component. The components can be combined in series, with the output of the previous component being the input for the next component. As the station numbering varies between papers, the numbering method used here is shown in Appendix B.2.

For all the calculations the assumption is made that all processes are adiabatic. This means that there is no heat transfer between the flow and its surroundings. It can not be assumed that compression and expansion are isentropic, since a multitude of pressure ratios for both the compressor and turbine will be analysed. With a higher pressure ratio more stages are required. While every stage can safely be assumed to have a similar isentropic efficiency, the isentropic efficiency of the entire component is

different depending on the number of stages. This can be explained by the constant pressure lines in a T-s diagram, shown in Figure 4.3. As can be seen these lines diverge for increasing entropy. If a large compression is divided in steps it can be seen that the individual isentropic temperature changes combined are larger than the single large temperature change. This indicates that the overall isentropic efficiency of a multi-stage compressor is smaller than the individual isentropic efficiency of a stage. Inversely, the isentropic efficiency of a turbine is larger than the isentropic efficiency of a stage.

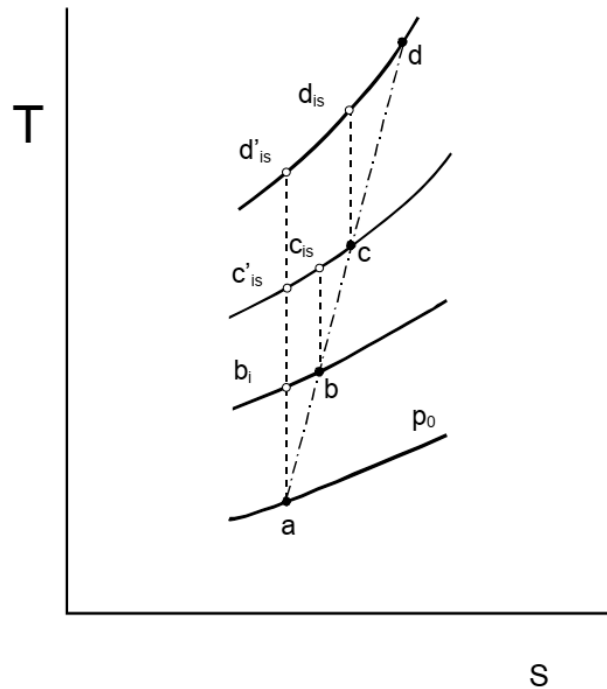


Figure 4.3: Single-stage versus three-stage compression [21]

As alternative to assuming isentropic compression and expansion a polytropic efficiency can be assumed. This can be defined as the isentropic efficiency of an infinitely small compression or expansion step. For these infinitely small steps it can be safely assumed that the isentropic efficiency is constant. Therefore, this polytropic efficiency can be used for calculating the compressor and turbine performance. Since the size and design pressure ratio for a component is unknown at the start of the engine design process, the polytropic efficiency is required as user input. The program will then calculate the isentropic efficiency based on the pressure ratio over the component.

Air is assumed to be a calorically perfect gas. The molecular composition of air is assumed to be either of the following options:

- pure air in International Standard Atmosphere (ISA) conditions: before any fuel is added in the engine, in the bypass flow and outside the engine
- air/fuel mixture: every part of the engine behind the combustion chamber

In the calculations it is assumed that the air and air/fuel mixtures are ideal gases. This means that pressure, temperature and volume are directly related as described in the ideal gas law and values like the specific heat capacities at constant pressure or volume,  $c_p$  and  $c_v$  are constant. This means that single values are assumed for the above air compositions, as shown in Table 4.1. In the following sections, values for pure air will be indicated with the subscript  $air$  and values for the air/fuel mixture will be indicated with  $gas$ .

Because of the above assumptions of adiabatic processes and ideal gases the concept of total enthalpy, temperature and pressure can be used. The definition of total properties is the level they would have if the flow would be brought to a stand still adiabatically, without adding or removing work. Since the velocity change inside the components is of little interest during this stage of research, using total

Table 4.1: Key values for the ideal gas used in the program

	$\gamma$	$c_p$	$R$
pure air	1.4	1000	287.06
air/fuel mixture	1.33	1150	287.06

properties is very useful. The total properties need to be calculated just once, after which all equations can use total pressure, temperature and enthalpy.

Every component influences pressure, temperature and/or mass flow, although the assumption is here that the mass flow rate at the exhaust is the same as the mass flow rate through the inlet, with exception of the fuel mass flow, so no losses like bleed air are taken into account. It is also assumed that the entry conditions for a component are exactly the same as the exit conditions of the previous component.

### Inlet

As the inlet does no work on the airflow, the total temperature across the inlet is constant. The inlet is assumed to have a fixed isentropic efficiency on which the pressure ratio over the inlet. Additionally, a ram recovery factor is applied in case of supersonic flight, based on the MIL-E-5008B standard stated in equation 4.1. The pressure and temperature ratios over the inlet are calculated using the isentropic relations (equations 4.2 and 4.3). The mass flow rate does not change.

$$f_{loss,M} = 1 - 0.075 (M - 1)^{1.35} \quad (4.1)$$

$$\frac{P_{0,2}}{P_{amb}} = \eta_{inlet} \cdot f_{loss,M} \left( 1 + \frac{\gamma_{air} - 1}{2} M^2 \right)^{\frac{\gamma_{air}}{\gamma_{air} - 1}} \quad (4.2)$$

$$\frac{T_{0,2}}{T_{amb}} = 1 + \frac{\gamma_{air} - 1}{2} M^2 \quad (4.3)$$

In the above equations  $f_{loss,M}$  is the Mach correction factor,  $P_{amb}$ ,  $P_{0,2}$ ,  $T_{amb}$ ,  $T_{0,2}$  are the ambient static pressure and the total pressure or temperature behind the fan respectively.  $\eta_{inlet}$  is the inlet efficiency and  $\gamma_{air}$  is the gas constant for pure air.

### Fan and compressor

The fan and compressor work similarly in the way they compress air. The only difference is the number of stages and the efficiency at which they compress the air. The isentropic efficiency depends on the pressure ratio and polytropic efficiency of the component, which can be calculated using Equation 4.4 [19]:

$$\eta_{is} = \frac{\Pi^{\frac{\gamma_{air} - 1}{\gamma_{air}}} - 1}{\Pi^{\frac{\gamma_{air} - 1}{\gamma_{air} \cdot \eta_{poly}}} - 1} \quad (4.4)$$

where  $\Pi$  is the pressure ratio and  $\eta_{poly}$  is the polytropic efficiency of the component. Since the pressure ratio will be user-defined, only the temperature ratio needs to be defined now, which is done using the isentropic relation in equation 4.5:

$$\tau = 1 + \frac{1}{\eta_{is}} \Pi^{\frac{\gamma_{air} - 1}{\gamma_{air}}} - 1 \quad (4.5)$$

where  $\tau$  can be used for either the fan temperature ratio  $\frac{T_{0,21}}{T_{0,2}}$  or the compressor temperature ratio  $\frac{T_{0,3}}{T_{0,21}}$ .

### Combustion chamber

The pressure ratio and temperature change over the combustion chamber will be predefined. The fuel flow rate can be calculated with an energy balance, shown in equation 4.6.

$$\dot{m}_{fuel} = \frac{\dot{m}_{core} \cdot c_{p,gas} (T_{0,4} - T_{0,3})}{LHV \cdot \eta_{cc}} \quad (4.6)$$

In this equation  $\dot{m}_{\text{core}}$  is the core mass flow rate, as specified by the bypass ratio.  $CP_{\text{gas}}$  is the pressure coefficient for the air/fuel mixture.  $T_{0,4}$  is the turbine inlet temperature which will be specified by the user and  $T_{0,3}$  is the compressor exit temperature.  $LHV$  is the lower heating value of the fuel. In this case Jet A fuel is assumed, which has a LHV of 43.1 MJ [22].  $\eta_{cc}$  is the efficiency of the combustion chamber.

### Turbines

Since the turbines provide power to the compressors, the compressor work needs to be evaluated before the turbine performance can be calculated. The work done by a compressor can be calculated using equation 4.7:

$$W = \dot{m} \cdot c_p \cdot \Delta T \quad (4.7)$$

with the mass flow rate through the component,  $c_p$  of the air through the component and the temperature change over the component. In this case of a fan with a single compressor, a two spool configuration is useful, with a high pressure turbine connected to the compressor and a low pressure turbine connected to the fan. The required turbine work can then be calculated by dividing the corresponding compressor work by the mechanical efficiency to account for mechanical losses.

For the flow characteristics through the turbines, equation 4.7 can be used inverted, resulting in the output temperature. The pressure ratio is the final unknown, but since the isentropic efficiency depends on the pressure ratio, it can not be calculated immediately. To deal with this, an iteration starts with calculating the pressure ratio using the polytropic efficiency. Then an isentropic efficiency is calculated using the initial pressure ratio. With this approximation a new pressure ratio can be calculated. This iteration is continued until the pressure ratio change decreases below a certain value.

### Nozzle

The nozzle calculations depend on whether or not the nozzle is choked. A choked nozzle means that the air inside the nozzle is completely expanded and can not expand further. In an unchoked nozzle the air is not fully expanded and therefore the nozzle is not used at its full potential. To calculate whether the nozzle is choked, equation 4.8 is used. The ratio  $\frac{p_{0,7}}{p_{crit}}$  is the critical pressure ratio which means that the nozzle is completely used. If the ratio  $\frac{p_{0,7}}{p_{amb}}$  is larger than the critical pressure ratio the nozzle is choked.

$$\frac{p_{0,7}}{p_{crit}} = \frac{1}{\left(1 - \frac{1}{\eta_{noz}} \cdot \frac{\gamma_{gas}-1}{\gamma_{gas}+1}\right)^{\frac{\gamma_{gas}}{\gamma_{gas}-1}}} \quad (4.8)$$

If the nozzle is unchoked, the thrust can be calculated by multiplying the mass flow rate with the difference in flow velocity over the engine (equation 4.9). If the nozzle is choked, this equation alone does not fully describe the flow potential. The pressure difference through the nozzle area describes the additional thrust coming from the nozzle (equation 4.10).

$$T_{unchoked} = \dot{m}_8 \cdot (V_8 - V_0) \quad (4.9)$$

$$T_{choked} = \dot{m}_8 \cdot (V_8 - V_0) + A_8 \cdot (p_{0,8} - p_8) \quad (4.10)$$

To obtain the required values the isentropic relations and gas equations were used.

For choked nozzles the total pressure equals the critical pressure calculated before:  $p_{0,8} = p_{crit}$ . Then, the density and velocity can be calculated using the equation of state (equations 4.12 and 4.13), following which the nozzle area can be calculated from the mass flow rate definition (equation 4.14).

$$\frac{T_{0,8}}{T_{0,7}} = \frac{2}{\gamma_{gas} + 1} \quad (4.11)$$

$$\rho = \frac{p}{R \cdot T} \quad (4.12)$$

$$V = \sqrt{\gamma \cdot R \cdot T} \quad (4.13)$$

$$A = \frac{\dot{m}}{\rho V} \quad (4.14)$$

For unchoked nozzles the static pressure inside the nozzle is set equal to the ambient pressure. The static temperature can then be calculated from the isentropic relations (equation 4.15).

$$\frac{T_{0,8}}{T_8} = \left( \frac{p_{0,8}}{p_8} \right)^{\frac{\gamma_{gas}-1}{\gamma_{gas}}} \quad (4.15)$$

The flow velocity results from the energy balance, equation 4.16

$$V_8 = \sqrt{2 \cdot c_p (T_{0,8} - T_8)} \quad (4.16)$$

Finally, the thrust can be calculated with equation 4.10

#### 4.1.2. Design steps

To actually design the engine based on the cycle calculations mentioned above, an optimisation routine was created. Since the cycle calculations return a value for thrust based on inputs for component efficiencies and pressure ratios, these were fixed as program inputs with the only variables being mass flow rate and thrust. The optimisation then tries to minimise the mass flow rate while keeping the thrust above the minimum threshold.

It was decided that the main engine parameters, listed below in Table 4.2, should be entered by the user before running the program. Mattingly has a useful list containing many of these variables with their values and (expected) changes for every 20-year period starting from 1945 [19]. These were validated using data from various older and newer engines, as shown in Appendix B.

Table 4.2: Input parameters for the engine module

BPR	bypass ratio [-]	$\eta_{inlet}$	inlet efficiency
OPR	overall pressure ratio [-]	$\eta_{polyfan}$	fan polytropic efficiency
$\Pi_{cc}$	combustion chamber pressure ratio [-]	$\eta_{polycomp}$	compressor polytropic efficiency
TIT <sub>max</sub>	maximum turbine inlet temperature [K]	$\eta_{cc}$	combustion chamber efficiency
		$\eta_{mech}$	mechanical efficiency
		$\eta_{polyturb}$	turbine polytropic efficiency
LHV <sub>f</sub>	fuel lower heating value [MJ]	$\eta_{noz}$	nozzle efficiency

Additionally, the atmospheric conditions and gas properties are set. The design point calculation for the engine will be based on the takeoff condition, with sea level standard altitude and no velocity.

To find the design thrust per engine the total thrust (as calculated by the design point module) is divided by the number of engines. By default this number can be either two or four. The three-engine option is not considered in this design for the additional design work that would be needed to add an engine along the centreline of the aircraft. The benefit of having three engines would be a reduced thrust (which also means smaller size and less complexity) per engine compared to a two-engine design. Additionally, less powerful engines generate less noise which may help in meeting noise requirements.

The only parameters that still need to be defined are the compressor pressure ratios, turbine inlet temperature (TIT) and the mass flow rate.

To divide the required overall pressure ratio (OPR) over the fan and compressor, some assumptions were made about the fan size. The pressure ratio over a single fan stage was assumed to be 1.4 [19]. Additionally, the fan was assumed to have two stages like the GE Affinity, so that the estimated fan pressure ratio (FPR) is 1.96. The compressor pressure ratio can then be calculated by dividing the OPR by the FPR.

After experimenting with various ways of determining a good TIT, a function was created which calculates a limit based on engine certification year:

$$TIT_{max} = 454.5 \cdot \ln(0.163 \cdot (\text{year} - 1950)) + 1000 \quad (4.17)$$

with the TIT in Kelvin. The data for this was found in [23]. It is also possible to manually enter the maximum allowed TIT.

The mass flow rate was decided to keep as variable in the optimisation. The goal of the optimisation is to minimise the fuel flow rate, given all the parameters like efficiency and pressure ratios. The mass flow rate is the only variable parameter with the thrust being limited by the minimum design thrust. The initial value for mass flow rate is calculated by dividing the design single-engine thrust by an estimation of the specific thrust. The bounds for the mass flow rate are set to 100 and 1,100 kg/s. This results in a configuration with minimum air and fuel mass flow rate for the required thrust, given the aforementioned engine parameters.

### 4.1.3. Engine size calculations

Since the engine calculations mentioned above are theoretical and not very detailed, not many details about the size of the engine can be obtained directly. Therefore, statistical methods are used to calculate the diameter, length and mass of the engine.

A large database of engine parameters was found online<sup>1</sup>. While the database is not updated recently, its large size will be useful in finding trends for size and mass. The accuracy of data was verified by comparing some entries to data found in Jane's<sup>2</sup>. The database contains engines with dry static thrust between 60 and 115,000 lbf (roughly 300 N to 500 kN) and bypass ratios between 0 and 16.6. This is a very large variation and therefore caution needs to be taken before using this statistical data.

A first attempt to calculate the length of the engine was by looking at the data set. Since Raymer uses a statistical relation between length, Mach number and thrust [14], the correlation between thrust and length was evaluated. As can be seen in Figure 4.4, there is no obvious correlation between length and thrust. Raymer distinguishes two engine categories: a supersonic, afterburning engine and a subsonic, non-afterburning one. At Mach 0.8 and 1.6 these approximately describe the bounds on the engine length.

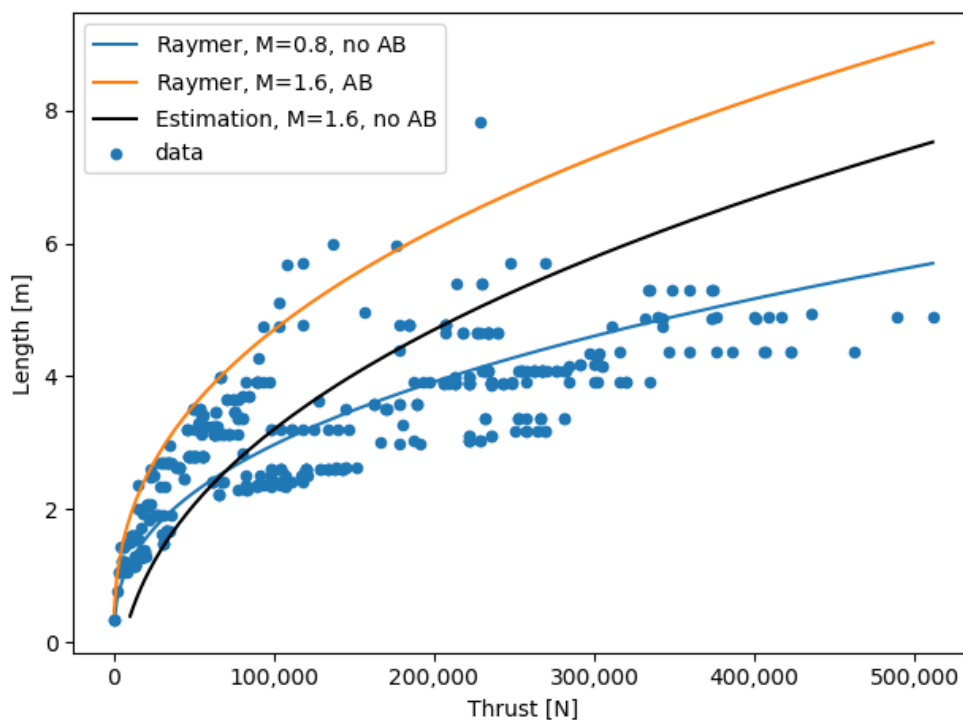


Figure 4.4: Relation between engine thrust and length

<sup>1</sup><https://www.jet-engine.net/>. Accessed 20 December 2019

<sup>2</sup><https://janes.ihs.com/AeroEngines/Reference>. Accessed 20 December 2019

As the engine for this aircraft will not have an afterburner, its length will be smaller than the afterburning engines. The length of an afterburner usually varies between 1.5 and 3 m [24–26]. Therefore, it was decided that the engine length would be defined by the equation given by Raymer reduced by 1.5m (equation 4.18). This should give enough room for mixing the bypass and core flow and for a variable-area nozzle. For low thrust engines this will give inaccurate results, but it is assumed that the minimum thrust per engine will always be above 150 kN. Note that the original equation is given in imperial units. Equation 4.18 is converted to SI units.

$$L_{engine} = \left( 3.06 \left( \frac{T}{4.448} \right)^{0.4} M^{0.2} \right) \cdot 0.0254 - 1.5 \quad (4.18)$$

To find the diameter of the engine and nacelle various methods were combined. As base parameter the air mass flow rate is used, since that seems to be the most influencing parameter on the engine's diameter. Figure 4.5 shows the relation between mass flow rate and fan diameter. To find a better linear fit the lowest and highest results were removed from the dataset, since the engine is not estimated to have a mass flow rate lower than 100 kg/s or higher than 1100 kg/s. This results in a linear regression with  $R^2 = 0.97$ .

The same was done to calculate the diameter of the engine itself, visible in Figure 4.6. Here the linear fit has  $R^2 = 0.94$ . Both regressions were evaluated using SPSS which resulted in statistically significant regressions. For subsonic aircraft the nacelle diameter is approximately 1.2 to 1.5 times the fan diameter [27, 28]. However, supersonic engines need much sharper nacelle edges and therefore can do with a smaller nacelle.

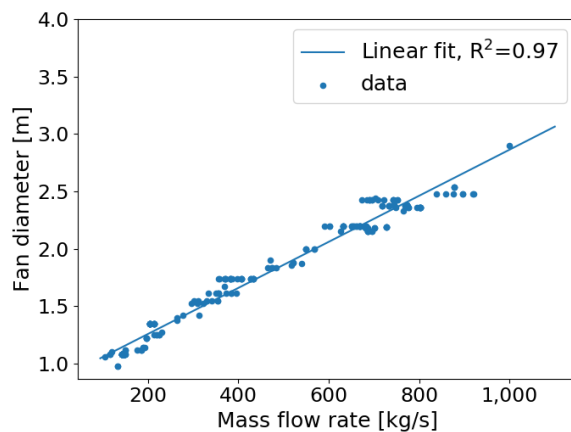


Figure 4.5: Relation between mass flow rate and fan diameter

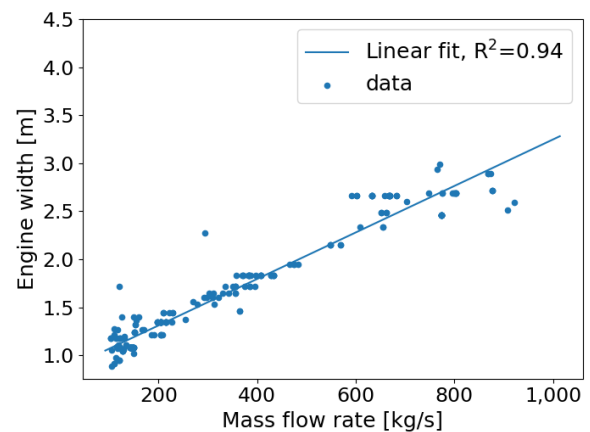


Figure 4.6: Relation between mass flow rate and engine diameter

For the aerodynamic calculations the capture area is required as input value. Raymer defines a preliminary capture area which is related to the cruise Mach number and mass flow rate. For a cruise Mach number of 1.6 the ratio  $\frac{A_{capture}}{\dot{m}}$  is approximately 3.7.

For the dry mass of the engine the relation between thrust and mass is evaluated. As shown in Figure 4.7 the data has a linear correlation with  $R^2 = 0.96$ . All related equations are listed below.

$$D_{fan} = 2.0 \cdot 10^{-3} \dot{m} + 0.85 \quad (4.19)$$

$$D_{engine} = 2.4 \cdot 10^{-3} \dot{m} + 0.83 \quad (4.20)$$

$$m_{engine} = 1.6 \cdot 10^{-2} T + 350 \quad (4.21)$$

Engines like Concorde's Rolls-Royce Olympus engines have extensive compression ramps to slow down the air without losing too much pressure. With Raymer as a guide [14], it was decided that for a cruise Mach number of 1.7 and higher a variable-geometry inlet would be used. For lower cruise Mach numbers a fixed-geometry inlet is assumed to be sufficient.

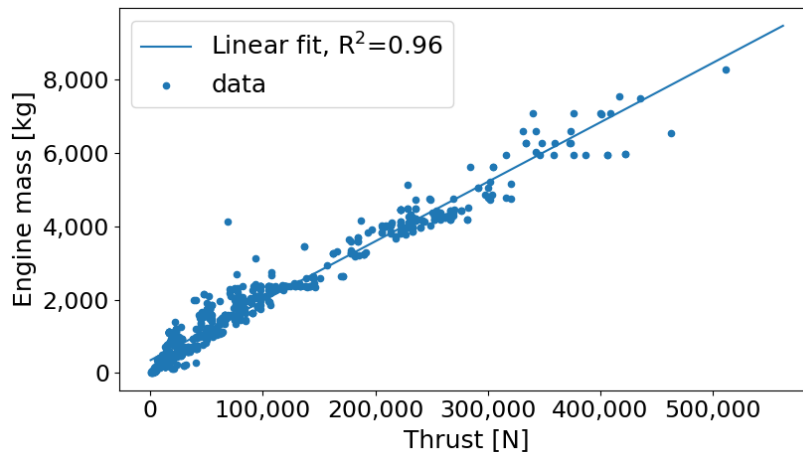


Figure 4.7: Relation between engine thrust and mass

## 4.2. Engine off-design calculation

Now the design performance of the engine is calculated, the off-design performance needs to be evaluated. The results of this analysis can then be used in the Class I weight estimation, where the fuel use at various mission segments needs to be estimated. This fuel use changes depending on atmospheric conditions, speed and thrust setting. The usual way of doing this is by changing the operating point on the compressor and turbine maps, which results in a different mass flow rate and pressure ratio [27, 29]. However, due to the low detail level of the engine design these are unknown. There are options to create hypothetical compressor and turbine maps, using software like Gas turbine Simulation Program (GSP) [30] or GasTurb [31]. These programs however are not suited to perform all design steps automatically, require additional assumptions and will likely not result in a more accurate result, since in the end the calculation steps are similar.

Because of this a more approximate method was looked for. Kurzke suggests to adapt existing cycle maps [32], but this method seems to be impractical to integrate in automated code. Finally, a method was found which does not use compressor or turbine maps but finds an equilibrium between operating lines of the low and high pressure spools related to compressor exit pressure [33, 34]. The method explained by Bos [34] could not be reproduced, so therefore the calculations as described by Mirza-Baig [33] were used.

For the cruise phase of the flight the method was verified by comparing it to the report data and data from Janes<sup>3</sup>. However, for supersonic flight the results were inaccurate as they were too low. Additionally, the results for the low-thrust phases loiter and final reserve were inaccurate. This was expected since Mirza-Baig mentions that agreement of the simulation was good at sea-level static condition for thrust levels above 50% of the maximum. However, due to the short duration of these phases it is expected that they are less relevant for the total fuel use during a flight, so it was accepted that they will be estimated with lower accuracy.

To solve this, the fuel data for the flight segments that were unknown were linked to the known data. The supersonic cruise fuel use is made dependent on the subsonic cruise data. The subsonic and supersonic specific fuel consumption (sfc) of various real and theoretic engines were compared as shown in Table 4.3. This shows that on average, the supersonic sfc is 1.28 times the subsonic sfc with a standard deviation of 0.04. Since there is a large difference between the Concorde engine (Olympus 593) and that of the Tu-144 and the Olympus is generally considered to be better optimised for both subsonic and supersonic flight, it is likely that better ratios can be achieved for current generation supersonic engines. Therefore, the ratio is by default set to 1.24, with a user option to change it if more information is available.

Although a 24% increase in sfc may seem acceptable for gaining time by flying supersonically, there

<sup>3</sup><https://janes.ihs.com/AeroEngines/Reference>. Accessed 20 December 2019

are more factors that influence the total fuel use. The Breguet range equation includes the sfc and  $L/D$ . A subsonic aircraft has a lower sfc and higher  $L/D$  than a supersonic aircraft in all flight phases. This combination results in a reduced fuel use with respect to supersonic flight. Based on the mission alone, the ratio of fuel weight to take-off weight for this supersonic aircraft will be around 0.57. For a subsonic mission with the same distance, the fuel weight will be approximately 0.30 times the takeoff weight. Since the takeoff weight of a supersonic aircraft will also be higher than that of a subsonic aircraft, the total fuel quantity required will be more than twice the fuel required for a subsonic aircraft having the same mission.

For loiter and final reserve it is assumed that the aircraft generates more drag and because the lower thrust setting will be a less efficient one, the sfc during loiter and final phase is 1.10 and 1.12 times the sfc during the diversion phase. Since the influence of these values is estimated to be low, not much effort has been taken into a detailed reasoning behind these numbers. Chapter 7 will show the effects of changing them.

Table 4.3: SFC data for various aircraft during subsonic and supersonic cruise. Imperial units are used for the sfc since they are the most widely used

Aircraft name	HELESA	HSTC	Concorde			Tu-144D	Edge
Engine type	MFTF <sup>4</sup>	MFTF	Olympus 593	MCV99	TF <sup>5</sup>	RD-36-51A	MFTF
Source	[35]	[36]	[37]	[37]	[37]	<sup>6</sup>	[38]
sfc <sub>crsub</sub> [lb/lb/h]	0.63	1.05	1.025	0.845	0.816	0.94	0.78
M <sub>crsub</sub> [-]	0.92	0.9	0.95	0.95	0.95	0.95?	0.7
sfc <sub>crsup</sub> [lb/lb/h]	0.83	1.3	1.195	1.1	1.094	1.23	1.0
M <sub>crsup</sub> [-]	1.6	2.4	2.0	2.0	2.0	2.0	2.4
sfc ratio	1.32	1.24	1.17	1.30	1.34	1.31	1.28

<sup>4</sup>Mixed-flow turbofan

<sup>5</sup>Turbofan

<sup>6</sup><http://www.tu144sst.com/techspecs/powerplant.html>. Accessed 4 February 2020

# 5

## Geometric design

Now the engine parameters are fixed, the geometry of the aircraft is designed. Using pre-set requirements and a number of assumptions the shape of the fuselage and wings can be defined.

The fuselage shape is defined in Section 5.1. Following that, the wing geometry is explained in Section 5.2. Section 5.3 shows the empennage design. Finally, the location and size of the fuel tanks will be explained in Section 5.4.

### 5.1. Fuselage design

The fuselage design is mostly based on the number of passengers and the Mach number. The shape is not yet optimised for noise generation. The fuselage is divided in a nose section, the cabin and the tail section (Figure 5.1). The nose and tail section have a fixed slenderness ratio, while the cabin section dimensions will be based on the number of passengers.

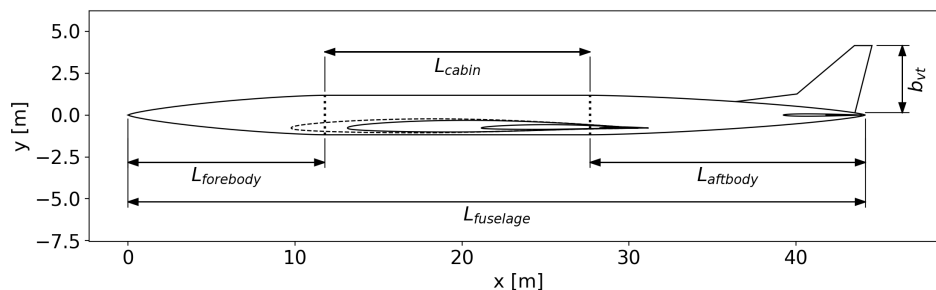


Figure 5.1: Example aircraft drawing with fuselage sections shown

#### 5.1.1. Nose and tail section

The shape of the nosecone and tailcone was chosen such that the theoretical drag contribution of these sections will be lowest. The largest contribution comes from wave drag and friction drag. The wave drag can be reduced by increasing the slenderness ratio of the conical section, while the friction drag will be reduced by choosing a shape with a surface area that is as low as possible. These requirements are conflicting, since a higher slenderness ratio, given a certain cabin diameter, will always result in a higher surface area. Therefore, the goal was to find the optimal slenderness ratio and curvature of the nosecone and tailcone in order to optimise the sum of wave drag and friction drag.

For low nose slenderness ratios, the Von Kármán nose has the lowest wave drag contribution [39]. Additionally, this nose type can be described by using just diameter and length, which are two variables that can easily be defined. At higher slenderness ratios, the pressure drag contribution becomes less than or equal to the wave drag. An example of this is shown in Figure 5.2, where a cone-cylinder

combination with varying thickness ratio ( $d/l$ , the inverse of slenderness ratio) is subjected to a  $M=2$  flow. Here it can be seen that around  $d/l = 0.125$  ( $l/d \approx 6.7$ ) the wave drag contribution is equal to the skin friction contribution. Below this value, at higher slenderness ratios, the skin friction contribution starts to raise which will increase the total drag. When this happens, elongating the nose further is not useful, due to the increase of weight that can not be offset by the drag reduction. The slenderness ratio where this transition happens is considered to be somewhere between 5 [39] and 8 [40, 41]. This corresponds to a thickness ratio between 0.125 and 0.2, indicated in Figure 5.2.

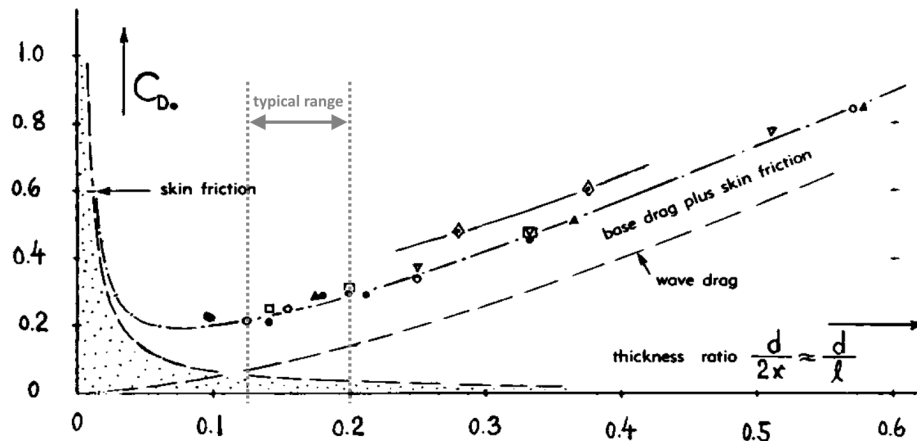


Figure 5.2: Buildup of total drag coefficient for a cone-cylinder configuration at  $M=2$  as a function of thickness ratio. Adapted from [42]

Additionally, a more slender body will generate less or smaller shock waves, which will result in less noise disturbance on ground. More about this will be explained in Chapter 9. It was decided to keep the slenderness ratios as secondary user input, with a nose slenderness ratio of 5 and a tail slenderness ratio of 7 as default values. More about this choice will be explained in Chapter 7.

It is assumed that the cockpit and the front and rear part of the cabin section will be located in the nosecone and tailcone. Having a traditional windowed cockpit would require a front window with a sharp angle to the fuselage to allow for a good visibility range for the pilots. This would increase the drag because the different shape compared to the Von Kármán shape. However, it is likely that modern supersonic aircraft will have an external vision system. This system is planned for the NASA X-59<sup>1</sup> and Boom XB-1<sup>2</sup>, among others. Research by NASA suggests that an external vision system is promising to meet all requirements for operational use [43]. Therefore, it is assumed that the cockpit will not influence the aerodynamics of the nose.

### 5.1.2. Cabin

Based on the total number of passengers a seating layout is defined. Based on the size of the aircraft, a certain percentage of passengers is assumed to use first class, premium economy or economy class. For each class seat dimensions are estimated, after which the width of the aircraft can be calculated. From the number of seats abreast the length of the seating area is calculated, which defines the cabin length.

The distribution of passengers over the different classes is listed in Table 5.1. The reasoning behind this is the following: a small aircraft is very likely to offer a premium experience, similar to business jets. On the other hand, aircraft with more than 130 seats are likely to be more like an average airliner, which means that it will probably need a mixed configuration of first and economy class. For aircraft with a number of passengers in between these values, a single class is assumed, but with seats comparable to premium economy class.

<sup>1</sup>Testing of X-59 Virtual Forward Window Successful. NASA, 26 August 2019 (last updated 28 August 2019). <https://www.nasa.gov/feature/langley/testing-of-x-59-virtual-forward-window-successful>. Accessed 26 March 2020

<sup>2</sup>Boom - XB-1. Boom Supersonic. <https://boomsupersonic.com/xb-1>. Accessed 26 March 2020

The seat dimensions are based on average numbers for long haul flights. They can be found in Table 5.2. Source data is listed in Appendix C. The aisle width is defined to be 20 in (0.508 m), the minimum value required by EASA CS 25.815. Since the seat widths only define the inner width of the plane, the calculated width is multiplied by a factor 1.06 to get the outer width of the aircraft [44].

Table 5.1: Passenger distribution over the classes

	Number of passengers		
	1-20	21-130	130+
seats abreast (standard)	2	2	4
distribution	100% business	100% premium economy	15% business 85% economy

Table 5.2: Seat dimensions for various classes

	pitch [in]	pitch [m]	width [in]	width [m]
Economy	32	0.81	20.5	0.52
Premium economy	38	0.97	22.5	0.57
Business	42	1.07	24.5	0.62

In the cabin design space for lavatories, closets, galleys and doors should also be taken into account. To calculate the extra cabin length, the method from the FLight OPTimization System (FLOPS) weight estimation is used [44]. Subsequently, it is assumed that 2 m of the front section and 2 m of the rear section of the cabin will be placed in the nose and tail sections of the aircraft. This is done because these parts (which likely are galleys or lavatories) will not need the full cross-section of the cabin and therefore will save space if they will be located in the nosecone or tailcone.

To make sure the fuselage is not excessively wide or long, there will be a minimum and maximum for the slenderness ratio. For the nose and tailcone this number will be fixed, but the cabin slenderness can be changed by changing the number of seats abreast. The slenderness ratio of the aircraft is set to be between 15 and 25, based on the slenderness ratios of previous supersonic aircraft [45]. To support this, data of some more recent supersonic aircraft were compiled in Figure 5.3. The data for this can be found in Table C.3 in Appendix C.

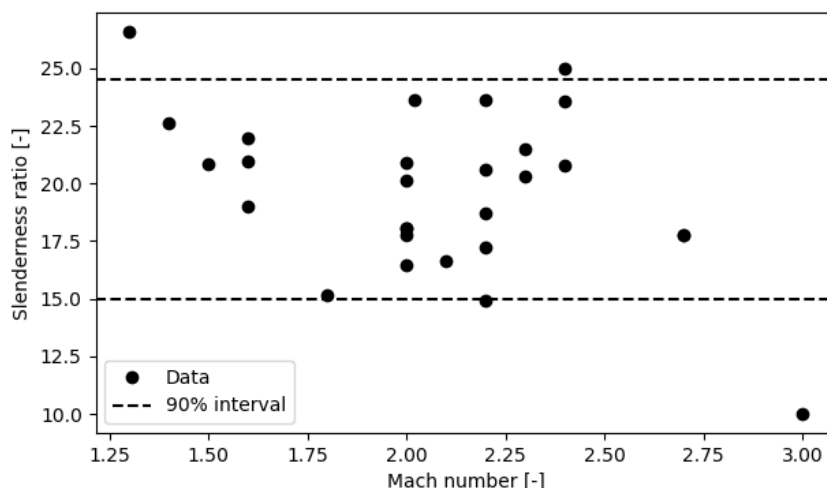


Figure 5.3: Slenderness ratio for various supersonic aircraft, compared to Mach number. More details in Appendix C

If the calculated slenderness is above the limit, the aircraft will be made wider by allowing more seats abreast. If the slenderness is below the limit the number of seats abreast will be decreased. This

results in a fixed fuselage length for a given number of passengers, which can be seen in Figure 5.4. The graph shows the small increases in aircraft length for every row of seats, with each new row being a flat segment in the graph. The changes in passenger distribution among seat types are visible at 21 and 131 seats, as well as the addition of new lavatories and galleys which are bigger jumps in the graph.

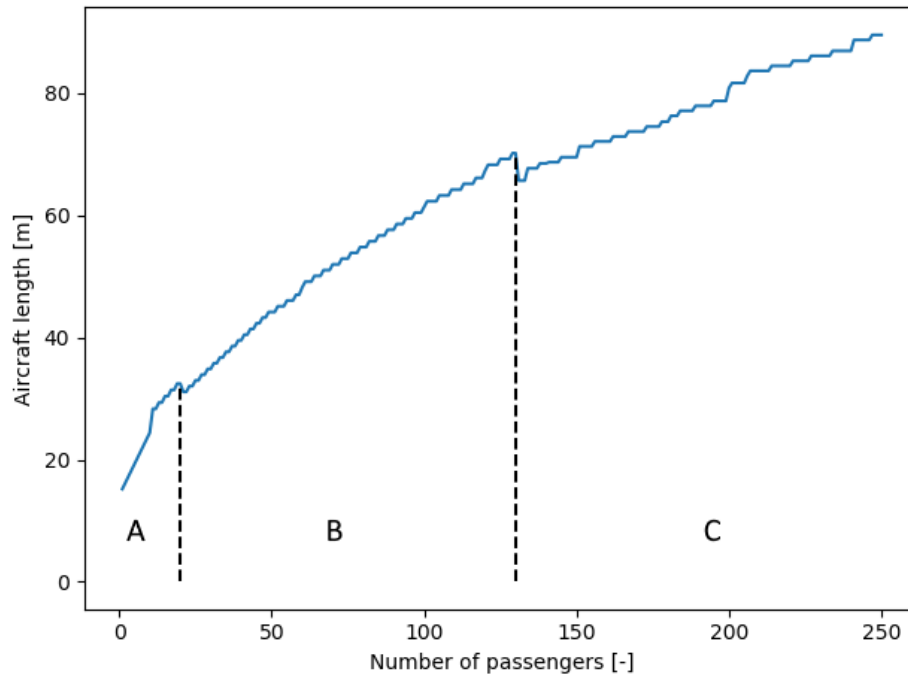


Figure 5.4: Aircraft length plotted against number of passengers. A: business class seats only, B: premium economy seats only, C: mixed seats

Figure 5.5 shows the seating layout and fuselage slenderness compared to the number of passengers. As can be seen the number of seats abreast increases for higher passenger numbers, but at a smaller rate than subsonic aircraft. For example, the Boeing 737 can seat around 110 passengers with a 6-abreast layout, while aircraft like the Airbus A330 usually have 8 or 9 seats abreast for a number of passengers greater than 250.

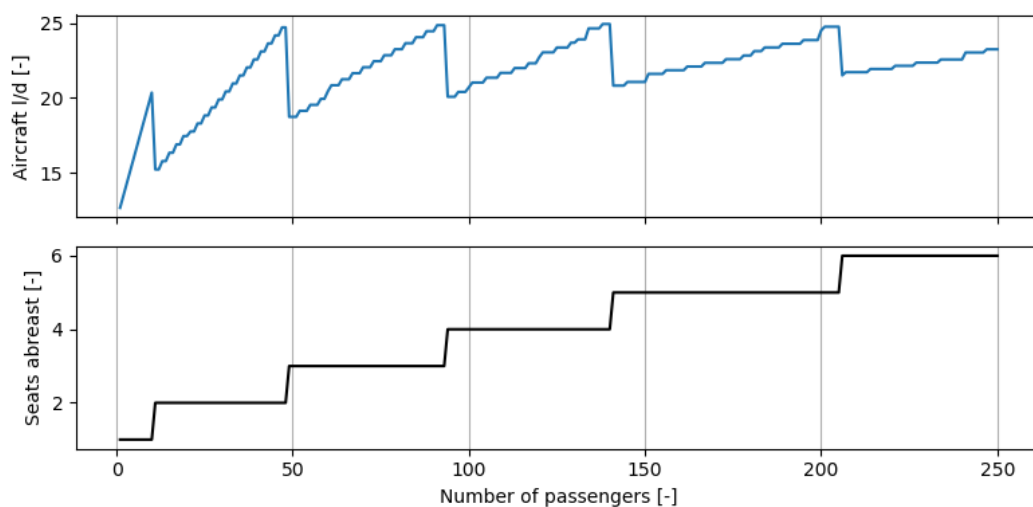


Figure 5.5: Fuselage slenderness ratio and seats abreast plotted against number of passengers

## 5.2. Wing design

The next step after the fuselage design is designing the wing. This section could be a thesis itself, however by taking a number of assumptions it was attempted to keep the wing design as simple as possible. This section will mainly talk about the geometry and planform of the wing. More about the aerodynamic properties of the wing can be found in the other thesis about this design program [5].

### 5.2.1. Planform shape

Numerous shapes have already been used for supersonic wing designs. They vary from simple delta wings to variable sweep wings and oblique wings. Each of these wing types has its own benefits and drawbacks, which will be discussed below. After that, a final choice will be made on the wing type.

#### Variable-sweep wing

Variable-sweep wings can hinge around a pivot and can therefore change their sweep angle. Due to this, the wing can be optimised for the actual flight speed. This allows for good high speed performance when the wings are swept back, without sacrificing low speed performance when the wings are (nearly) perpendicular. Notable examples of aircraft with variable sweep wings are the Grumman F-14 Tomcat and the Rockwell B-1 Lancer. The greatest benefit of this type of wings is for aircraft that need to fly multiple subsonic and supersonic flight phases for a long time. For example, the F-14 could use its swept back wings for supersonic dash and could reduce its sweep for manoeuvring in tight turns [46]. The biggest drawback of this system is that these wings are much heavier than fixed wings. This is mainly due to the hinge system that has to support the movable wings. However, for a mission that justifies using variable sweep wings this probably saves weight compared to a fixed-wing design [46].

#### Oblique wing

The oblique wing is a special type of variable sweep wing. Instead of sweeping both wings backward, the wings are now regarded as a single wing which is able to rotate around a single point at the centre of the fuselage. This design comes very close to the theoretical optimum lift distribution at subsonic speeds, but then turned at an angle to the flow [47]. Therefore, the drag of this type of aircraft will be lower and therefore they will require less fuel and will have a lower MTOW. A variant of an oblique wing aircraft is the oblique flying wing (OFW). This concept is just a flying wing which will be able to change its yaw angle during flight. The maximum speed limit for oblique wing designs may be around Mach 2. Otherwise, the sweep angle would become too high, resulting in lower performance and reduced controllability [48]. Others say that even lower Mach numbers would be limiting the oblique wing-body aircraft, down to 1.4 or 1.6 [47].

The biggest disadvantage of an OFW is the need for many passengers. To allow reasonable room for passengers, the wing must have a minimum thickness which also limits the minimum size of the wing itself. Van der Velden suggests a minimum of at least 200 passengers [49], which will probably be too high for an economically viable SST at this moment. A supersonic flying wing-body may be more suitable for lower passenger numbers, but there is little data about this kind of aircraft. OFWs also need a very wide runway, due to the low sweep during takeoff. An OFW with more than 200 passengers may be more than 100 m wide [49].

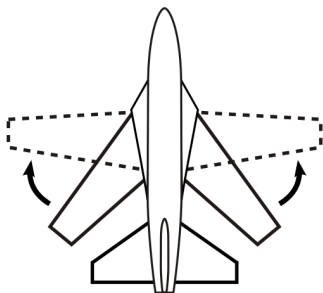


Figure 5.6: Variable-sweep wing planform<sup>3</sup>

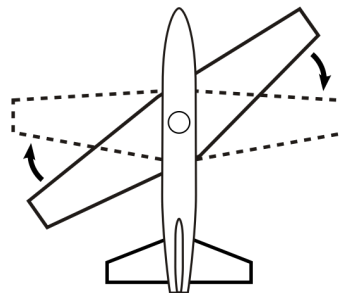


Figure 5.7: Oblique wing planform<sup>4</sup>

### Delta wing

A wing type with geometry that is somewhat easier to describe is the delta wing. In its most basic shape a delta wing is a sharp triangle. Due to its high sweep angle the volume wave drag is reduced. The large root chord results in a lower wing weight while having increased stiffness. This also results in a larger wing area compared to normal wings, therefore having a lower wing loading [46]. Drawbacks of a delta wing are the lower lift efficiency. Due to the low aspect ratio and high sweep angle a delta wing aircraft needs to fly at a higher angle of attack. Another consequence of this is the need for higher thrust, which then causes additional noise, which will mainly be noticed during takeoff and landing [47]. A delta wing without tailplane or canard also is unable to use flaps, since it can not counter the nose down pitching moment caused by the flap deflection.

### Ogive wing

A variation of delta wings used by Concorde and a few other aircraft is the ogive wing. Instead of a straight leading edge, this wing type has a curved leading edge. This was done to keep the inboard leading edge sharp to introduce a strong vortex and keep the aerodynamic centre as far forward as possible. This allows for better transonic and supersonic performance when the aerodynamic centre will move aft [1]. To counter the drawbacks of a highly swept wing the outboard leading edge sweep is decreased and a little bit of trailing edge forward sweep is introduced [50].

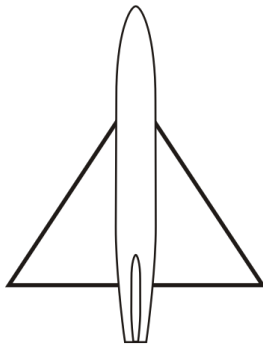


Figure 5.8: Delta wing planform<sup>5</sup>

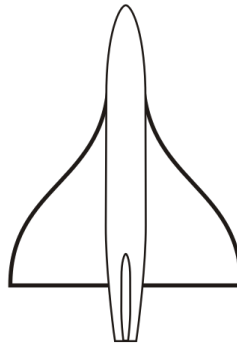


Figure 5.9: Ogive wing planform<sup>6</sup>

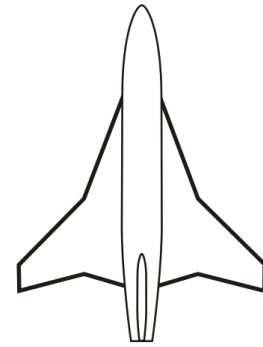


Figure 5.10: Cranked arrow wing planform<sup>7</sup>

### Cranked arrow wing

The more conventional variant of the ogive wing mentioned above is the cranked arrow wing. This wing type has two sections with different sweep angles. This simplifies production and gives more room for possible leading edge high-lift devices. Furthermore, this type of wing allows for a better volume distribution to decrease supersonic wave drag [51].

### Trade-off

Based on the above research on wing planforms, the wing planform selected was a cranked arrow wing. OFWs and other variable geometry wings were considered to be too impractical for real use. The reason for this is that variable geometry wings come with a large weight penalty that probably can not be justified for the mission, since a typical mission for the SST considered here mainly consists of a long supersonic cruise and subsonic segments only during the accelerating and deceleration phases of the flight. OFWs also will require airport adaptations for their different shape and size compared to

<sup>3</sup>Image by Steelpillow, [https://commons.wikimedia.org/wiki/File:Wing\\_variable\\_sweep.svg](https://commons.wikimedia.org/wiki/File:Wing_variable_sweep.svg). CC BY-SA 3.0 (<https://creativecommons.org/licenses/by-sa/3.0>)

<sup>4</sup>Image by Steelpillow, [https://commons.wikimedia.org/wiki/File:Wing\\_oblique.svg](https://commons.wikimedia.org/wiki/File:Wing_oblique.svg). CC BY-SA 3.0 (<https://creativecommons.org/licenses/by-sa/3.0>)

<sup>5</sup>Image by Steelpillow, [https://commons.wikimedia.org/wiki/File:Wing\\_delta.svg](https://commons.wikimedia.org/wiki/File:Wing_delta.svg). CC BY-SA 3.0 (<https://creativecommons.org/licenses/by-sa/3.0>)

<sup>6</sup>Image by Steelpillow, [https://commons.wikimedia.org/wiki/File:Wing\\_ogival\\_delta.svg](https://commons.wikimedia.org/wiki/File:Wing_ogival_delta.svg). CC BY-SA 3.0 (<https://creativecommons.org/licenses/by-sa/3.0>)

<sup>7</sup>Image by Steelpillow, [https://commons.wikimedia.org/wiki/File:Wing\\_cranked\\_arrow.svg](https://commons.wikimedia.org/wiki/File:Wing_cranked_arrow.svg). CC BY-SA 3.0 (<https://creativecommons.org/licenses/by-sa/3.0>)

today's aircraft. Additionally, an OFW will be too unconventional for many calculation methods used and will probably be too large to be economically viable.

A problem with using a delta wing is that it has an unswept trailing edge. This means that the length-wise area distribution will see a sharp drop at the wing trailing edge, which will result in additional shock waves resulting in more noise. Additionally, the possible control problems for a tailless delta configuration make this option less favourable.

To increase low-speed performance it was chosen to divide the wing into two parts with different sweep angles. This allows for a good high-speed performance for the inboard wing, and a better low-speed performance for the outboard wing due to the lower sweep angle.

### 5.2.2. Subsonic leading edge

A special design requirement for the wings was to have a subsonic leading edge. When the leading edge would be supersonic, a normal shock would occur at the wing leading edge. This results in a drag rise over the wing. Additionally, supersonic aerodynamics suddenly plays a role in the airfoil design, such as the need for a sharp leading edge [52]. Supersonic airfoils have a bad subsonic performance and therefore they are not very useful in the design of SSTs, because of the additional thrust that will be required. This will cause more noise, which is unwanted.

To make sure the wing leading edge is subsonic, it must be within the Mach cone of some disturbance upstream. For the wing this is the leading edge root. The Mach cone is defined as the cone enclosed by the Mach angle, which is defined as equation 5.1, where  $\mu$  is the Mach angle and  $M$  the Mach number. As can be seen, the Mach angle increases with increasing Mach number, therefore narrowing the Mach cone.

$$\mu = \sin^{-1} \frac{1}{M} \quad (5.1)$$

The wing planform is defined using the leading edge sweep angle and taper ratio. The default leading edge sweep angle is set to a high value to ensure the leading edge stays within the Mach cone generated by the wing-fuselage root leading edge. During testing it was found that  $\Lambda_{LE} = 68^\circ$  resulted in the lowest takeoff weight (see Chapter 7). For the inboard leading edge sweep angle  $7^\circ$  is added to the effective sweep angle. The outboard sweep angle then depends on the area as defined during the design point calculation. The default taper ratio is 0.15.

The inboard trailing edge sweep angle is kept at  $0^\circ$  for increased flap effectiveness. The outboard trailing edge sweep angle is defined by the taper ratio combined with the quarter chord sweep angle. An example of this wing design output is shown in Figure 5.11.

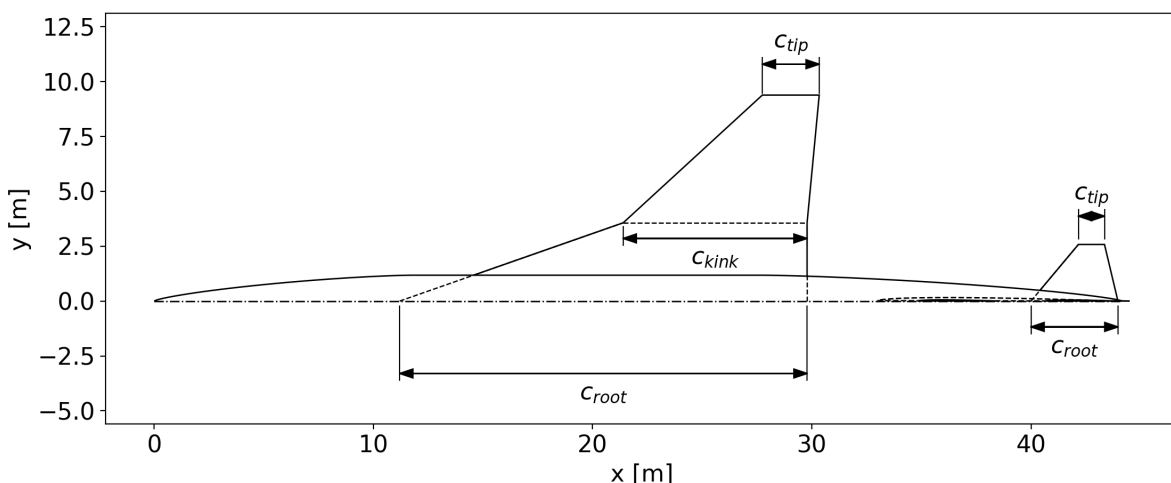


Figure 5.11: Example wing and horizontal stabiliser with fuselage section shown

### 5.3. Empennage design

Since the choice was made earlier to not make stability calculations, the empennage design was based mostly on estimates, earlier designs and handbook calculations.

The horizontal stabiliser is optional by user input. If it is included, the calculations are done using a modified volume coefficient and a geometric factor as described in FLOPS [44]. The leading edge sweep angle, taper ratio and aspect ratio are set as secondary user inputs. The FLOPS method requires assumptions for the elevator sizing and stabiliser positioning. The ratio between elevator area and total area is assumed to be  $\frac{1}{3}$ , which is the default value suggested, and the stabiliser is assumed to be mounted to the fuselage. With these values the entire horizontal stabiliser is defined (see Figure 5.11).

It was attempted to design the vertical stabiliser in a similar way, but this resulted in inaccurate values. Therefore, the required surface area is calculated using a volume coefficient of other supersonic aircraft, combined with geometry variables as shown in equation 5.2:

$$S_{vt} = \frac{V_{vt} \cdot S_w \cdot b_w}{l_{h,vt}} \quad (5.2)$$

where  $S_{vt}$  is the surface area of the vertical tail,  $V_{vt}$  is the vertical tail volume coefficient,  $S_w$  and  $b_w$  are the wing surface area and span and  $l_{h,vt}$  is the tail arm: the distance between the mean aerodynamic chords (MACs) of the wing and vertical tail.

Again the leading edge sweep angle, taper ratio and aspect ratio are secondary user inputs, based on which the dimensions are calculated.

To increase the effectiveness of the vertical stabiliser, a dorsal fin is added. To do this, a kink location was defined, following which the outboard sweep angle was increased by  $10^\circ$ . This results in a lower kink chord, which then reduces the surface area. To compensate for this, the inboard sweep angle is increased. This is shown in Figure 5.12.

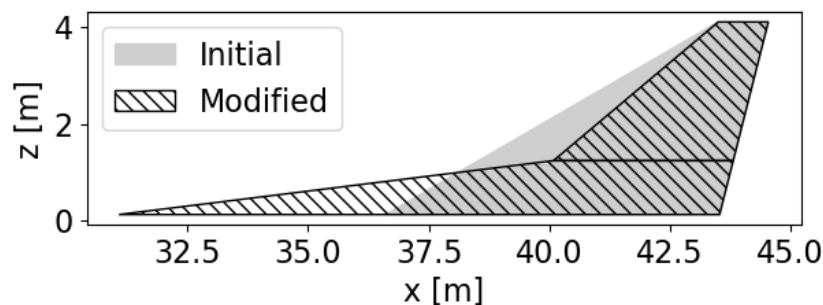


Figure 5.12: Example horizontal tail; distances on axes are measured from fuselage centerline and nosecone front

### 5.4. Fuel tanks

Now the various aircraft sections that may contain fuel have been designed, it is time to calculate the maximum fuel volume and whether that is suitable to perform the design mission. As a start, the wing, horizontal stabiliser (if present) and a part of the tailcone was designated as fuel tank. Since the engines will be wing-mounted, the wing will house the engine feed tanks, as well as the main fuel tanks. Since at supersonic speeds the aerodynamic centre will shift backward, the tail tanks will be used as trim tanks, so that fuel will be shifted backward as well to balance the centre of gravity with the aerodynamic centre and keep the trim drag as close as possible to zero [53].

The volume available in the wing is calculated using the estimated position of the front and rear spar of the central wing construction. The front spar is estimated to be located at 12% of the chord length (or at 5% if no leading edge high-lift devices are used) and the rear spar location depends on the flap size as calculated in the aerodynamics module. Based on this and the planned airfoil, the cross-sectional area of a wing section is calculated, which is then integrated over the wing, up to 90% of the wing span.

The horizontal stabiliser fuel tank is calculated in the same way. The front and rear spar locations are estimated to be 20% and 75%. Due to the low thickness this volume is negligible compared to the total fuel tank volume, but due to the probable importance for trimming this tank is still kept in the design.

The tailcone fuel tank is assumed to occupy 60% of the tailcone. The pressure bulkhead will be put right behind the aft galley, which continues up to 2 m into the geometric tailcone. 60% of the remaining volume will be used for the fuel tank.

It was discovered that available fuel tank volume does not increase linearly with the fuel requirement for a mission. Large aircraft do have sufficient fuel volume, but early versions of the smallest aircraft variant with 18 passengers could only store 60-70% of the required fuel. To solve this, additional fuel tanks were planned in other fuselage parts, such as the nosecone and fuselage bottom. Additionally, the tailcone fuel tank will be enlarged to 85% of the total volume of the tailcone.

If this still does not solve the problem the fuselage can be lengthened as a last resort. Optionally, wing tip tanks or a belly tank could be added too. All of these options will increase drag, but lengthening the fuselage or adding wing tip tanks could help in finding a good area ruled aircraft shape.

Further research will have to show which of these options would result in the lowest weight addition. The latest version of the aircraft design did have sufficient space for fuel by only using the wing, tailcone and horizontal stabiliser tanks, so it currently is expected that the planned size of the aircraft will leave enough space for fuel storage.

A picture of the planned fuel tank layout is shown in Figure 5.13.

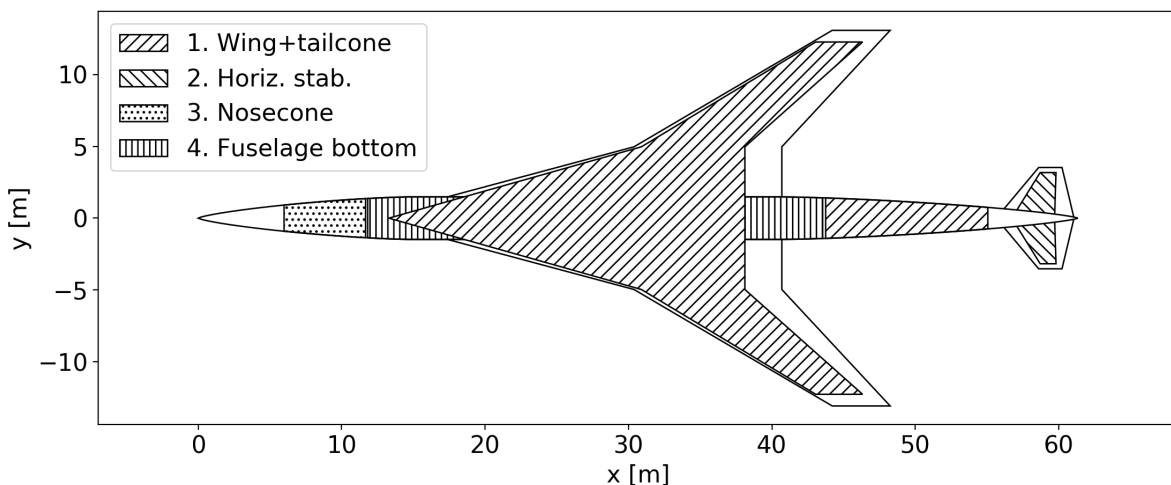


Figure 5.13: Fuel tank layout



# 6

## Aerodynamics and Class II weight estimation

In the previous chapters the aircraft design has been shown. To know more about the flight characteristics of supersonic aircraft, an aerodynamic analysis has been performed. These analyses are required for knowing the lift/drag ratios which play an important role in the calculation of the aircraft's key parameters. Additionally, lift data is required for the Class II weight estimation which is another important part of the aircraft design programme. The Class II weight estimation is a more detailed weight analysis by defining the OEW not as statistical relation to the MTOW, but as a combination of component weights. Therefore, this analysis is more precise than the Class I weight estimation.

One key assumption for the lift and drag analyses is that the wing has a subsonic leading edge. This allows selecting a subsonic airfoil instead of supersonic airfoils with sharp leading edges that experience stall at lower angles of attack. To make sure the wing leading edge encounters subsonic flow the wing is positioned inside the Mach cone, as explained in section 5.2.

This chapter is a summary of the aerodynamics and class II weight estimation chapters in the first thesis on the supersonic aircraft design program. For a more detailed explanation and reasoning, the reader is referred to Den Boer [5].

Section 6.1 will explain the lift analyses for the various flight phases. After that, the drag buildup is shown in Section 6.2. Finally the Class II weight estimation is summarised in Section 6.3.

### 6.1. Lift analysis

As the main goal for the aerodynamics module is to provide lift/drag ratios at specific mission points, the first step is to estimate the lift based on flight parameters and the angle of attack. For subsonic flight ( $M \leq 0.9$ ) the USAF Stability and Control DATCOM is used [54]. This collection of methods gives an equation to calculate the lift curve slope mainly depending on the wing aspect ratio and Mach number. This equation however only covers the ideal case. Lift divergence during transonic flight and the fuselage generating lift is not taken into account.

$$C_{L\alpha} = \frac{2\pi A}{2 + \sqrt{4 + \frac{A^2 \beta^2}{\eta^2} \left(1 + \frac{\tan^2 \Lambda_{0.5c}}{\beta^2}\right)}} \frac{S_{exposed}}{S_{ref}} F \quad (6.1)$$

In this equation,  $C_{L\alpha}$  is the lift curve slope,  $\beta = \sqrt{1 - M^2}$ ,  $\Lambda_{0.5c}$  is the half-chord sweep angle and  $\eta$  the airfoil efficiency factor.  $\frac{S_{exposed}}{S_{ref}}$  is the ratio between exposed and reference wing area, while  $F$  is a correction factor for the additional lift generated by the fuselage [14]. Besides this a factor is used to take transonic lift divergence into account. Torenbeek mentions that this method underestimates the

wing lift gradient by 5-10% for transonic airliners at maximum flight speed. Therefore, the lift gradient resulting from equation 6.1 is multiplied by a factor 1.08 above Mach 0.90. This factor linearly increases from 1.0 between Mach 0.75 and 0.90.

For even lower speeds during the takeoff and landing phases of the flight a different method was used, since this method underestimates the lift coefficient at high angles of attack (above 10°). To solve this a separate method by Polhamus [55] was applied which is specifically aimed at including the vortex lift. The method is shown in equation 6.2 where the first term describes the potential flow and the second term describes the vortex lift. This equation does not take into account fuselage lift or reduced exposed wing area.

$$C_L = K_p \sin \alpha \cos^2 \alpha + K_v \sin^2 \alpha \cos \alpha \quad (6.2)$$

where  $C_L$  is the lift coefficient and  $\alpha$  is the angle of attack.  $K_p$  and  $K_v$  are coefficients that can be found using graphs in the source. These coefficients depend on Mach number, sweep angle and aspect ratio. Using this equation the deviation from real data was found to be acceptable for Mach 0.25 (Table 6.1).

Table 6.1: Polhamus method lift coefficient for M=0.25 compared to source data [50, 56]

Concorde				NLR			
Angle of attack [deg]	$C_{L_{ref}}$ [-]	$C_{L_{Polh}}$ [-]	Deviation	Angle of attack [deg]	$C_{L_{ref}}$ [-]	$C_{L_{Polh}}$ [-]	Deviation
0	0	0	0%	0	0	0	0%
5	0.192	0.201	4.90%	4	0.187	0.186	-0.53%
10	0.417	0.442	6.02%	8	0.392	0.405	3.29%
15	0.696	0.708	1.72%	12	0.631	0.648	2.63%
20	0.979	0.982	0.31%	14	0.761	0.775	1.84%
Average			2.59%	Average			1.45%

Because of the different behaviour of air at supersonic speeds, a separate calculation is performed for  $M \geq 1.4$ . Here the digital DATCOM is used [57]. This is an updated version of DATCOM merged into a computer program. To use this program an input file has to be created containing Mach number and angle of attack data. The DATCOM program then reads the file and produces an output file with the calculation results. The exact way this was done is stated by Den Boer [5]. While the digital DATCOM has some shortcomings like not taking into account the influence of airfoil thickness on the lift curve slope and only being able to calculate the linear part of the lift curve for supersonic flight, these are not considered to be limiting. A study suggests the effect of airfoil thickness on supersonic lift can be ignored for thin airfoils [58], which is assumed to be true for the airfoils used here, too. Furthermore it is rightly assumed that the aircraft will only operate in the linear part of the lift curve. For validation again data from the Nederlands Lucht- en Ruimtevaartcentrum (Netherlands Aerospace Centre) (NLR) is used. The method described above is compared to the lift curve for Mach 1.6 and 1.8, shown in Table 6.2.

Table 6.2: Digital DATCOM lift coefficient for M=0.95 compared to source data [56]

M=1.6				M=1.8		
Angle of attack [deg]	$C_{L_{ref}}$ [-]	$C_{L_{calc}}$ [-]	Deviation	$C_{L_{ref}}$ [-]	$C_{L_{Polh}}$ [-]	Deviation
0	0	0	0%	0	0	0%
2	0.088	0.089	1.34%	0.077	0.082	5.98%
4	0.179	0.177	-1.04%	0.156	0.163	4.69%
6	0.278	0.266	-4.24%	0.238	0.245	2.82%
	Average		-0.99%	Average		3.37%

For transonic flight the lift a curve is fit through the calculated lift at  $M = 0.9$ ,  $M = 0.95$  and  $M = 1.4$ , and through the estimated lift at  $M = 1.0$ . This gives an indication of the lift curve slope for the clean aircraft at the entire flight regime. As an example, the resulting lift curve slope by using data from NLR

is shown in Figure 6.1. The kinks in the curve are caused by the transonic lift divergence from Mach 0.75 and the begin and end of the transonic interpolation from Mach 0.90 and Mach 1.4. While little data is available for additional validation the lift curve slope has a 2% deviation from the NLR data point of  $C_{L_{\alpha}}$  at  $M=0.95$  [56].

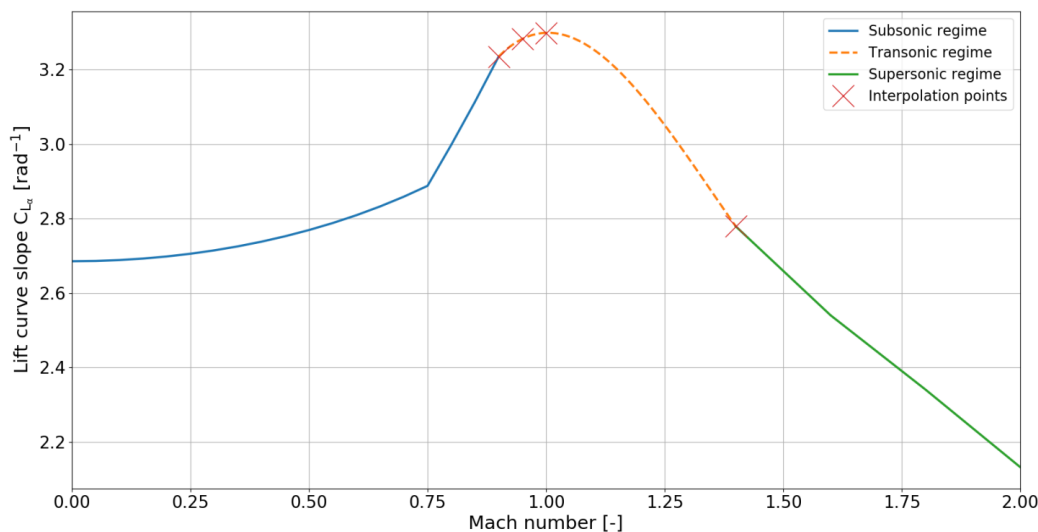


Figure 6.1: Example lift curve slope variation with Mach number [5]

As with most other aircraft, the aircraft needs high-lift devices during takeoff and landing to improve low-speed lift. The extra lift required at takeoff and landing is calculated at two points: for takeoff at an angle of attack of  $10^\circ$  in ground effect, and for landing at an angle of attack of  $12^\circ$  without ground effect. The reason for choosing these specific angles is that  $10^\circ$  is assumed to be the maximum angle with a reasonable wheel strut length (larger angles would require longer struts to avoid tail strikes) and angles above  $12^\circ$  would result in visibility problems for the pilots. This could be solved by using a movable nose like Concorde but this adds more weight which would be unnecessary otherwise.

Depending on the flap type, the  $C_{L_{max}}$  increase varies between 0.4 and 1.0. During the sizing process either a user-selected flap type will be used, or cycle through the flap types until an option is found that fulfils the  $C_{L_{max}}$  requirements. If the requirements can not be met by any high-lift device combination, the top-level requirements are relaxed a bit which reduces the maximum required lift. This keeps going until the lift requirements can be met. More about the high-lift devices and their sizing calculations can be found in [5]

## 6.2. Drag analysis

The drag generated by an aircraft can be split up in two categories: lift-independent drag and lift-dependent drag. Lift-independent drag is generated by the shape of the aircraft itself, for example friction drag. Lift-dependent drag is caused by the generation of lift. Examples of this are vortex drag and induced drag. These will first be explained for subsonic speed in section 6.2.1 and after that for supersonic speed in section 6.2.2.

### 6.2.1. Subsonic drag

The lift-independent drag can be divided into two parts: low-speed drag, containing friction drag and parasite drag, and high-speed drag containing compressibility drag and wave drag. The friction drag is the sum of the friction drag of all components, based on the whether the flow is laminar or turbulent, the geometry and slenderness of the component and their interference. Additionally, factors are included for leakage, landing gear and flaps.

At high subsonic speeds local shocks will form on the aircraft. These shocks generate additional drag, here called high-subsonic compressibility drag. Using two methods, the drag divergence Mach number

was estimated to be slightly above 1.0. While the anticipated cruise Mach number of 0.95 is below  $M_{DD}$ , a drag increase of about 2.5 counts can still be expected.

The most important lift-dependent drag factor at subsonic speeds is the induced drag. This is the component that has the largest contribution to the quadratic shape of the drag polar, due to the quadratic dependence on  $C_L$ . Other parameters required to calculate the induced drag are the wing aspect ratio and the Oswald efficiency factor  $e$ . While most estimation methods are unable to calculate  $e$  at high subsonic speeds, a method was found that calculates the viscous  $e$  from the inviscid  $e$ . A factor to calculate the influence of flap deflection on  $e$  is also included. Furthermore, it is assumed that no vortex will be created from the wing leading edge due to the normally low angles of attack. The  $L/D$  during take-off or landing is not required to be known, so therefore it is currently not taken into account.

Another component of the lift-dependent drag is trim drag. Aircraft having a horizontal stabiliser usually require a downward force on that surface to balance the aircraft, which requires additional lift on the main wing. This increases induced drag. Since no balance estimation is performed in this early design stage, it is estimated that the trim drag accounts for 2% of the total aircraft drag.

Now all drag components are mentioned above, the combined drag for subsonic and supersonic flight can be calculated. The subsonic lift/drag curve consists of the friction drag, high-subsonic compressibility drag (if applicable), induced drag and trim drag.

### 6.2.2. Supersonic drag

To calculate the drag during supersonic flight, a method used by NLR [56] is applied. This method first models the zero-lift drag of the fuselage, wings, horizontal stabiliser and vertical stabiliser and sums them. This was multiplied by a factor of 0.85 to get closer to the real value simulated by supersonic area ruling. Then the lift-induced wave drag is calculated by combining the vortex-induced drag and the minimum wave drag for an elliptic streamwise lift distribution. The total lift is then calculated using the suction parameter which can be estimated by using the design lift coefficient. This method is rather elaborate and is further specified by Den Boer [5].

A second method that was evaluated is one described by Raymer [14] which however had large deviations from real data and therefore is only used as a backup. The lift/drag curves of both methods are shown in Figure 6.2.

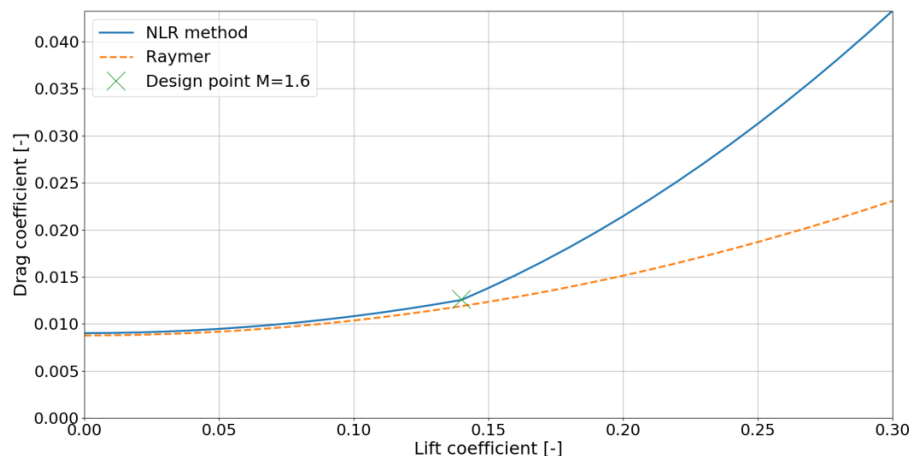


Figure 6.2: Supersonic lift/drag methods applied to the NLR aircraft design in [56] (source: [5])

When the NLR method was applied to the NLR aircraft design, this resulted in a lift/drag ratio of 11.16, indicated with a cross in Figure 6.2. This is 0.54% more than the 11.1 found in [56]. For Concorde the cruise  $L/D$  is estimated to be 8.24. The calculation method finds a lift/drag ratio of 7.89, which is 4.3% less. Both numbers are acceptable for this design stage, although more validation data need to be found for further proving the validity of this model. For now it is expected that the accuracy of the model is within 10% of the real data.

## 6.3. Class II weight estimation

Now the aerodynamics parameters are known, the Class II weight estimation can be performed. By dividing the OEW into various components, it can be estimated more accurately, resulting in a better estimation of the MTOW.

### 6.3.1. V-n diagrams

The first step in creating the Class II weight estimation is the generation of V-n diagrams to calculate the limiting load factor of the aircraft. Two V-n diagrams are to be created: a manoeuvre diagram and a gust diagram which is based on the manoeuvre diagram. Both diagrams are constructed by calculating the load factor at certain speeds during various flight phases.

The manoeuvre diagram consists of six points, listed below:

- A Along the stall speed line when reaching the limiting load factor (usually 2.5) while operating at 1.1 times the maximum lift coefficient
- C Cruise speed at limiting load factor
- D Dive speed at limiting load factor
- E Dive speed at load factor 0
- F Cruise speed at maximum negative load factor (usually -1.0)
- H Negative stall speed at maximum negative load factor while operating at -0.85 times the maximum lift coefficient

The gust diagram is created in a similar way. At certain reference speeds the gust load is calculated from a reference gust speed, the gust intensity, wing loading and lift curve slope. The gust diagram starting point is a load factor of 1.0 which is the normal condition in-flight. Since the gusts can either have a positive or negative influence, the positive gust points are also mirrored around the line of load factor 1.0. The points that define the gust loading diagram are shown below.

- B' The intersection of the stall line and the gust load/speed relationship, or a minimum value required by certification limits
- C' Gust load factor at cruise speed
- D' Gust load factor at dive speed
- E' Negative gust load factor at dive speed
- F' Negative gust load factor at cruise speed
- G' Negative point B'

These V-n diagrams combined show the maximum allowable load depending on flight speed. An example graph is shown in Figure 6.3.

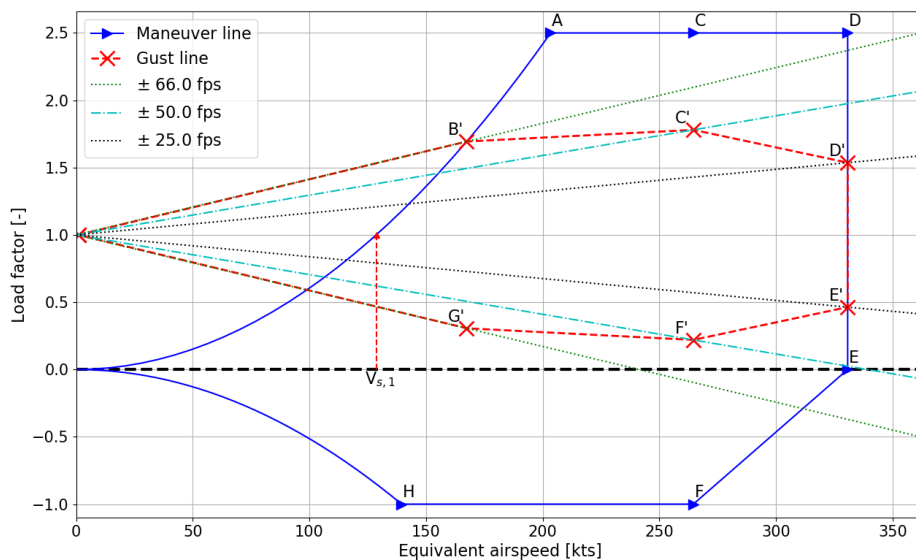


Figure 6.3: Example V-n diagram

### 6.3.2. Weight estimation

With the load limits calculated the Class II estimation of the OEW can be performed. To do this the aircraft is divided into several components. For every component the weight is estimated by using methods of Raymer [14], Torenbeek [6], Roskam [59], FLOPS [44], Nicolai [60] and Kroo [61]. The primary method used is from FLOPS but methods from the other authors are used when they were found to be more accurate. Note that this section is a short summary of the method. More detailed component information and calculations are included by Den Boer [5].

#### Structures

The first component group evaluated is the structures group. This consists of all structural parts like fuselage, wing, empennage, nacelles and landing gear. Particularly the wing weight was hard to be estimated by the methods evaluated, since most methods are aimed at subsonic wings and tailplanes. However, enough data were available to adjust the methods by adding weight penalties or by calibration.

#### Propulsion

The propulsion group contains the bare engine and its accessories, like engine controls. The engine dry weight is calculated using equation 4.21. Most engine accessories for supersonic aircraft will have approximately the same weight. The only exception is the inlet, which is longer and has more moving parts for supersonic aircraft. To estimate the weight of these components accurately, methods tailored for supersonic aircraft were found and used.

#### Equipment

The last group containing parts of the empty weight is the equipment group. This group consists of different kinds of systems like avionics and hydraulics. The elements of this group sometimes are difficult to estimate due to their rapid change with new technology developments or the difference between subsonic and supersonic aircraft. For example, newer aircraft require more electric power to supply the digital systems in the cockpit and the passenger entertainment. There also is a trend of increasing the cabin pressure to reduce the effect of flight altitude on passengers. However, supersonic aircraft like Concorde had electric systems and cabin pressure that is much like current aircraft. Therefore not much had to be changed to the methods found.

#### Operations

The difference between empty weight and OEW is the operations group. This includes crew weight, unusable fuel and oil, among others. This group could be evaluated as a whole by methods found in FLOPS [44].

### 6.3.3. Calibration

To improve the accuracy of certain methods, they are validated using data from two aircraft: the Boeing 737-200 and Concorde. The reason for choosing the 737-200 as subsonic aircraft is that this is an aircraft from about the same era as Concorde with much information known about it. If weight differences between the methods and real data could not be explained they were recalibrated using data from multiple aircraft so that they matched better. This resulted in absolute deviations to be reduced from a maximum of 67% to a maximum of 12%.

### 6.3.4. Technological developments

Since both the methods and the validation aircraft are old, weight savings can be expected for aircraft that are currently being built. New construction methods or materials will reduce weight, but are not included in the weight estimations. Therefore component weights are multiplied by a factor that accounts for weight savings due to technology developments. While testing the method this resulted in a 16.8% OEW decrease with respect to Concorde for a current-generation aircraft with the same requirements as Concorde.

To account for unforeseen weight growth, every component weight is increased by 5%. The resulting OEW is then used in a new Class I weight estimation to calculate a new MTOW. This is compared to the MTOW calculated at the start of the iteration. If the difference is less than a user-set limit (by default 0.1%), the iterative part of the program is stopped and the final methods are executed.

# 7

## Exploring the design space

After the methods were finished the program was validated. Since all methods were verified and validated separately, it was expected that the full program results are valid too. This was indeed the case, as shown by Den Boer [5]. Since some calculations were changed after the publication of that thesis a second validation was performed. The new validation results will be shown in Section 7.1. Besides that, an analysis was performed to check the validity of some earlier assumptions and to ensure that the model matches the expectations when changing parameters. This will be explained in Section 7.2. Finally, a set of aircraft was generated with varying size on which the noise and emissions calculations were based. They will be shown in Section 7.3.

### 7.1. Full program validation

A full program validation was performed for a second time after the changes in the modules for the design point, engine and geometry were validated. This was done to check whether any previous results would still be valid. To make sure the results are comparable, exactly the same dataset as in [5] is used. The takeoff masses are compared, which is shown in Table 7.1. For Concorde and the Tu-144 new, improved versions are designed as well.

Table 7.1: Aircraft take-off mass comparison for program validation

Aircraft	$W_{TO,ref}$ [kg]	$W_{TO,calc,prev}$ [kg]	$W_{TO,calc}$ [kg]	Delta w.r.t. [5] [%]	Delta w.r.t. ref [%]
Concorde	185,066	186,723	202,775	9	10
Concorde new	185,066	126,075	129,592	3	-30
Tu-144	206,794	213,095	232,695	9	13
Tu-144 new	206,794	145,134	148,804	3	-28
Boom SST	77,100	118,888	100,947	-15	31
Boom SST mod	77,100	82,226	81,867	0	6
Aerion AS2	54,884	55,699	51,030	-8	-7
HELESA	43,100	46,009	42,557	-8	-1
Cranfield SSBJ	44,900	48,918	43,794	-10	-2
NLR M1.6	340,000	355,184	342,849	-3	1
SC-13	140,160	149,074	154,796	4	10

The largest differences (not counting the new Concorde and Tu-144) can be seen in the results of Concorde, Tu-144 and Boom SST. The main reason is a change in thrust correction factor during the design point calculations. The original version included an additional factor to take bypass ratio into account in a relation with Mach number. However, it was found out that a large part of this correction already was taken into account by the pressure effect and therefore the resulting thrust was corrected too much or too little at Mach numbers outside the original scope of 0.8-1.8. At Mach 2 and BPR 3 this

resulted in a thrust that was three times higher than without this correction. At Mach 0.3 the resulting thrust was about 15% lower. This could be seen in performance during the low-speed flight segments like climb performance and supersonic cruise performance.

Concorde and Tu-144 had the climb performance as active constraint on thrust loading. This makes the new MTOW of Concorde and Tu-144 around 10% higher than their real MTOW, since there also were changes that resulted in a decreasing MTOW. For the Boom SST the supersonic cruise defined the lower limit of the thrust loading. The reduced thrust correction resulted in a lower supersonic cruise constraint and therefore the thrust loading reduced by nearly 15%.

The OEWs of the aircraft were also compared to the calculation results. This is shown in Table 7.2. Here the trend from the take-off mass for Concorde, Tu-144 and Boom SST can also be seen. Apart from that, the empty mass increased with 2 to 6%. The outlier here is the Aerion AS2. The reason for this may be found in the differences between the model aircraft and the real design. The current design<sup>1</sup> has a wing with laminar flow and a low sweep angle and three engines, while the model has a highly swept wing and two engines.

Table 7.2: Aircraft empty mass comparison for program validation

Aircraft	$W_{OE,ref}$ [kg]	$W_{OE,calc,prev}$ [kg]	$W_{OE,calc}$ [kg]	Delta w.r.t. [5] [%]	Delta w.r.t. ref [%]
Concorde	79,264	75,793	87,381	15	10
Concorde new	79,264	51,257	55,940	9	-29
Tu-144	99,199	90,427	105,626	17	6
Tu-144 new	99,199	59,236	64,892	10	-35
Boom SST	34,464	47,036	42,747	-9	24
Boom SST mod	34,464	33,335	37,794	13	10
Aerion AS2	26,218	22,105	22,180	0	-15
HELESA	19,577	18,697	18,761	0	-4
Cranfield SSBJ	21,000	19,269	19,040	-1	-9
NLR M1.6	136,000	136,786	139,273	2	2
SC-13	62,489	60,704	64,182	6	3

When comparing the empty mass and takeoff mass it can be seen that the differences between them decreased. When the outliers of new Concorde, new Tu-144 and unmodified Boom SST are not counted, the average takeoff mass was 5% higher and the average operational empty mass was 6% lower than the real value [5]. Now, the average takeoff mass is 6% higher and the average operational empty mass is 7% higher than the real value. Although the values are higher, it can be seen that the deviations between MTOW and OEW are very similar. Probably, the difference to the reference data can be solved by adjusting the calibration of the Class II weight estimation.

In conclusion it can be said that on average the aircraft's calculated masses deviate with less than 10% from their real masses, which is acceptable for this stage of the design.

## 7.2. Design space exploration

To further check the validity of the model a parameter variation analysis was performed. This was done to get more insight in the behaviour of the program and the importance of certain input variables and to find out whether the program outputs are logical.

There are different ways to perform sensitivity analyses. The most simple analysis is to change one input variable and check the change in output. A limitation of this method however is that interactions between variables can not be detected. However, this method can be executed multiple times with different variations, so that a matrix can be generated for multiple parameter variations.

For this analysis the influence of the most important input parameters on the takeoff mass will be

<sup>1</sup>On April 15th 2020, Aerion published an updated design featuring a highly swept delta wing instead of a laminar flow low-sweep wing. This new design is not taken into account for this thesis.

investigated. The selection process for these parameters is described below in section 7.2.1, following which the variation of these parameters is shown in section 7.2.2.

### 7.2.1. Parameter selection

Not every parameter has the same influence on the resulting MTOW. Therefore, only a few parameters will be investigated in detail here. Most of the other parameters have only little influence on the model or were only relevant during verification. The program inputs are divided into two sections: primary and secondary inputs. The primary inputs define the flight conditions and constraints like runway length. This input list also contains estimations for the initial run of the iterator where not all data have been calculated yet.

The primary inputs and constraints are likely to have a large impact on the program results. These are the number of passengers, mission range, supersonic Mach number, number of engines, wing aspect ratio, takeoff and landing distance and stall speed.

The initial run estimations have no influence on the final result of the program. Depending on how far the estimations deviate from the final result, the number of required iterations changes. A good estimation gives a result in 2 or 3 iterations, while a bad estimation requires 20 or more runs, or may not give a result at all. Checks are built in that terminate the program when the calculated MTOW becomes too large. This is the main way to find out that the initial estimations are incorrect for the aircraft that is to be modelled. Apart from that, these estimations should be defined by trial-and-error.

The secondary inputs are divided in technical options for the program and specific options for the various methods. For example, the Class I weight estimation method contains parameters like loiter time and speed. The aerodynamics inputs contain many parameters defining the flap placement and airfoil shapes. Examples of geometry inputs are front and rear spar locations and sweep angles of wings and stabilisers. Also the engine parameters are listed here. In total there are close to 150 parameters, all of which are listed in Appendix D.

To determine which parameters need to be evaluated, a parameter variation was performed for every input parameter. The effect of changing any input both up and down by 20% on the takeoff mass was evaluated. A change of 20% was chosen in favour of smaller percentages since any takeoff mass variations are more pronounced with a larger input change. Larger variations were deemed unnecessary since they resulted in unrealistic input values like Mach number, wing aspect ratio and stall speed.

Any parameter change that resulted in a more than 10% increase or decrease of the takeoff mass was considered worth a more detailed look and is described below in section 7.2.2. The results of the parameter variations are listed in Appendix D.

### 7.2.2. Parameter variations

As mentioned before, this sensitivity analysis only looks at trend data from a number of parameter variations. Some parameters are tested in combination with others to check their interference. The inputs that are varied for the sensitivity analysis are listed below. The reasoning behind the choice for these parameters is detailed in Appendix D. The nosecone and tailcone slenderness ratios are added to verify assumptions from the geometry module, as explained in Chapter 5.

- Number of passengers
- Design mission range
- Supersonic cruise Mach number
- Number of engines
- Stall speed
- Nosecone slenderness ratio
- Tailcone slenderness ratio
- Wing aspect ratio
- Wing leading edge sweep angle
- Combustion chamber efficiency
- Supersonic sfc scaling factor

### Number of passengers

It is interesting for an aircraft design to know whether it can be scaled with passenger number. Increasing passengers will result in a longer fuselage and therefore a higher takeoff mass. To evaluate this, the influence of the number of passengers on the design takeoff mass was tested by adapting from a baseline 100-seat model. The results are shown in Figure 7.1.

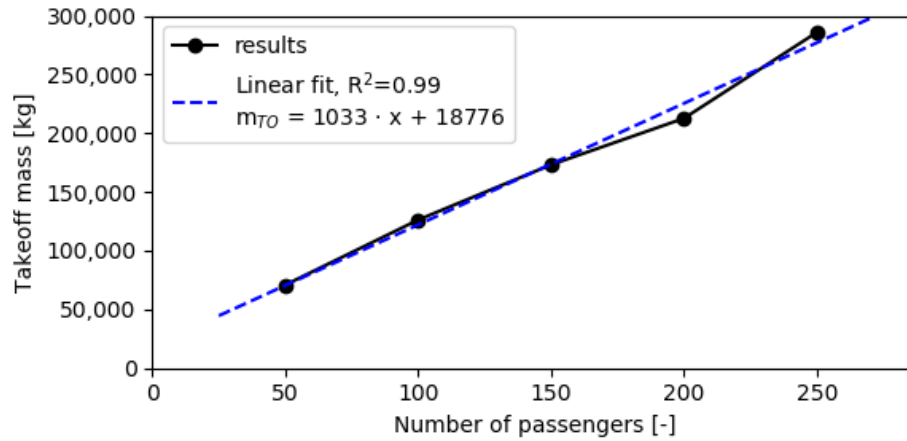


Figure 7.1: Takeoff mass variation with number of passengers

As can be seen in the graph the relation is increasing almost linearly. The linear trendline fit shows that for every passenger more than 1,000 kg will be added to the takeoff mass. Table 7.3 additionally shows that increasing the number of passengers has an effect on the contributions of OEW and fuel mass to the takeoff mass. The contribution of the OEW grows while the fuel mass contribution decreases. This is likely due to the need for extra fuselage length and structural weight. While this additional weight will require more fuel, the mission itself does not change. Therefore, the relative fuel mass contribution decreases.

Table 7.3: OEW and fuel mass data for passenger variation

Passengers	50	100	150	200	250
$W_{OE}$ [kg]	30,032	53,718	73,753	90,843	124,433
$W_{OE}/W_{TO}$ [-]	0.42	0.43	0.43	0.43	0.44
$W_{f_{max}}$ [kg]	38,954	68,045	91,855	110,836	148,519
$W_f/W_{TO}$ [-]	0.55	0.54	0.53	0.52	0.52

### Design mission range

The mission range also has a large contribution on the takeoff mass. The range is used in the Breguet range equations in the Class I weight estimation. In that equation, a longer range will result in a larger fuel fraction and thus in a higher takeoff mass. Figure 7.2 shows the relation between range and takeoff mass for multiple passenger numbers.

The graph shows that the takeoff mass increases almost linearly with an increase in mission range. A higher number of passengers comes with a steeper slope. This means that the takeoff weight of a larger aircraft increases faster than that of a smaller aircraft when the mission range grows. Table 7.4 shows the results of a linear trend line fit for each data set. This data shows that there is indeed a linear relation between mission range and takeoff mass. This data also seems to suggest that doubling the number of passengers results in approximately doubling the mass increase per added distance to the mission range as indicated by the curve's slope.

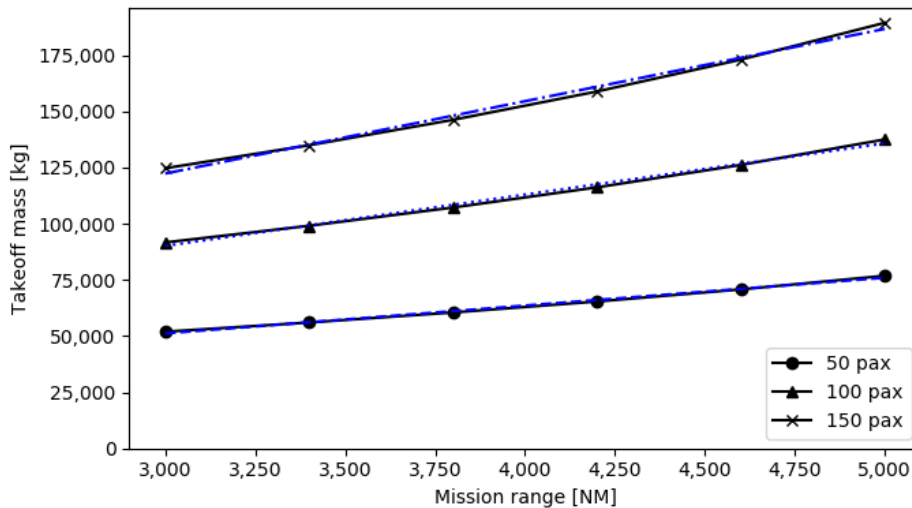


Figure 7.2: Takeoff mass variation with design mission range

Table 7.4: Linear fit for relation between mission range and takeoff mass

Number of passengers	Linear relation	R <sup>2</sup>
50	$W_{TO} = 12 \cdot R + 14,012$	0.99
100	$W_{TO} = 23 \cdot R + 21,726$	0.99
150	$W_{TO} = 32 \cdot R + 25,784$	0.99

Table 7.5 shows the contribution of empty mass and fuel mass to the takeoff mass. It can be seen that the trend for increasing range is a decreasing empty weight contribution and an increasing fuel mass contribution. This is in line with expectations, because increasing the mission range does not change anything to the aircraft itself, but it does change the fuel requirements.

Table 7.5: OEW and fuel mass data for range variation of 100 seat aircraft

Range [NM]	4,000	4,200	4,400	4,600	4,800	5,000
$W_{OE}$ [kg]	49,676	50,948	52,284	53,718	55,308	56,940
$W_{OE}/W_{TO}$ [-]	0.45	0.44	0.43	0.43	0.42	0.41
$W_{f,max}$ [kg]	56,552	60,186	64,006	68,045	72,365	76,908
$W_f/W_{TO}$ [-]	0.51	0.52	0.53	0.54	0.55	0.56

The fuel mass fractions for various passenger numbers and ranges are shown in Figure 7.3. Here it can be seen that larger aircraft have a lower fuel mass fraction. This likely is the result of an increasing lift-drag ratio for larger aircraft caused by a more slender fuselage and a larger subsonic fraction of the wing leading edge. This effect is already described by Den Boer [5]. Additionally, the growth rate of the fuel mass fraction decreases with increasing mission range. This may seem strange since fuel mass fraction is expected to grow nearly exponentially with increasing range, similarly to the takeoff mass. The fuel mass itself does increase with mission range and is the largest driver of the takeoff mass increase, but the relative growth of the fuel mass compared to the takeoff mass actually decreases. This becomes visible in Table 7.6 where the relative fuel mass difference is the largest of the three parameters, but is decreasing for larger design ranges.

### Supersonic cruise Mach number

What speed is the optimal cruise speed for supersonic aircraft is still a subject of discussion. Concorde flew at speeds around Mach 2 and while data in Appendix C suggests a decreasing trend towards Mach 1.6, current SST design projects still aim at speeds varying from Mach 1.4 to Mach 2.2. A test was

Table 7.6: Relative variation with mission range of takeoff, operational empty and maximum fuel mass

Design mission range [NM]	3,000	3,400	3,800	4,200	4,600	5,000
$W_{TO}$	51,933	56,040	60,498	65,375	70,766	76,813
Difference to 400 NM shorter range [%]		7.9	8.0	8.1	8.2	8.5
$W_{OE}$	25,239	26,275	27,401	28,638	30,024	31,602
Difference to 400 NM shorter range [%]		4.1	4.3	4.5	4.8	5.3
$W_{f_{max}}$	23,624	26,969	30,598	34,562	38,924	43,790
Difference to 400 NM shorter range [%]		14.2	13.5	13.0	12.6	12.5

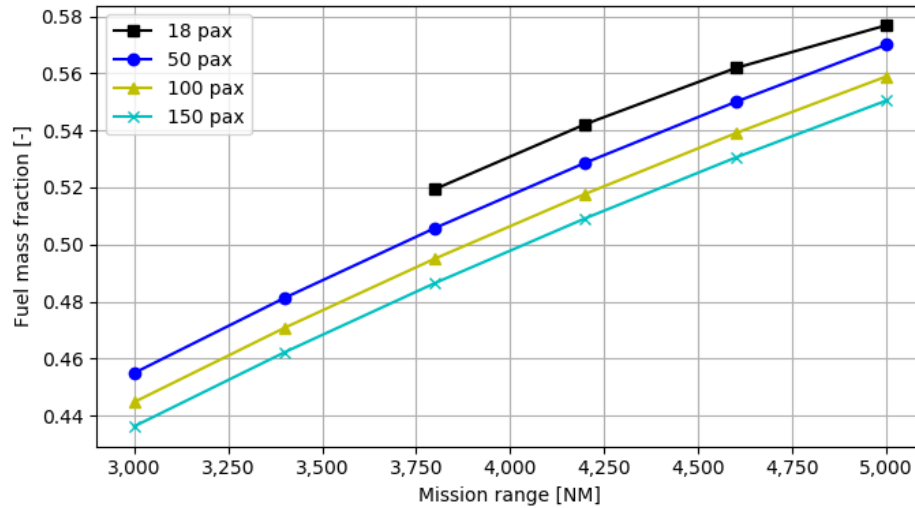


Figure 7.3: Fuel mass fraction variation with mission range

performed for these Mach numbers for various passenger numbers to see their effect on the aircraft design. The resulting takeoff mass is shown in Figure 7.4.

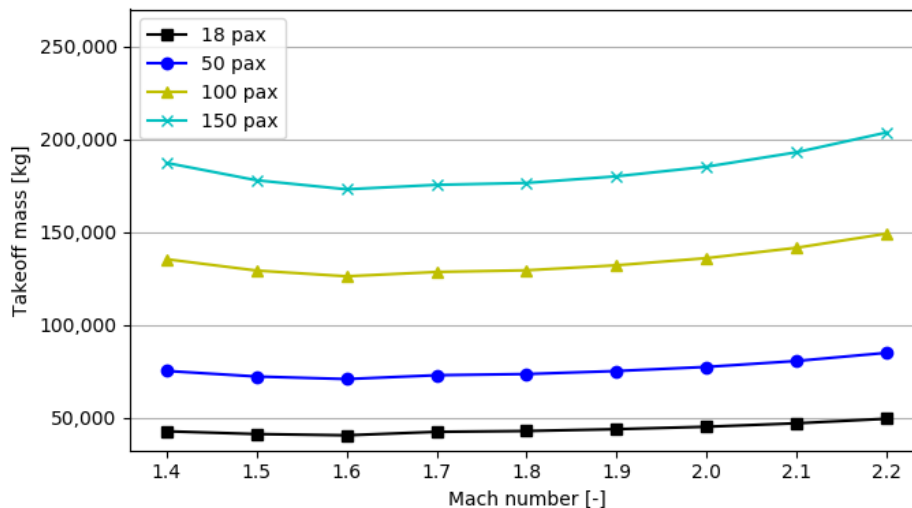


Figure 7.4: Takeoff mass variation with cruise Mach number

As can be seen in the graph that the mass decreases between Mach numbers of 1.4 and 1.6. For higher Mach numbers the mass starts growing again, with an increasing speed for Mach numbers above 1.8. These effects are more visible for higher passenger numbers.

The main reason for the decreasing mass between Mach 1.4 and 1.6 is the decrease in mission fuel. Since the range is kept equal but the speed increases, the acceleration and deceleration segments will require more flight distance. Therefore, the total distance flown supersonically decreases. This reduces the required fuel mass and therefore the weight of all other components. This was shown by Den Boer [5].

However, due to the higher Mach number the wave drag increases. This results in a lower lift-to-drag ratio, requiring more thrust, more fuel and a larger takeoff mass. This counteracts the weight decrease from the lower fuel usage. The reason why this happens at Mach 1.7 is the introduction of a variable-geometry inlet for the engines for speeds at or above Mach 1.7. This adds between 50 and 200 kg to the engine weight, depending on the size of the engine. Along with this the snowball effect of increasing weight, lift, drag and thrust is started, which is more pronounced at larger passenger numbers.

Figure 7.5 shows the relative change in Mach number with  $M=1.6$  as reference. It is worth noting that changing the Mach number below  $M=1.6$  has the lowest impact on the aircraft with 18 passengers while doing that above  $M=1.6$  has the lowest impact on the larger aircraft. A reason for this is that the addition of the variable geometry inlet has a larger influence on smaller propulsion systems than on larger variants. For instance, for the 18 seat aircraft the propulsion weight increases with 15% from Mach 1.6 to 1.7, while the 150 seat aircraft has a propulsion weight increase of 8%. Therefore, the relative weight increase is much higher for smaller aircraft. The difference in takeoff mass decrease between Mach 1.4 and 1.6 is almost 50% larger for the 150 seat aircraft than for the 18 seat aircraft. The reason for this is the larger contribution of the empty mass to the takeoff mass for the larger aircraft.

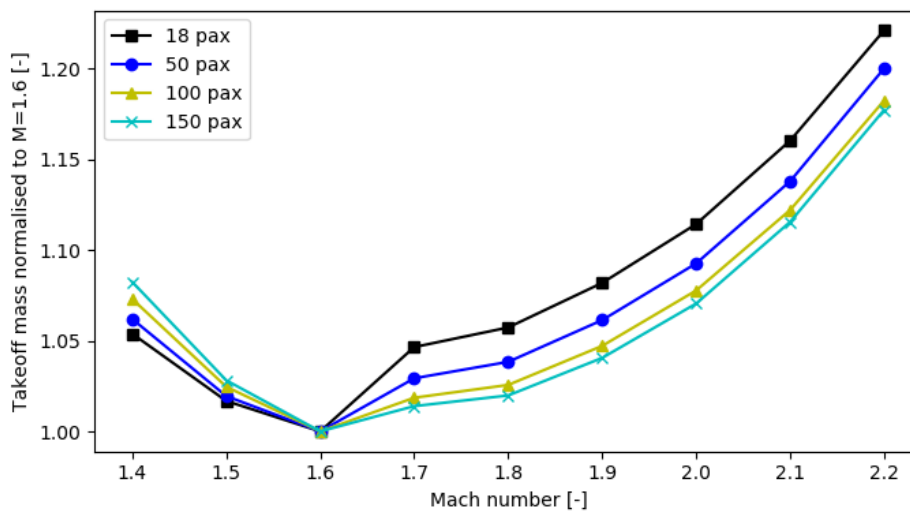


Figure 7.5: Normalised takeoff mass variation with cruise Mach number

### Number of engines

The choice for the number of engines is only relevant for a small fraction of the aircraft design. Since having three engines was not considered for this design, the only choice is between two and four engines. To show the effect of this choice on the takeoff weight, a number of experiments were performed showing the effect of the number of engines on multiple variables. The number of passengers is plotted against the takeoff weight for both engine options in Figure 7.6.

The graph shows a linear relationship between the number of passengers and the takeoff mass, as indicated before. The configuration with two engines always results in a higher takeoff mass than a four-engine variant, although the difference is small for low passenger numbers. The reason for this is that a two-engine aircraft requires larger engines to produce the same thrust as a four-engine aircraft. While larger engines do have a better thrust-to weight ratio and comparable sfc, they have a higher dry mass. This results in better engine performance and lower weight for the 4-engined aircraft due to the smaller overall engine mass. The relative difference between the engine numbers is shown in Table 7.7. Note that the 20 passenger aircraft already has a total thrust of almost 200 kN, which is comparable to that of a Boeing 737.

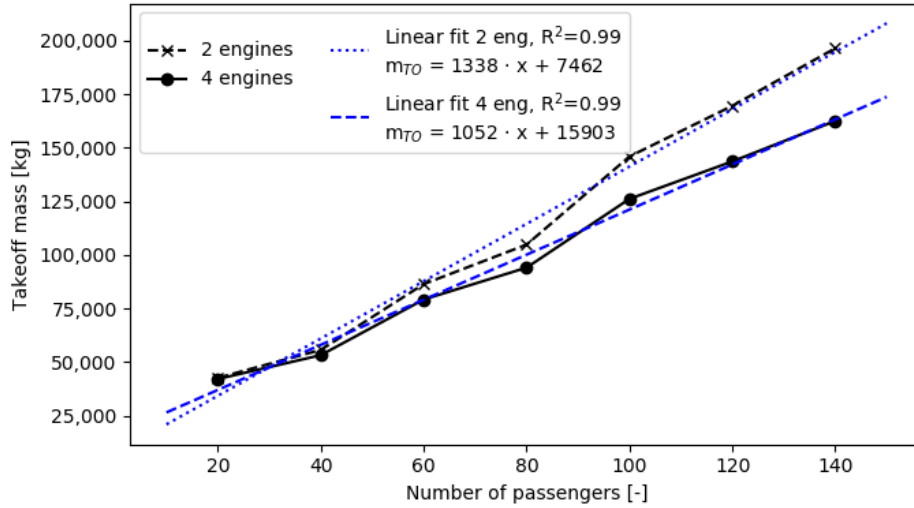


Figure 7.6: Takeoff mass variation with passenger number for 2 and 4 engines

Table 7.7: Engine data compared for 2-engine and 4-engine option

npax	2 engines			4 engines		
	thrust [kN]	sfc [kg/N s]	engine mass [-]	thrust [kN]	sfc [kg/N s]	engine mass [-]
20	192	0.95	3,815	131	0.98	3,523
40	256	0.95	4,851	166	0.98	4,088
60	397	0.95	7,129	247	0.98	5,401
80	485	0.94	8,563	293	0.98	6,153
100	671	0.94	11,575	393	0.98	7,772
120	783	0.94	13,393	448	0.97	8,657
140	903	0.94	15,329	507	0.97	9,613

A similar graph can be made for the mission range of a 100-seat aircraft (Figure 7.7). This shows the same trend as Figure 7.6 that for larger required thrust the difference between 2 and 4 engines increases.

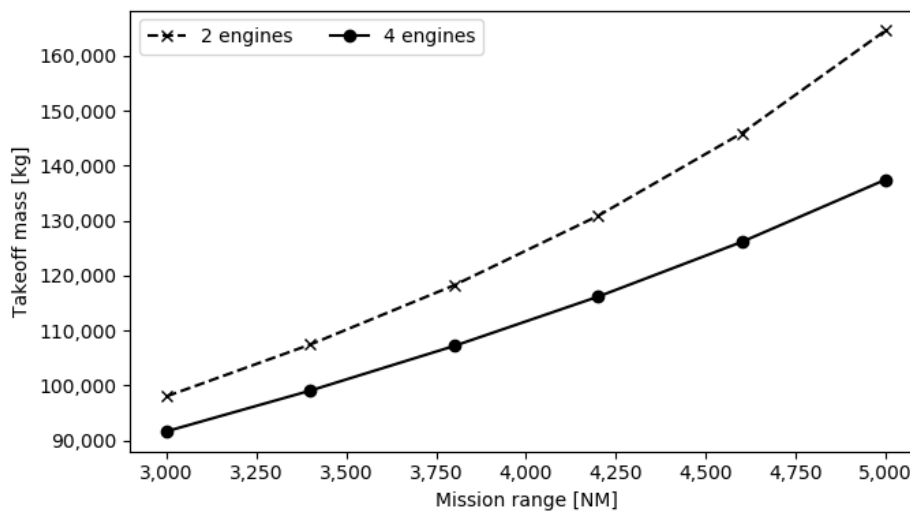


Figure 7.7: Takeoff mass variation with mission range for a 100-seat aircraft with 2 or 4 engines

**Stall speed**

The clean stall speed at sea level was found to have a large impact on the design as well. As explained in Chapter 3, this speed is used in calculating the maximum allowed wing loading for the design point. It turns out that this usually is the limiting constraint and therefore it influences the takeoff mass, as can be seen in Figure 7.8.

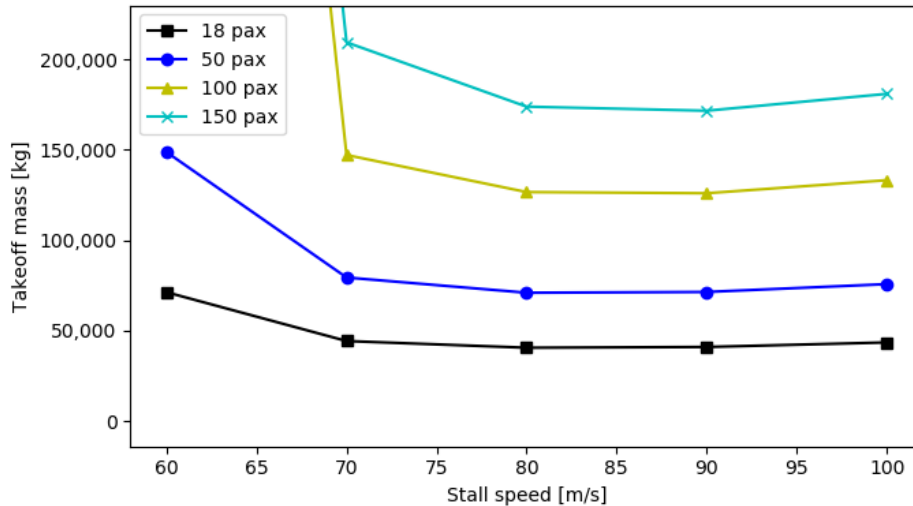


Figure 7.8: Takeoff mass variation with clean stall speed

The figure shows that the takeoff mass initially decreases to a minimum around a stall speed of 80 m/s and then starts increasing again. The reason for the mass decrease is the increasing wing loading which is directly influenced by the stall speed. The higher wing loading results in a smaller wing area resulting in a lower takeoff mass. However, a higher wing loading in this configuration also results in a higher thrust loading for wing loadings above 4,000 N/m<sup>2</sup>. From that moment the takeoff distance also is a limiting constraint where the thrust loading increases almost linearly with the wing loading. This starts happening around a stall speed of 80 m/s. Around 90 m/s this effect starts to become visible in the graph, after which the wing weight decrease is smaller than the propulsion and fuel weight increase, resulting in a higher takeoff mass.

**Nosecone and tailcone slenderness ratio**

As pointed out in Chapter 5, it is interesting to find out the influence of the slenderness ratios of the nosecone and tailcone on the design. Therefore, the nosecone and tailcone slenderness were varied between 3 and 8 to find out their influence on the takeoff mass. Figure 7.9 shows the influence of the nosecone and Figure 7.10 shows the influence of the tailcone.

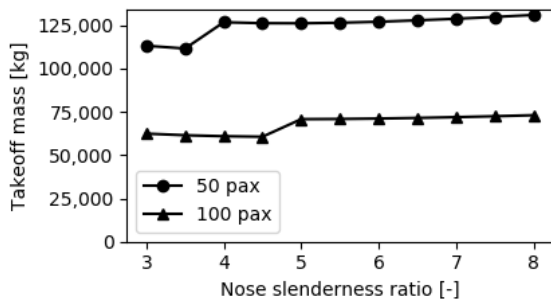


Figure 7.9: Takeoff mass variation with nosecone slenderness

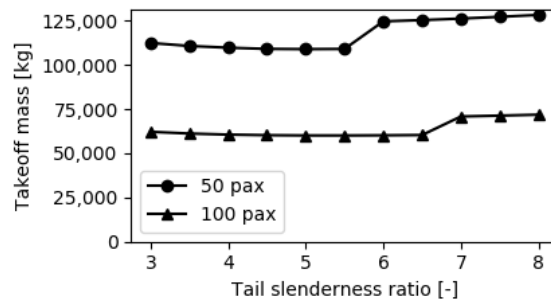


Figure 7.10: Takeoff mass variation with tailcone slenderness

What stands out in both graphs is the jump disturbing an otherwise convex curve. This jump is caused

by the fuselage exceeding the total slenderness constraints. As explained in Chapter 5 the fuselage slenderness should be between 15 and 25. The jump in the 50 passengers graph is when the seat arrangement increases from two to three seats abreast. For the 100 passenger aircraft this happens when the configuration jumps from three to four seats abreast. The increase in takeoff mass is around 15%.

If the total fuselage slenderness is not limited to 25, the effect of only changing the nosecone or tailcone slenderness is more visible. This is shown in Figure 7.11. It can be seen that the curve is somewhat parabolic. This indicates that there is an effect of the nosecone slenderness ratio, but this is caused by multiple factors. The lift-to-drag ratio always increases for increasing nose slenderness, but as the empty weight grows, this benefit is offset by the additional weight. The optimal point here is around 5.5.

The effect from changing the total slenderness is negligible as well, as shown by the case with the tailcone slenderness ratio of 5, where the difference in takeoff mass is less than 1% of the original values.

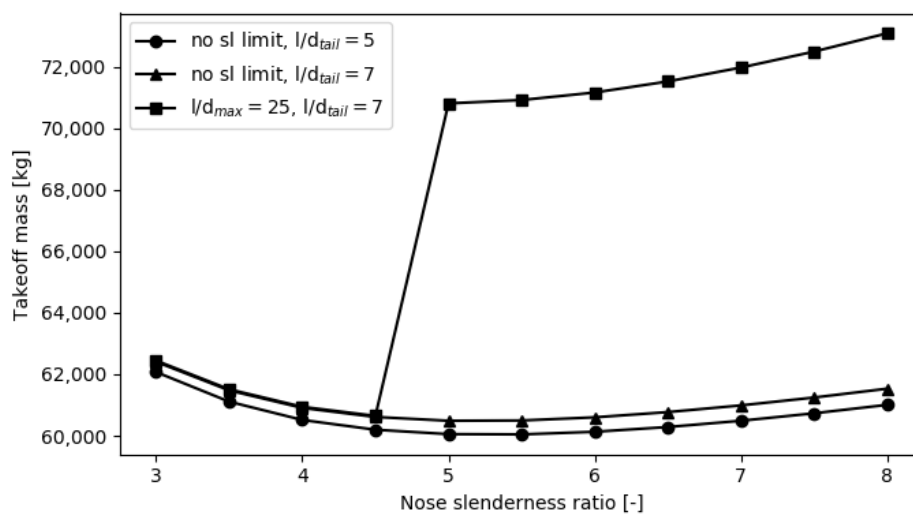


Figure 7.11: Takeoff mass variation with various nosecone and tailcone slenderness ratios for a 50-seat aircraft

### Wing aspect ratio

Certain wing parameters also have an important influence on the takeoff mass. One of these is the wing aspect ratio. Because the aspect ratio is included in the basic drag equation  $C_D = C_{D_0} + \frac{C_L^2}{\pi e AR}$ , the drag reduces with increasing aspect ratio. Figure 7.12 shows the takeoff mass variation with aspect ratio for various passenger numbers.

Based on the drag equation there should be an inverse relation between aspect ratio and takeoff weight. Although the graph has some similarities to an inverse relation it is approximately linear for aspect ratios above 1.8. It can be seen that for larger aircraft a change in aspect ratio results in a larger takeoff mass decrease. This is likely a result from larger aircraft having a larger subsonic leading edge fraction, which results in less drag.

The main reason for the decreasing mass is in the design point calculations. Since the takeoff distance, climb performance and cruise speed constraints all depend on the aspect ratio via the lift/drag ratio, they decrease. Since the lift increases with increasing aspect ratio (Chapter 6) the stall speed constraint is increased. This results in a higher wing loading (a smaller and lighter wing) and a lower thrust loading (a smaller and lighter engine).

The 18 seat aircraft can be seen to have a relatively larger takeoff mass for low aspect ratios. This also has to do with the subsonic leading edge fraction, since this changes more for a small wing than for a large wing. The takeoff mass at an aspect ratio of 1.6 is nearly 25% lower than with AR=1.4, compared to an approximately 10% decrease for the 50 and 100-seat aircraft.

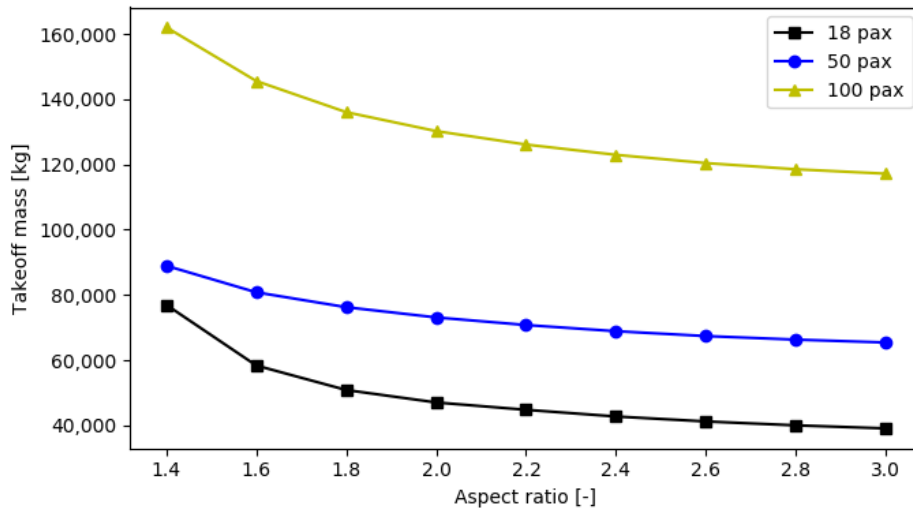


Figure 7.12: Takeoff mass variation with wing aspect ratio

**Wing leading edge sweep angle**

The sweep angle has a large influence on the aerodynamic properties of the wing. As explained in Chapter 5 the wings should be swept at such an angle that most of the wing’s leading edge is in subsonic flow. To examine the influence of changing the sweep angle, it is varied between the minimum and maximum values where the program still gives valid results. This was done for a single Mach number. If the sweep angle is too small, a too large part of the wing becomes supersonic, resulting in more drag and a weight growth of over 100%. On the other hand, if the sweep angle becomes too large, it is impossible to find a possible wing shape since chord lengths may become negative. The usable range of sweep angles with the resulting takeoff masses is presented in Figure 7.13.

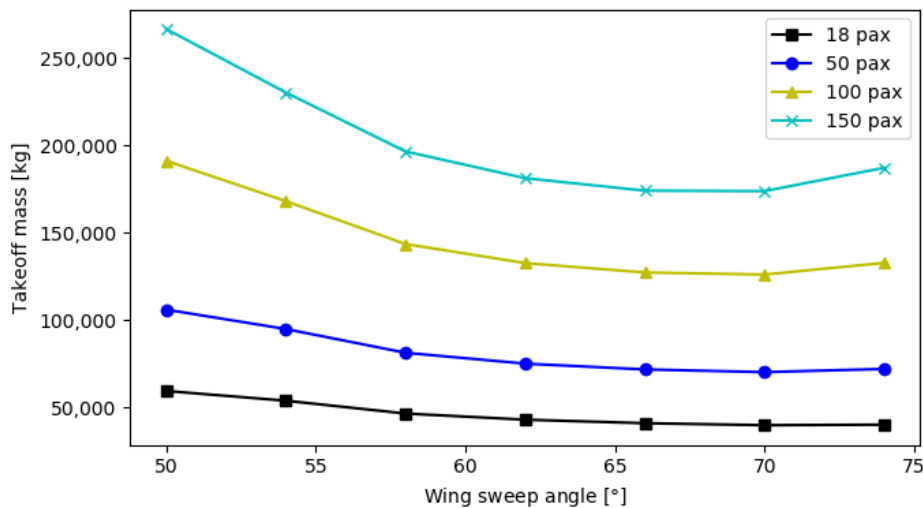


Figure 7.13: Takeoff mass variation with wing leading edge sweep angle at M=1.6

The graph shows a parabolic curve with a minimal mass around a sweep angle of 70 degrees for M=1.6. At 50 degrees sweep the wing was found to have a fully supersonic leading edge. The takeoff mass found here likely is unrealistic since methods for wings with supersonic leading edges are not included in the program. For sweep angles above 58° the leading edge is subsonic.

While the lift decreases for increasing sweep angles, the drag decreased even further, resulting in an increase in lift/drag ratio. This resulted in a smaller wing and lower takeoff weight. However, at a certain point the maximum lift coefficient becomes too small, resulting in a lower maximum wing loading, requiring a larger wing. This increases the takeoff weight starting around  $\Lambda_{LE} = 70^\circ$ .

### Combustion chamber efficiency

The only engine component parameter having a sufficiently important impact on the takeoff mass is the combustion chamber efficiency. With most other parameters in the combustion chamber predefined, the efficiency is the parameter that defines how much fuel is required to reach the turbine inlet temperature. Chapter 4 explains more about this and Appendix B lists the minimum and maximum values for this parameter. Figure 7.14 shows the resulting takeoff masses.

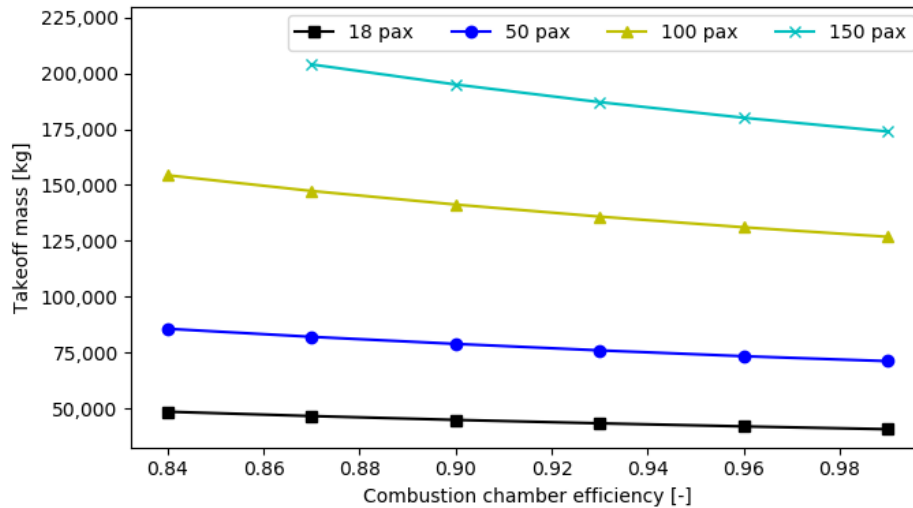


Figure 7.14: Takeoff mass variation with combustion chamber efficiency

The graph shows a linear decreasing trend with increasing efficiency. This is expected since a higher efficiency means less fuel is needed for a sufficient temperature rise. The difference between an efficiency of 0.84 and 0.99 is a 15% decrease in sfc. Besides this, the takeoff mass for a 100-seat aircraft decreases with nearly 2,000 kg for every percent increase in combustion chamber efficiency.

### Supersonic sfc scaling factor

The final parameter that was found to have an important impact on the model's outcome is the sfc scaling factor. The reason for using this factor and its value is described in Chapter 4. While the numbers itself may be accurate, it is interesting to see the influence of the supersonic sfc on the model, since it only relates supersonic engine performance to takeoff mass. The scaling factor was varied between 1.0 (exactly the subsonic performance) and 1.3, as shown in Figure 7.15.

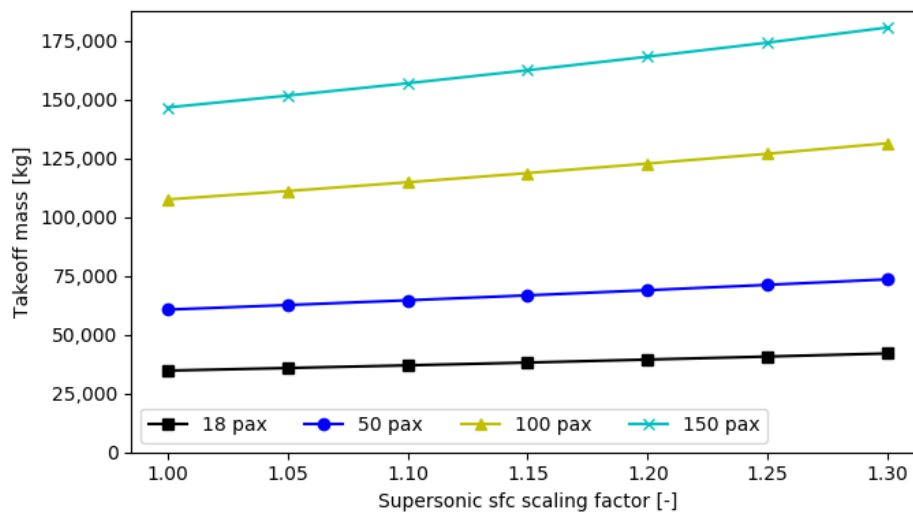


Figure 7.15: Takeoff mass variation with supersonic sfc scaling factor

The figure shows that the takeoff mass increases when the scaling factor increases. This is expected, since a higher sfc requires more fuel which results in a larger empty mass and a larger takeoff mass.

The relative changes in takeoff mass are independent of the number of passengers: a 30% increase in supersonic sfc results in a 20% increase in takeoff mass.

### 7.3. Aircraft designs

The above sections prove that the program returns valid results for the range of parameters that were evaluated. The requirements for these aircraft were set so that they provide a wide range of passenger numbers. These passenger numbers may not all be realistic for supersonic aircraft that will enter service in the (near) future, since it is estimated that the market for supersonic aircraft will be rather small, even when the FAA ban on supersonic overland flights would be lifted [2].

A selection of top-level design requirements of the selected aircraft is shown in Table 7.8. These are the same as in [5] except for the SSBJ engine bypass ratio, since there was no reason to expect an SSBJ engine to have a smaller bypass ratio than larger supersonic aircraft. The basis for these numbers are the parameter analysis in Chapter 7 and other studies of supersonic aircraft [56, 62]. The noise requirements are not used as design constraints, but will be used in Chapters 8 and 9.

Table 7.8: Selection of aircraft design requirements

Parameter	Unit	SSBJ	SST50	SST100	SST170	SST250
Number of passengers	[-]	18	50	100	170	250
Range	[NM]	4,600	4,600	4,600	5,000	5,000
Cruise Mach number	[-]	1.6	1.6	1.6	1.6	1.6
Takeoff distance	[m]	1,900	2,400	2,800	3,000	3,200
Number of engines	[-]	2	4	4	4	4
Wing aspect ratio	[-]	2.1	2.2	2.2	2.5	2.5
Bypass ratio	[-]	3.0	3.0	3.0	3.0	3.0
Sonic boom strength	[EPNdB]			75-85		
Airport noise	[-]		Stage 5 / Chapter 14 compliant			

Since some calculations in the design program were changed after the publication of [5], the weights and performance of these aircraft is summarised in Table 7.9.

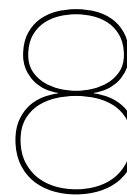
Table 7.9: Selection of aircraft design outputs

Parameter	Unit	SSBJ	SST50	SST100	SST170	SST250
$W_{TO}$	[kg]	43,696	70,690	126,133	203,036	314,434
$W_{OE}$	[kg]	18,953	30,305	53,699	86,033	136,969
$W_{OE} / W_{TO}$	[-]	0.43	0.43	0.43	0.42	0.44
Design fuel efficiency	pax·km/kg	4.48	8.88	11.67	14.23	13.78
W/S	[N/m <sup>2</sup> ]	4,219	4,173	4,173	4,210	4,210
T/W	[-]	0.49	0.34	0.32	0.30	0.30
Thrust per engine	[kN]	104	59.5	98.3	148.1	231

The improved wing design and other improvements made after the publication of the earlier thesis [5] decreased the aircraft weight and increased the fuel efficiency. Combined with the increased engine bypass ratio for the SSBJ its takeoff mass decreased with 16% while the takeoff mass of the other aircraft decreased with 5-10%.

It may be worth noting that some of these aircraft may not be practically usable. The SST100 already has a predicted length of 61 m, comparable to a Boeing 777-200. The SST250 will have a length of 91 m which is longer than any aircraft currently in service. Besides the requirement for long landing gear legs to achieve a sufficient rotation angle during takeoff and landing, airport modifications will likely be required to handle these large aircraft.





# Low-speed noise analysis

This chapter describes the methodology to estimate the noise production of new SSTs. First of all, current noise regulations are described in section 8.1 with a small part reflecting on the relevance for supersonic aircraft. Following this, some noise modelling methods are explained with their applicability to this project in section 8.2. Since the most common methods can not be used, the noise estimation method that will be used will be explained in section 8.3.

## 8.1. Noise regulations

Noise regulations for aircraft are defined by ICAO in Annex 16 Volume I [63]. This chapter defines the noise limits for aircraft in the vicinity of airports. The most current set of regulations is Chapter 14 which applies to subsonic aircraft with a takeoff mass of 55,000 kg and above with a type certification application submitted on or after 31 December 2017. From 31 December 2020 this category will be expanded to include all subsonic aircraft. This volume includes a chapter on supersonic aircraft noise, but does only advise to use the maximum subsonic noise levels as a guideline, since no standards have been developed yet for these aircraft. For this reason the supersonic aircraft will be compared with the subsonic regulations in Chapter 14.

The noise limits in Annex 16 are defined as Effective Perceived Noise Level (EPNL). This is a measure for the perceived noise integrated over the duration of an overflight. The Perceived Noise Level (PNL) is calculated from the measured sound pressure level (SPL) which is corrected for noisiness [63]. This happens because the human perception of loudness depends on the sound frequency. For this the noy scale was created which converts sound pressure level to equal loudness for a 1,000 Hz reference sound [64].

The maximum noise levels for aircraft are defined at three points as listed below and shown in Figure 8.1.

- **Lateral full-power reference point:** the point on a line parallel to the runway at 450 m distance where the noise level is maximum during takeoff
- **Flyover reference point:** the point at 6,500 m from the start of the takeoff roll on the extended runway centreline
- **Approach reference point:** the point at 2,000 m from the runway threshold on the extended runway centreline

At each of these points a maximum noise level is defined as shown in Figure 8.2. For every point a margin of 1 dB should be applied and additionally, when the margins are summed, this number should be larger than or equal to 17. This means that the generated noise summed for all conditions should always be at least 17 dB lower than the summed noise limits. This limit is the one that makes the difference between the regulations of Chapter 3, 4 and 14. The individual noise levels were kept equal, while the cumulative margin changed (Figure 8.3).

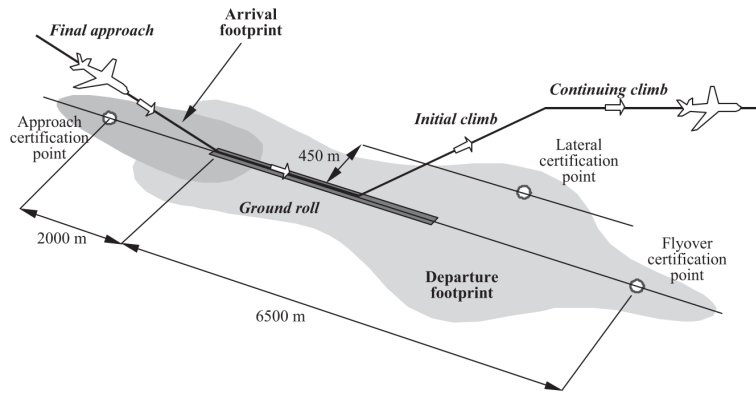


Figure 8.1: Reference noise measurement points [65]

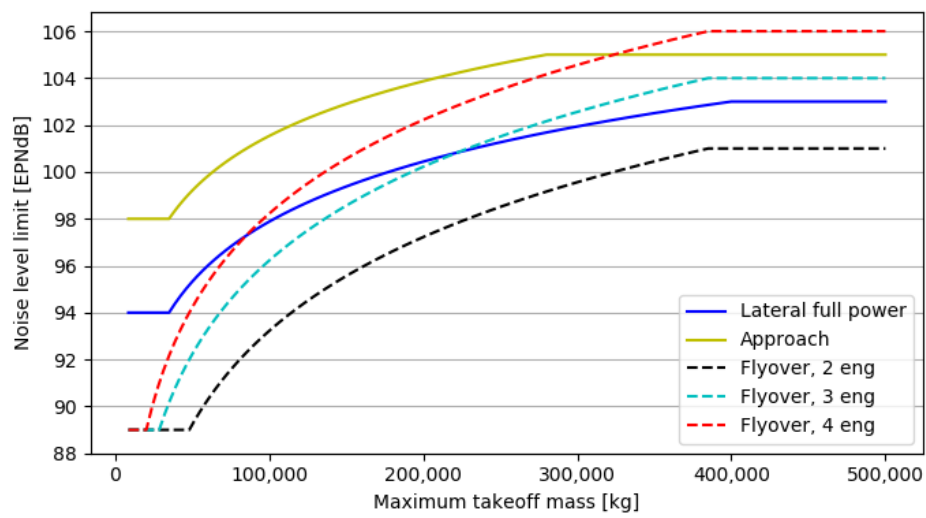


Figure 8.2: Annex 16 chapter 14 limit noise values for the different reference points

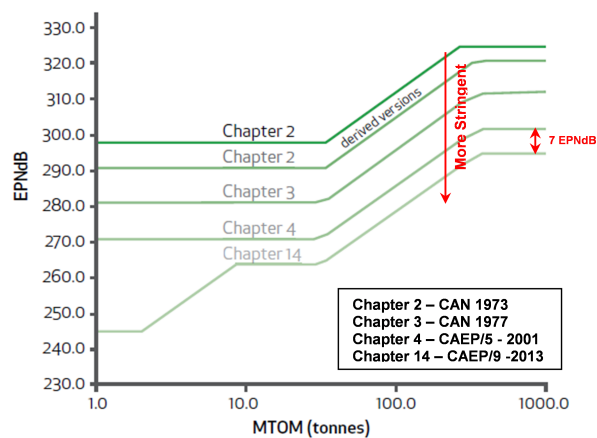


Figure 8.3: Cumulative noise limits for the various Annex 16 chapters<sup>1</sup>

<sup>1</sup><https://www.icao.int/environmental-protection/Pages/Reduction-of-Noise-at-Source.aspx>. Accessed 29 July 2020

## 8.2. Noise modelling

To be able to model the noise generation of an arbitrary supersonic aircraft, it is essential to know what noise sources need to be modelled and what is the state of available knowledge to make those models. Farrasat [66] makes a distinction between four model categories: fully analytical methods, Computational Fluid Dynamics (CFD) combined with acoustic analogy, fully numerical methods and semi-empirical methods. Each of these categories has its own benefits and shortcomings and can be applied to different design stages.

### 8.2.1. Fully analytical methods

This group of methods consists of an analytical approach for both the fluid dynamics and acoustics. Usually the source is modeled as a combination of monopoles, dipoles or quadrupoles and planes. This allows for an insight in the dependence of noise intensity on input parameters and the directivity of the noise pattern [66, 67]. Additionally, they can form the basis on which semi-empirical methods are developed.

However, the required simplicity of analytical models can result in a too simple model which is unable to represent real situations. Although they can give useful insights on theoretical noise prediction, some of the examples used by these methods can not be realised in practice [68].

### 8.2.2. CFD combined with acoustic analogy

A method that combines the strength of analytical methods while being able to model more complex sources is combining aerodynamic flow calculations with analytical methods for the acoustic propagation. Based on the aerodynamic analysis sound sources are located. These sources can then be used to calculate the acoustic propagation.

The theoretical basis of this method is the fact that the Navier-Stokes equations can be rewritten to a form of a linear wave equation with a source term similar to a quadrupole [69, 70].

### 8.2.3. Fully numerical methods

The fully numerical methods depend on single simulations using CFD. To accurately simulate the flow both the sound source and receiver should be included in the computational domain. However, to model a turbulent flow the number of mesh points should be proportional to the Reynolds number for the turbulent eddies raised to the  $\frac{9}{4}$ th power. Since the Reynolds number for jet exhausts is around  $10^5$  to  $10^7$ , this would mean that approximately  $10^{12}$  to  $10^{15}$  mesh points would be required [71]. This is more than current computers would be able to calculate in a reasonable amount of time.

### 8.2.4. Semi-empirical methods

The final category is that of the semi-empirical methods. Mainly driven by the need for reliable noise prediction for aircraft designs semi-empirical codes have been developed. Because of the large amount of acoustic data that has been collected this data can be linked to aircraft configurations and characteristics. With this method high lift noise and other broadband noise can be estimated with reasonable accuracy. Although this accuracy is less than the other methods, the broad applicability of this method allows it to be used on early design stages when no detailed geometry is known yet.

### 8.2.5. Method applicability

Each of the methods listed above are only useful for a select type of calculations. For instance, applying a numerical method to a conceptual design will not result in reliable data since the conceptual design will not have an accurate geometry description to fit a mesh around the aircraft for generating CFD data. A similar reasoning is true for fully analytical methods, which can not be used to model an entire aircraft because these methods depend too much on simplifications.

Figure 8.4 shows what methods can be used for what applications. The division is roughly similar to the one described above. Categories 1 and 2 are the fully numerical and acoustic analogy methods, mainly focused on component noise modelling and simulation. Category 3 comprises the analytical methods, but adapted to the fact that known models usually combine analytic methods with CFD or empirical data [72]. The semi-empirical methods are divided into two categories. The 4a category contains methods that only use empirical data, while in 4b methods use empirical data in case analytical or

numerical solutions are not available.

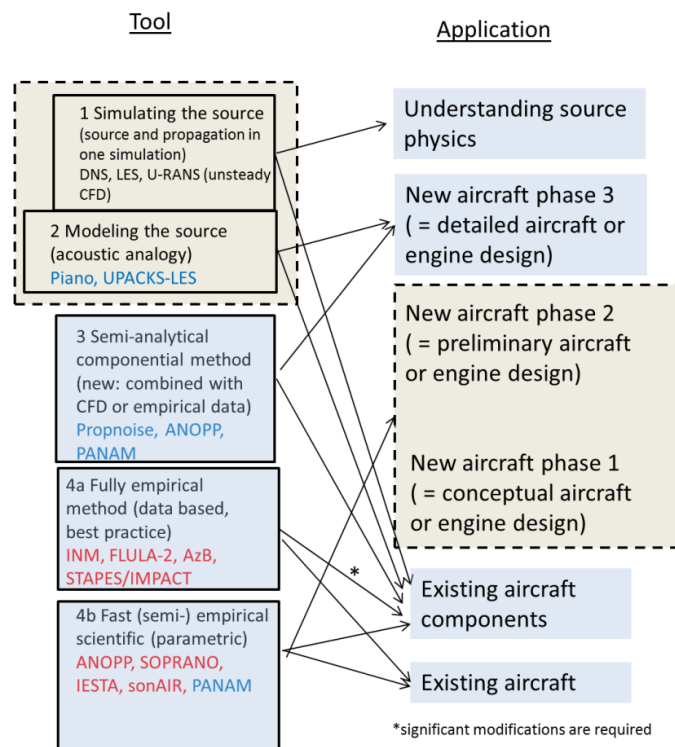


Figure 8.4: Existing noise estimation methodologies and tools with their applications. Adapted from [72]

As can be seen in the figure, the suggested tools to evaluate conceptual or preliminary designs are the semi-empirical methods in category 4b. This category covers the methods ANOPP, SOPRANO, IESTA, sonAIR and PANAM.

Aircraft NOise Prediction Program (ANOPP) is developed by NASA in the 70s to become an integrated noise prediction program, combining source noise models with exposure contour estimation [73]. This was later expanded into ANOPP2 which introduced physics-based methods to also allow the program to predict noise for non-conventional aircraft and aircraft components [74].

SOPRANO is a noise prediction tool created by the Spanish engineering firm ANOTEC. Further information could not be found publicly about this tool.

IESTA is a tool created by the French aerospace laboratory ONERA for estimating the environmental impact of air traffic around airports [75]. Its noise component consists of three modules: noise source, installation effects and noise propagation, all depending on the state of the aircraft [76].

SonAIR is developed by the Swiss Federal Laboratories for Materials Science and Technology (Empa) due to not many noise prediction tools being publicly available or suitable for a wide range of aircraft types. Therefore a tool was developed that combines sound emission models, sound source data and sound propagation into a single model [77].

PANAM was developed by the German Aerospace Laboratory (DLR) to integrate noise prediction in the conceptual aircraft design process [78]. The program uses source models developed by DLR based on modern aircraft [79].

Unfortunately, none of these tools are available for the general public. Therefore, they can not be used for this thesis. Although many of the underlying equations used are shown in reports for PANAM [78] and ANOPP [80], the full and current methods are not accessible, or require too many input variables that are unknown at this stage of the design. Therefore, a combination of various methods and data is used to give an accurate description of the noise generation of future supersonic aircraft in the vicinity of airports.

### 8.3. Low-speed noise estimation method

As a starting point for the low-speed noise estimation of supersonic aircraft, Concorde can be used. Although this aircraft was exceptionally loud, it is a good example of the additional noise associated with supersonic aircraft compared to subsonic aircraft. Figure 8.5 shows the development of noise levels for entry into service aircraft between 1955 and 1990 with Concorde included. As can be seen average noise levels of subsonic aircraft decreased by more than 20 EPNdB in this time, but Concorde produced more noise than the loudest jet aircraft. These differences can only be explained by the large difference in design requirements between supersonic and subsonic aircraft. Therefore, section 8.3.1 will explain the main noise sources of an aircraft and section 8.3.2 will show the differences between subsonic and supersonic aircraft and their effect on the generated noise. Although there are ways to reduce the noise, chances are low that these measures are sufficient or will be available in a short timeframe, as section 8.3.3 explains.

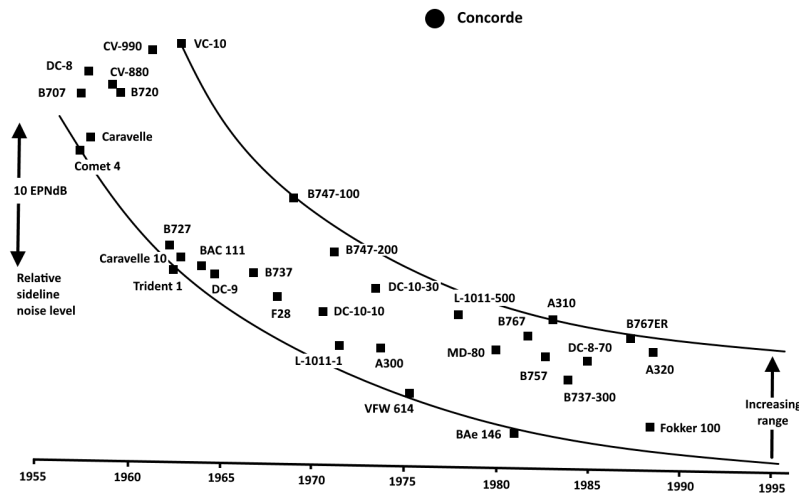


Figure 8.5: Jet aircraft noise levels at entry into service until 1990. Redrawn from [81]

#### 8.3.1. Aircraft noise sources

Aircraft have only a few distinctive noise sources. These sources can be divided into airframe noise and engine noise. The most important mechanism of airframe noise is turbulence [70]. Therefore the components that contribute the most to the airframe noise are the wings and tailplanes, high-lift devices and landing gear (Figure 8.6). The extent to which these components contribute to the airframe noise varies with speed, aircraft size and shape. Speed is an important factor since it was found that airframe noise at ground level increases with the fifth power of flight speed [82]. Aircraft shape influences the noise since components that generate more turbulence also generate more noise. Larger aircraft also generate more noise and therefore also produce more noise.

The landing gear is the most important airframe noise source of large aircraft. Smaller aircraft do not have a dominant airframe noise contributor, since the high-lift devices and the landing gear both generate similar noise levels [83]. However, this effect is more prominent during approach because the high-lift devices are extended further during this flight phase.

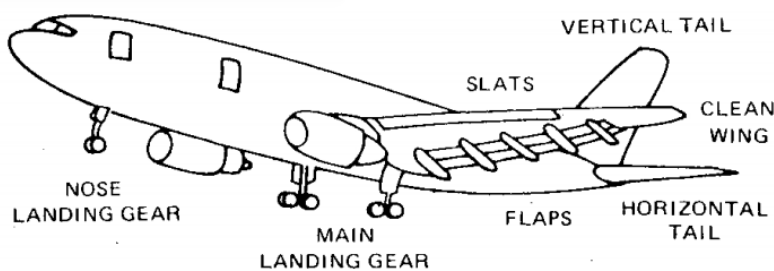


Figure 8.6: Noise generating airframe components [84]

All engine components that have air flowing through them contribute to the engine noise, although in various degrees. The highest contributions for high-bypass engines are from the fan and jet exhaust. For low-bypass engines the jet exhaust is the primary noise source. As shown in Figure 8.7 the takeoff fan noise and jet noise of a typical 2000-2010 widebody are nearly equal, while the approach fan noise is almost 15 dB higher than the jet noise. This can be explained by the larger engine thrust during takeoff. A larger thrust results in a higher jet velocity. With less thrust during approach the compressor emits more noise, which may seem counterintuitive. However, this can be explained by the lower flow velocity through and in front of the engine. Therefore, the sound pressure waves from the compressor can now propagate forward, resulting in a larger compressor noise contribution.

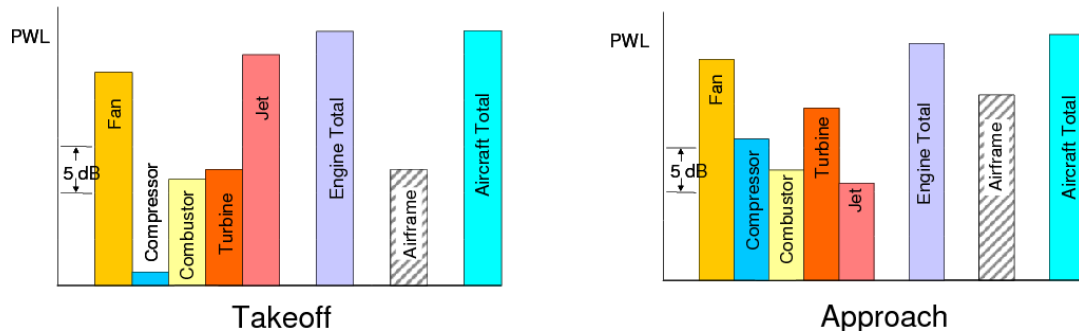


Figure 8.7: Relative power levels of aircraft noise sources at takeoff and approach for a typical 2000-2010 widebody aircraft with high BPR engines [85]

Figure 8.7 also shows that the airframe noise during approach is a larger fraction of the total aircraft noise than during takeoff. This is the result of the extended high-lift devices and landing gear which generate more noise than the clean wing itself.

### 8.3.2. Supersonic aircraft noise

In order to say something about the noise generated by supersonic aircraft during approach and takeoff, the differences between supersonic and subsonic aircraft need to be identified.

The most visible physical difference between subsonic and supersonic aircraft is the different wing shape. However, the wing shape itself has not much influence on the total noise generated. The most important factor for wing noise is turbulence. Therefore, the most influential parameters are velocity, wing span and boundary-layer thickness [84]. The sound pressure depends on the fifth power of velocity while it has a linear relation with the other parameters. This means that it is by far the most contributing parameter to the sound pressure. For this reason it is expected that the wing shape itself does not influence the generated noise. This seems to be confirmed by ANOPP models where the wing noise has the lowest contribution of all airframe noise sources [86].

A decision that will have more influence on the noise generation is not having leading edge high-lift devices. The additional turbulence and increased boundary layer thickness generated by the slats will not be present and therefore reduce the noise. This would mainly make a difference for aircraft with advanced high-lift systems since slat noise for these systems is dominant for frequencies between 3,000 and 3,500 Hz [86, 87]. This is also visible in Figure 8.8 where the slat noise is the second largest contributor to the airframe noise.

The removal of slats will likely reduce the total aircraft noise production by only 1 or 2 dB. As can be seen in Figure 8.8 the slat noise of the long range aircraft contributes less to the airframe noise than that of the short range aircraft. Removing slats from the short range example aircraft would result in an airframe noise reduction of 2-3 dB, while the total noise reduction would account for approximately 1 dB. For the long-range aircraft with higher landing gear noise the airframe noise reduction will be around 1 dB so the total noise reduction for removing slats will be less than 1 dB. Due to the expected high landing gear noise (explained below) it is believed that removing slats will reduce the total aircraft noise by 1 dB at most. The reasons for not using slats can be found in [5].

The most important change compared to subsonic aircraft is the longer landing gear legs. Supersonic aircraft are longer than subsonic aircraft for the same number of passengers due to their required

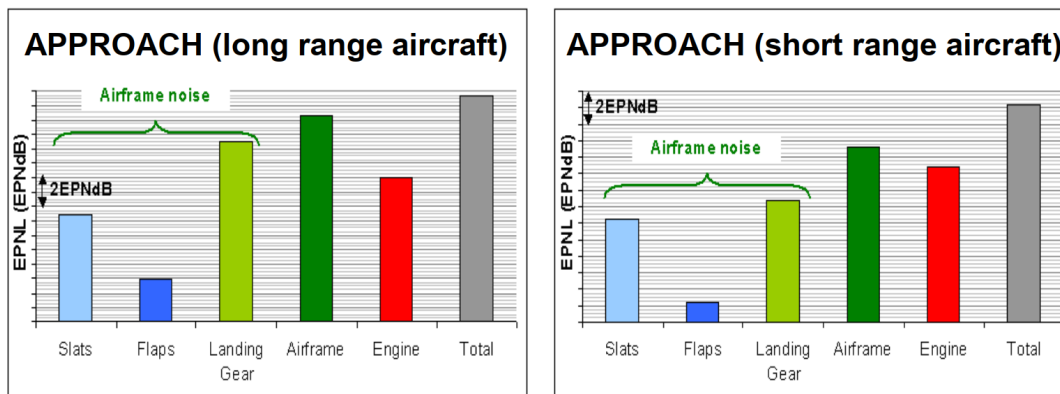


Figure 8.8: Approach noise breakdown for long range and short range aircraft. Source: Airbus via [83]

slenderness and they have a larger angle of attack during takeoff or landing because of the wing that is optimised for supersonic flight. Therefore, they need to have increased ground clearance when rotating for takeoff or during landing. Placing the landing gear further aft likely is not possible, since the main landing gear must be in front of the centre of gravity during rotation to avoid tipover [45]. Concorde<sup>2</sup> had a landing gear length of more than 3 m, which is longer than any subsonic passenger aircraft by Airbus or Boeing. The maximum value found here is 2.59 m for the Boeing 777-9<sup>3</sup>. Since the landing gear is the largest contributor to approach noise [88], the longer landing gear length of supersonic aircraft will result in noticeably louder noise than subsonic aircraft.

An additional factor that increases the aircraft's noise is the optimised engines for supersonic flight. For acceptable efficiency supersonic engines need engines with a low bypass ratio. Current subsonic engines<sup>4</sup> can have a bypass ratio of up to 12.5. In comparison, the bypass ratio selected for this engine is around 3. This lower bypass ratio results in a higher exhaust flow speed, which generates more noise. This was also the main cause for the loud noise of Concorde. Its engines had an exhaust speed of around 900 m/s when afterburning was applied, compared to 300 m/s or lower for the fully mixed exhaust of high bypass-ratio engines [81]. Figure 8.9 shows how the engine noise level decreases with increasing bypass ratio. Due to the logarithmic dB scale, the total engine noise depends the most on the highest noise contribution. Around BPR=5 the bypass noise level equals the core noise level. At lower bypass ratios the total noise level decreases with core flow noise level. Above BPR=5, the total noise level scales with the bypass flow noise. Therefore, increasing the bypass ratio from 0 to 3 results in a 10 dB noise reduction of the core flow. While the bypass flow noise level does not change, the total engine noise will decrease with approximately 10 dB as well.

Besides this, the lower aerodynamic performance of the wings at low speeds requires higher thrust to control the aircraft and counter the increased drag. Furthermore, this requires a higher approach speed since wings optimised for supersonic flight likely have a higher stall speed. Since noise scales with the fifth power of flight speed, this may be the most important factor in both approach and departure noise compared to subsonic aircraft.

When the above differences are summed, it is clear that a supersonic aircraft will generate more noise than subsonic aircraft during both approach and takeoff. The lower bypass ratio (and thus the higher jet exhaust speed), longer landing gear and increased flight speed will cause an increase in noise and supersonic aircraft are not expected to have features that produce less noise than subsonic aircraft.

### 8.3.3. Noise reduction measures

Ever since the start of aircraft noise research the problem of how to reduce aircraft noise has been investigated. This resulted in large noise reductions, illustrated by Figure 8.10. The regulatory noise limits have been decreased by almost 40 dB over the past 50 years which means that the generated

<sup>2</sup><http://www.concordesst.com>. Accessed 27 July 2020

<sup>3</sup>[http://www.boeing.com/resources/boeingdotcom/commercial/airports/acaps/777-9\\_RevA.pdf](http://www.boeing.com/resources/boeingdotcom/commercial/airports/acaps/777-9_RevA.pdf). Accessed 8 October 2020

<sup>4</sup>[https://customer.janes.com/Janes/Display/jae\\_a032-jae\\_](https://customer.janes.com/Janes/Display/jae_a032-jae_). Accessed 27 July 2020

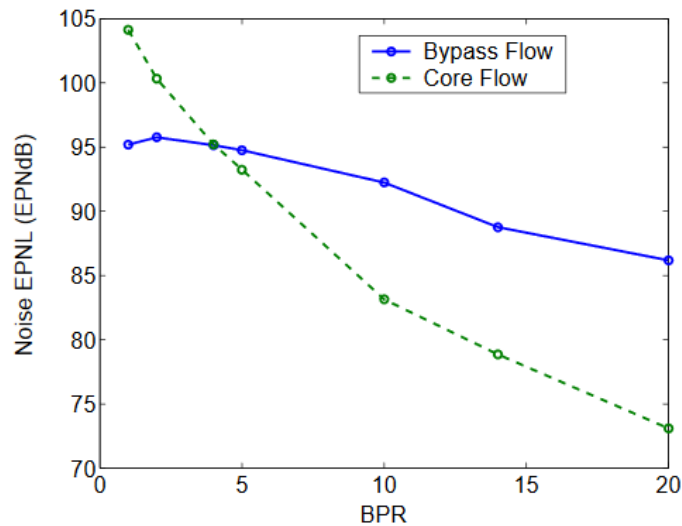


Figure 8.9: EPNL vs. bypass ratio for a 40,000 lb (178 kN) sea-level thrust engine [89]

aircraft noise has decreased in a similar way. Starting from the Chapter 4 limits, the limits for the individual measurement points have not changed, but a certain margin to the cumulative limits is now required to meet the standards.

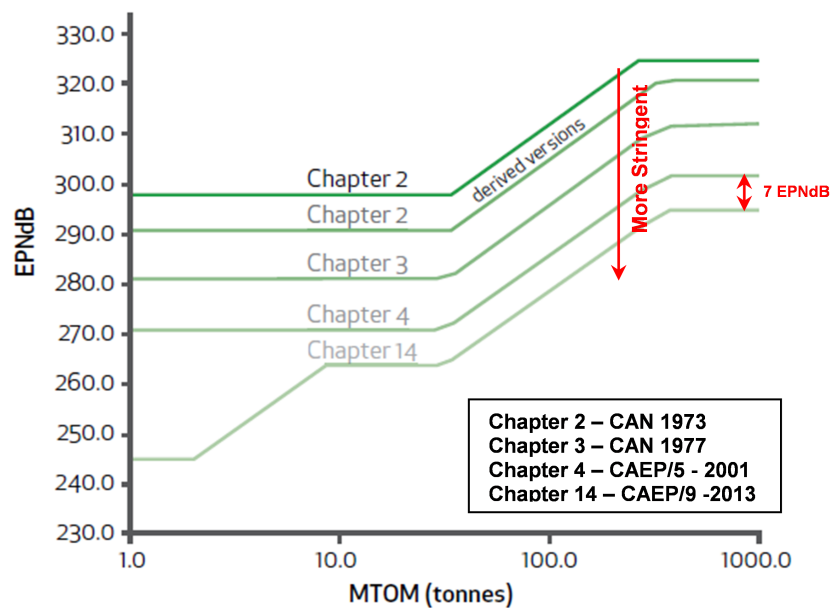


Figure 8.10: Development of ICAO noise limits over time<sup>5</sup>

No noise reduction technologies were used on Concorde. The only ways to have some control over the emitted noise was by changing the engine settings [81]. This resulted in cumulative noise levels that were higher than the loudest jet aircraft of that time when measured according to the ICAO Annex 16 procedure (Table 8.1). To make community noise a bit more acceptable a special flight profile was flown on takeoff and landing to reduce community noise [90].

Noise reduction measures that are used on current subsonic aircraft can (and most likely will) be applied to new supersonic aircraft, but due to the key differences between subsonic and supersonic aircraft

<sup>5</sup><https://www.icao.int/environmental-protection/Pages/Reduction-of-Noise-at-Source.aspx>. Accessed 29 July 2020

Table 8.1: Noise levels of subsonic jet aircraft and Concorde compared to regulatory values [1]

Observation point	B707-320B [EPNdB]	DC-8-50 [EPNdB]	Concorde [EPNdB]	ICAO Chapter 2 limit [EPNdB]
Takeoff	114	115	119.5	105
Sideline	108	106	112.2	107
Approach	120	117	116.7	107
Cumulated noise	342	338	348.4	319

described above it is unlikely that supersonic aircraft will ever have similar noise levels to subsonic aircraft. After all, any specific noise reduction measure developed for supersonic aircraft can also be applied to subsonic aircraft, since it is desired to reduce subsonic aircraft noise even further below current levels [91].

Specific noise measures for supersonic aircraft have been presented for a long time, mainly by proposing new engine designs. These are considered necessary to combine low noise with efficient subsonic and supersonic operations [92, 93]. However, despite being the subject of research at least since the early 1970s [94, 95] supersonic aircraft that reached the final conceptual design stages would not have such engines. With the NASA X-59, the Boom XB-1 and the Aerion AS2 all featuring more or less 'standard' turbofans, it is unlikely that revolutionary engine designs will be used any time soon.

Therefore, the only realistic option to reduce supersonic aircraft noise during takeoff and landing to acceptable levels is to fly a different approach and/or departure profile. This may include a faster climb or reducing thrust right after clearing the obstacle height behind the runway. However, ICAO Annex 16 does not allow changing the thrust setting during takeoff or flying faster than 20 knots above the safety speed [96].

The likelihood that it is inevitable for supersonic aircraft to generate more noise than allowed by regulations for subsonic aircraft is illustrated by a recent FAA notice of proposed rulemaking (NPRM) [97]. This notice proposes a new standard for supersonic aircraft with a maximum takeoff weight of 150,000 lbs (68,039 kg) having two or three engines and a maximum operating speed of Mach 1.8. The notice keeps the ICAO Annex 16 chapter 14 rules intact, but changes the required margins to 0 for the individual points and allows a 13.5 EPNdB margin to the cumulative noise limits, instead of the 17 EPNdB in Chapter 14. Additionally, it creates an option for aircraft manufacturers to include a Variable Noise Reduction System (VNRS). This will make deviations from the standard reference path possible.

This proposed rule may be just enough for supersonic aircraft to meet the noise limits. A recent study predicted that a three-engine aircraft with an MTOW of 55,000 kg has a Chapter 4 cumulative noise margin of 1.6 EPNdB [98], which is already higher than the limit in the FAA proposal. Aircraft closer to the limit of 68,039 kg may be louder than this.

The FAA proposal also shows that larger supersonic aircraft are currently deemed infeasible. The NPRM will only be applicable to aircraft with a MTOW below 68,039 kg and a maximum operating cruise speed of Mach 1.8. This decision was based on NASA models and data from supersonic aircraft manufacturers, indicating most current designs and developments fit within these parameters. According to the design program created for this thesis a takeoff mass of 68,039 kg corresponds to an aircraft with 47 seats.

### 8.3.4. Noise prediction

With only the general description of the supersonic aircraft designed in this thesis it is not possible to accurately predict the noise they produce. To still give an estimate for the produced noise, two options were explored:

- Use the cumulative noise from an existing supersonic aircraft and make assumptions on the cumulative noise of the new aircraft
- Break down the noise from an existing supersonic aircraft at each measurement point for airframe and engine noise and make assumptions on the component noise

The first option is less accurate, although less detailed assumptions are required. The second option requires more assumptions on how much noise levels have changed between different aircraft. These are not available at this point. For this reason only the cumulative noise method will be shown in more detail below.

### Cumulative noise prediction

The starting point for this method is Concorde, since this is the only supersonic passenger aircraft that has noise measurements available [1, 99]. The cumulative noise of Concorde is almost 348.4 EPNdB [1]. This is almost 30 dB above the ICAO Chapter 2 limit established in 1973. If a new version of Concorde would be designed today with the same weight the cumulative noise must not be higher than 283 EPNdB.

To estimate the noise for an improved Concorde all the differences affecting the noise output need to be evaluated. These will likely be the following:

- More silent engines with a higher bypass ratio
- Airframe noise improvements

To determine the effects of these improvements, a comparison is made with subsonic aircraft. Similar improvements were made with for example the Boeing 747-200 and the Fokker 28 and Fokker 100. Data from the EASA jet aircraft noise database<sup>6</sup> shows that various Boeing 747-200B variants had cumulative noise margins relative to the Chapter 3 limits varying between -6.8 and 12.2 dB with bypass ratios between 4.1 and 5.0 (see Table 8.2). Although the engines vary in maximum thrust this variation is only about 10% of the total thrust and does not seem to be related to the noise production. Since all these aircraft/engine combinations were registered at the same time it can be assumed that the only difference between these aircraft is the engine type. This shows that the engine has a large influence on the noise output from an aircraft, also for engines with a bypass ratio above 3.

Table 8.2: Boeing 747-200B cumulative noise margin relative to Chapter 3 limits for various engine variants

Engine model	Certification year	Bypass ratio [-]	Noise margin [EPNdB]
RB211-524B2-19	1970	4.3	-6.8
CF6-50E	1970	4.1	2.9
JT9D-7R4G2	1970	4.8	3.4
RB211-524D4-19	1970	4.2	5.0
CF6-80C2B1	1970	5.0	12.2

The same database shows the Fokker 28 variants with the Fokker 100, listed in Table 8.3. Here the aircraft model changed together with the engine types. These most pronounced changes among these variants are fuselage and wing stretches and the use of new engine types. Here it is visible that even though the fuselage and wings are stretched, the F28-4000 produces less noise than its smaller variants. This again happens with the Fokker 100 where the engine bypass ratio is increased as well.

Table 8.3: Fokker 28 and Fokker 100 cumulative noise margin relative to Chapter 3 limits for various aircraft and engine variants

Aircraft type	Engine model	Certification year	Bypass ratio [-]	Noise margin [EPNdB]
Fokker F.28 Mk 1000	RB 183 Mk 555-15	1969	1.015	-14.6
Fokker F.28 Mk 2000	RB 183 Mk 555-15	1972	1.015	-15.5
Fokker F.28 Mk 4000	RB 183 Mk 555-15H	1976	1.015	-6.1
Fokker F.28 Mk 4000	RB 183 Mk 555-15P	1976	1.015	-3.6
Fokker 100	Tay 620-15	1987	3.0	15.7
Fokker 100	Tay 650-15	1987	3.0	16.2

<sup>6</sup><https://www.easa.europa.eu/eaer/topics/technology-and-design/figures-and-tables>. Accessed 29 July 2020

This indicates that just improving the engine without changing the bypass ratio can have a large influence on older aircraft where engine noise is the dominant noise component. Additionally, this can overcome any negative results from enlarging the aircraft itself. Increasing the engine bypass ratio will add even more to this benefit.

As a final example, the Airbus A320 and A320neo were compared in Table 8.4. Here the noise difference between various engine variants were smaller than for the Boeing 747-200, but again a difference is visible between the A320 and A320neo.

Table 8.4: Airbus A320 cumulative noise margin relative to Chapter 3 limits for various aircraft and engine variants

Aircraft type	Engine model	Bypass ratio [-]	Noise margin [EPNdB]
Airbus A320-211	CFM56-5A1	6.0	12.1
Airbus A320-212	CFM56-5A3	6.0	12.2
Airbus A320-214	CFM56-5B4	6.0	16.6
Airbus A320-216	CFM56-5B6/3	6.0	15.1
Airbus A320-231	V2500-A1	5.3	13.3
Airbus A320-232	V2527-A5	4.8	18.9
Airbus A320-253N	LEAP-1A33	11.0	30.0
Airbus A320-271N	PW1127G-JM	12.2	28.7

From this data it can be concluded that engine developments combined with increasing the bypass ratio can cause a cumulative noise reduction of 20-30 EPNdB.

A new Concorde would likely not feature afterburners. This would reduce the takeoff noise by around 5-10 dB<sup>7</sup>.

Airframe noise reduction measures often achieve reductions of a single EPNdB per measure [72], so these can maybe result in a 10-15 EPNdB total airframe noise reduction.

Therefore, a new Concorde would be able to reduce its cumulative noise from almost 350 EPNdB to 295-315 dB. Assuming the weight is kept similar the Chapter 14 limit is 283 EPNdB which is still at least 12 dB lower than what could be reached in this example. The chapter 4 limit is 7 dB higher: 290 EPNdB. If the aircraft weight would be reduced by these improvements, the limit would be even lower. This makes it unlikely for supersonic aircraft to meet the Chapter 4 limits, let alone the Chapter 14 limits. Besides this, every airliner introduced after 2010 already meets the Chapter 14 limit, so the 'noise gap' between subsonic and supersonic aircraft is likely to remain for the foreseeable future.

The relative size of the aircraft will likely not influence this gap. The regulatory noise limits scale with takeoff weight and it is estimated that the parameters that have the highest influence on noise output (which are described above in section 8.3.1) will not decrease the noise production to below the limits. The reason for this is that the landing gear length will only scale with aircraft length, the approach speed does not change and the engine bypass ratio will be kept constant. Therefore, the only parameters that change with takeoff weight are engine thrust and, for a small part, landing gear length. Since engine thrust is accounted for by the weight-dependent noise limits, the relationship between takeoff weight and noise is expected to follow the logarithmic trend like the ICAO Annex 16 limits.

<sup>7</sup>Concorde noise measurements indicated a 10 dB noise reduction from 125 to 115 EPNdB during takeoff at Dallas-Ft. Worth airport [99]



# 9

## Supersonic noise prediction

For subsonic aircraft generally the area of interest for generated noise is the takeoff and landing phase. This is the reason why the noise regulations only cover noise in the vicinity of airports. Because of the high cruise altitude, lower noise levels are received on ground. Despite this, aircraft flying at cruise altitude can still be heard on ground, especially in areas with low background noise [100]. However, not much attention is given to aircraft noise in the cruise phase in literature and symposia. The only symposium held on this topic was joint NASA/FAA symposium on enroute noise in 1989 [101].

The major noise concern of supersonic aircraft is not the noise generated by any component, but the shocks generated by the aircraft when flying at supersonic speeds. The complex shock pattern generated by the aircraft is propagated through the air and forms a wave pattern with a sharp pressure rise at the beginning and the end of the signal. Since the duration of this wave signal usually is less than 0.1 second, the pressure rises are heard as a single bang, the sonic boom.

It is expected that the component noise (excluding the sonic boom noise) emitted by supersonic aircraft is roughly equal to that of subsonic aircraft. The main difference here is the higher jet exhaust speed which can be partially offset by the higher cruise altitude. Therefore, the assumption is that the ground noise without the sonic boom of supersonic aircraft is roughly similar to that of current subsonic aircraft and only sonic boom noise will be treated in this chapter. To confirm this more research is required.

This chapter will explain the methods used to estimate and compare the sonic boom generated by the aircraft described in this thesis. For this reason, section 9.1 will give some background information about sonic boom generation, after which the boom prediction methods will be explained in section 9.2.

### 9.1. Sonic boom background

Any object moving at supersonic speed usually creates shock waves. The moving object creates pressure disturbances which are propagated with the speed of sound. When the velocity exceeds the speed of sound, the pressure disturbances can not propagate upstream anymore. This results in a pressure rise and a shockwave is formed [102]. This is the reason for supersonic aircraft to generate a sonic boom. The shock pattern generated by the aircraft is propagated to the ground. During that propagation the shape of the pressure pattern usually changes to an N-shape, visualised in Figure 9.1.

There is a consensus that the distribution of the effective area is the most influential aircraft characteristic for the sonic boom strength. The smoother the area distribution, the softer is the sonic boom. This means for example that the cockpit canopy can not extend upward as is the case with many fighter aircraft, but should rather be an integral part of the fuselage, like the Boom XB-1 and NASA X-59 demonstrate (figure 9.2- 9.4). More background information about the influence of the aircraft's shape on the boom strength can be found in Appendix E.

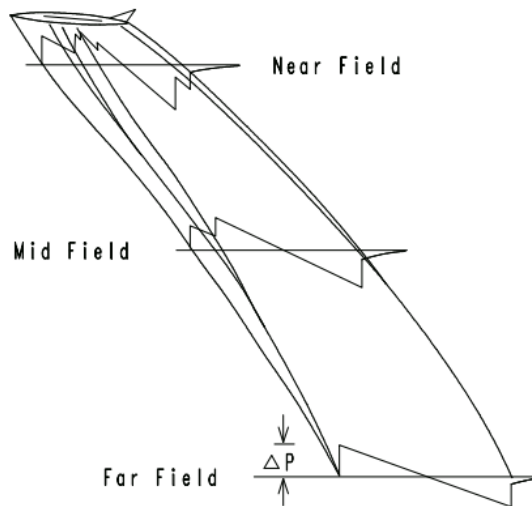


Figure 9.1: Sonic boom pressure wave propagation [103]

Figure 9.2: F-16 cockpit canopy<sup>1</sup>Figure 9.3: XB-1 blended cockpit<sup>2</sup>Figure 9.4: X-59 blended cockpit<sup>3</sup>

The strength of a sonic boom can be measured by the overpressure. This is the increase in pressure relative to the ambient pressure caused by the shock waves when they reach ground. However, not only the maximum pressure is important. The time in which this maximum pressure is reached is important as well. Seebass and George distinguished three different boom signatures resulting from boom minimisation (figure 9.5).

The top signature has a similar shape to the 'standard' N-wave. It is a result of minimising the sonic boom impulse. The second signature shows a signature with a flat top. This is caused by minimising the maximum pressure that occurs anywhere on the aircraft. The third signature is a result of minimising the shock wave pressure rise. This allows for a smaller initial pressure rise, denoted by  $p_s$ , after which the pressure gradually rises to  $p_{max}$ . Reducing the overpressure or shock pressure however increases the impulse of the shock wave [104]. This impulse may have a strong effect on people and buildings, especially for larger aircraft [105]. It is defined as the integral of the overpressure in the positive half of the signature.

As a unit for sonic boom overpressure pound per square foot (psf) is often used. As said before, this value indicates the pressure difference relative to the ambient pressure. A different way to describe sonic boom strength is by using a loudness scale. Since the sonic boom is a pressure disturbance just like any other sound, its strength can also be expressed in PNL. The boom loudness mainly depends on the maximum overpressure and the pressure rise time. The higher the maximum overpressure and the shorter the pressure rise time, the higher the sonic boom loudness will be.

For boom minimisation there are essentially two options: limiting the shock strength or preventing the

<sup>1</sup>Image source: <https://www.defensie.nl/binaries/content/gallery/defensie/content-afbeeldingen/actueel/nieuws/2018/02/12/d130725as1023-a.jpg?download>. Accessed 24 June 2020.

<sup>2</sup>Image source: <https://www.lockheedmartin.com/en-us/news/features/2020/shaping-x59-quesst.html>. Accessed 24 June 2020.

<sup>3</sup>Image source: <https://boomsupersonic.com/press>. Accessed 24 June 2020.

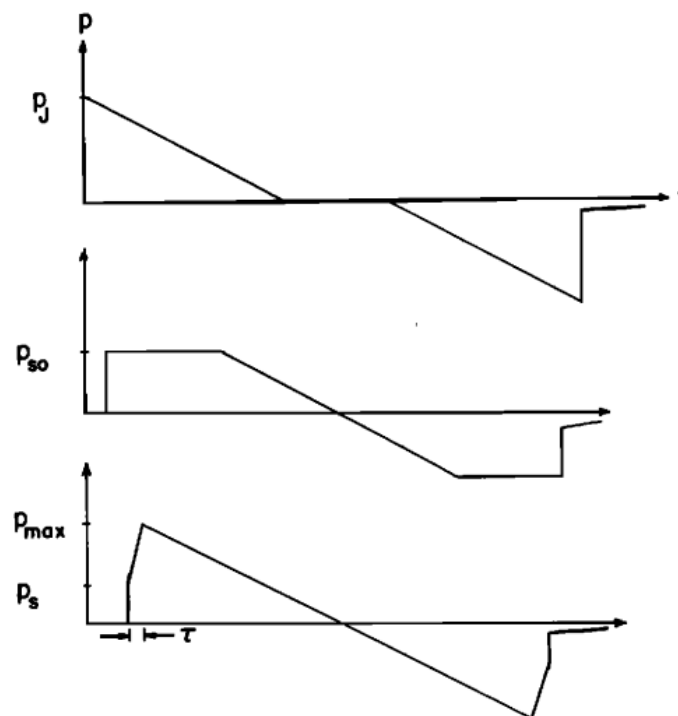


Figure 9.5: Various sonic boom signatures [104]

shock from happening at all. In the first case the F-function should be made as large as possible as early as possible. In the second case shock waves should be prevented by limiting the growth rate of F [105]. Examples of these two approaches can be seen in the F-5 Shaped Sonic Boom Demonstration (SSBD) on one hand, and most new SST designs on the other hand.

### Shock limitation

The goal of the F-5 Shaped Sonic Boom Demonstration (SSBD) was to reduce the sonic boom generated by a modified Northrop Grumman F-5E in order to produce a flat-top signature, opposed to the N-wave produced by the regular F-5E. This was tested by fitting a longer and thicker nose section to the aircraft (Figure 9.6). This indeed resulted in a flat-top signature and an overpressure reduction from 1.2 psf to 0.8 psf for a Mach 1.4 flight at 32,000 ft [106]. This modification looks a lot like the first mentioned case of shock reduction. Thickening the nose section causes that the largest cross-sectional area is reached earlier, therefore having an earlier large F-function.

### Shock prevention

New supersonic aircraft designs like the NASA X-59 that is currently in production feature a very slender fuselage. This matches the desire to have shocks that are virtually inaudible on ground [107]. The slender fuselage limits the growth rate of effective area and therefore the growth rate of the F-function, allowing for a much softer boom.

## 9.2. Sonic boom prediction

For the prediction of the sonic boom generated by the designed aircraft, multiple methods will be employed. Using CFD methods will not be possible due to the complexity of these methods and the low accuracy of the aircraft model, more simplified methods need to be used.

The first method will be the simplified sonic boom prediction method by Carlson [108]. This method is based on an estimation of the equivalent area distribution due to lift in combination with the aircraft's

<sup>4</sup>Image source: <https://www.dfrc.nasa.gov/Gallery/Photo/SSBD/HTML/EC03-0210-1.html>. Accessed 25 June 2020.

Figure 9.6: F-5 SSBD in flight<sup>4</sup>

cross-sectional area distribution. Based on these data a shape factor  $K_S$  can be defined. For the atmospheric propagation two factors  $K_p$  and  $K_t$  can be defined based on the altitude and speed. Following this, the overpressure and signature duration can be calculated with equations 9.1 and 9.2.

$$\Delta p_{max} = K_p K_R \sqrt{P_v P_g} (M^2 - 1)^{1/8} h_e^{-3/4} l^{3/4} K_S \quad (9.1)$$

$$\Delta t = K_t \frac{3.42}{a_v} \frac{M}{(M^2 - 1)^{3/8}} h_e^{1/4} l^{3/4} K_S \quad (9.2)$$

where  $P_v$  and  $P_g$  are the ambient and ground pressure,  $K_R$  is the ground reflection factor,  $h_e$  is the effective altitude and  $a_v$  is the ambient sound speed.

Carlson's report shows good coincidence of this method with real data (Figure 9.7). The maximum difference in overpressure between measurements and predictions is approximately 10 Pa or 0.21 psf. Additionally, the method was tested with F-5 data from [106]. This resulted in a nearly exact fit with the measured F-5 signature (Figure 9.8). As can be seen, the predicted boom has an overpressure of 1.21 psf and a duration of 77 milliseconds, while the measured boom has an overpressure of 1.23 psf and a duration of 84 milliseconds. However, evaluating the F-5 also showed a shortcoming in this method. Evaluating the F-5SSBD did not result in an equally large decrease in overpressure compared to the F-5E as the measurements showed. The predicted overpressure here was 1.1 instead of 0.9 which is more than 20% higher than the experimental data. From this it can be concluded that this method works well for aircraft designs that are not optimised for low-boom noise, like most older aircraft, but is unable to predict overpressures of reshaped aircraft for low sonic booms.

Because of this, a different method needs to be applied to find out what would be the minimum achievable overpressure. Seebass and George presented a method giving a theoretical minimum overpressure for a given set of aircraft parameters [104]. The only aircraft characteristics used are the altitude, Mach number, length and mass. Using these parameters, the minimum overpressure for a flat-top signature can be calculated (equation 9.3). This was indicated as  $p_{so}$  in Figure 9.5.

$$p_{so} = P_g \frac{4e^{-h/(2H)}}{3ak\sqrt{2\beta}} \frac{l}{h} \left( \sqrt{1 + \frac{9}{8}\tilde{W}} - 1 \right) \quad (9.3)$$

where  $H$  is the atmospheric scale height,  $a$  is the atmospheric advance ratio and  $k$  is a relation between Mach number and specific heat ratio.  $l$  and  $h$  are the aircraft's length and altitude and  $\tilde{W}$  is a relation between the aircraft's flying conditions and its mass.

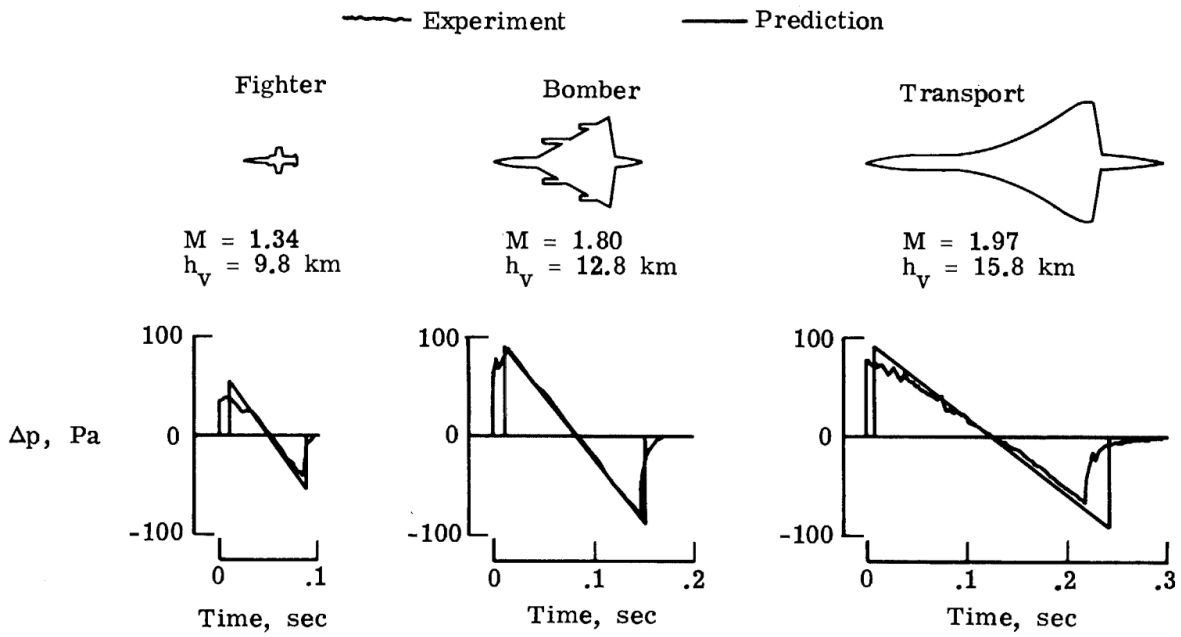


Figure 9.7: Experimental data and prediction for sonic boom signature for various aircraft types [108]

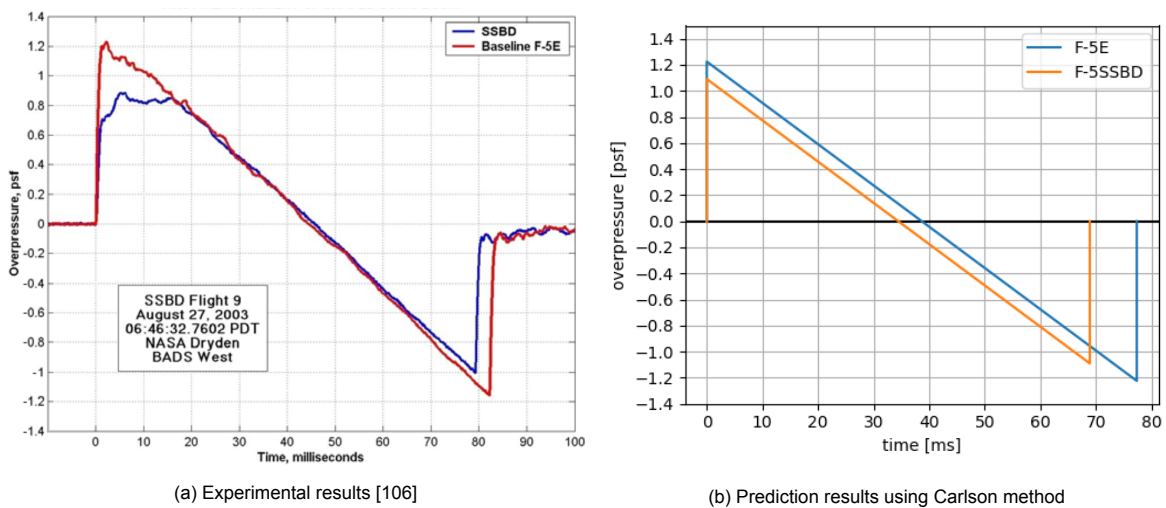


Figure 9.8: sonic boom signature for F-5E and F-5 SSBD

Additionally, Seebass and Argrow show a figure of merit which gives an indication of the relative loudness of sonic booms compared to other aircraft [105], based on the equations presented earlier [104]. This method is based on the same relationship as the minimisation method by Seebass and George mentioned above, as shown in equation 9.4.

$$FOM = \frac{\beta W}{P_0 l^{3/2} \sqrt{h}} e^{h/(2H)} \cdot 10^3 \quad (9.4)$$

Another way to predict the sonic boom signature is to use the Whitham F-function. By calculating the effective cross-sectional area a near-field pressure distribution can be calculated which can then be used as input for a boom propagation calculation. However, this method requires a more detailed definition of the fuselage shape than the current design stage can provide.

Table 9.1 provides an overview of the different methods applied to various aircraft and compared to the measured boom overpressure. As the methods used are quite simple, only the cruise altitude, length, mass and Mach number were required inputs for the model. For aircraft that did not fly in reality, the design overpressure was used for comparison. The NASA X-59 has a design boom loudness of 75 PLdB [107] which corresponds to an overpressure of around 0.4 psf<sup>5</sup>.

Table 9.1: Boom prediction methods compared to the real overpressure

Aircraft	Boom strength	Minimum overpressure [psf]	Figure of merit [-]	Carlson method [psf]	Real overpressure [psf]
F-5E	high	0.19	0.18	1.22	1.2
F-5SSBD	low	0.18	0.17	1.09	0.8
Concorde	high	0.92	1.45	2.18 <sup>6</sup>	2
X-59	low	0.20	0.20		0.4
Low-boom SSBj [109]	low	0.41	0.54	1.03	0.4
High-boom SSBj [109]	high	0.37	0.46	1.27	1.23
Low-boom SSBj [110]	low	0.48	0.69		0.5

The above table shows close matches (<10%) between the Carlson method and the real overpressure for the F-5E, Concorde and high-boom SSBj. On the other hand, the F-5SSBD and low-boom SSBj match better with the Seebass minimum overpressure. The Carlson method clearly is a method only suitable to calculate boom strengths for non-optimised aircraft shapes. In that case it gives accurate results. The reason for this is that the Carlson method assumes an N-shaped pressure signature. This is an accurate approximation for high-boom supersonic aircraft, but shaped boom designs either have a flat top signature or a gradual pressure rise as shown in Figure 9.5. The Carlson method also predicts the duration of the signature, but for now this is not considered important for this research.

While the Carlson method shows an accurate boom strength representation of the high-boom aircraft, the low boom aircraft are not well represented by either of the Seebass methods. The figure of merit described by Seebass and Argrow is an interesting number for the comparison for different aircraft sizes, but apart from that it does not give much insight on the real boom strength. As it uses the same dependencies as the minimum overpressure method, the trends are the same for both methods. Therefore, the figure of merit will not be used for describing the sonic boom properties in this thesis.

The minimum overpressure method does not always match with the real overpressures of the low-boom aircraft. The fact that the minimum overpressure method is mainly theoretical may be a reason why values this low can not be achieved. The F-5SSBD is not expected to have an optimal boom strength since it was only a partially improved design. The low-boom SSBjs by Aronstein [109] and Mack [110] nearly exactly match the method's prediction while the X-59 will have a 0.15 psf stronger boom than the theoretical minimum. This can be explained by the F-5SSBD only having minor modifications and the

<sup>5</sup>Iosifidis, P. Concept Development of the Quiet Supersonic Technology Aircraft. Presentation during AIAA AVIATION 2016. <https://lbpw-ftp.larc.nasa.gov/aviation-2016/aiaa-2016-talk-losifidis-quesst-aircraft.pdf>. Accessed 4 July 2020.

<sup>6</sup>Calculated using an even further simplified method by Carlson [108], which does not require the effective area distribution

low-boom SSBJs being very optimised design due to the conceptual level of the designs while the X-59 is somewhat in between due to probable practical limitations to boom optimisation. In conclusion it can be said that the minimum overpressure method is a good method to approximate the lowest achievable boom strength.

Since the aircraft designed for this thesis will have their effective cross-sectional area distribution calculated, the Carlson method can be fully applied to them and it is expected that this will result in a similar, non-optimised boom overpressure. This means that with careful shaping the overpressure can be brought down to close to the theoretical flat top minimum described by the minimum overpressure method. At typical cruise altitudes the overpressure of an optimal flat top boom can be around 50% lower than that of an optimal N-shaped boom [104]. This may be enough for small aircraft like business jets, but for larger aircraft the boom will likely still be too loud. Therefore, different, stricter boom shaping methods will likely be required for larger supersonic aircraft to reach an acceptable boom level. For smaller supersonic aircraft the theoretical flat top minimum can be seen as the desired goal, as will be explained below. Therefore, these two methods were used to describe the sonic booms created by the generated aircraft designs.

### 9.3. Prediction results

This section shows the results of the application of Carlson's method and the Seebass minimum overpressure. Both methods were applied to the selected aircraft that were shown in Chapter 7. Following this, the acceptability of these overpressures were analysed and an assessment was made on the acceptability of expected sonic boom loudness of future supersonic aircraft.

#### 9.3.1. Method comparison

For each aircraft the sonic boom overpressure was calculated at three points during cruise: start, mid and end. The only changing factor here is weight, which decreases by using the stored fuel. For each of these points the non-optimised boom overpressure and ideal theoretical overpressure are calculated. Figure 9.9 shows the non-optimised overpressure for the set of aircraft.

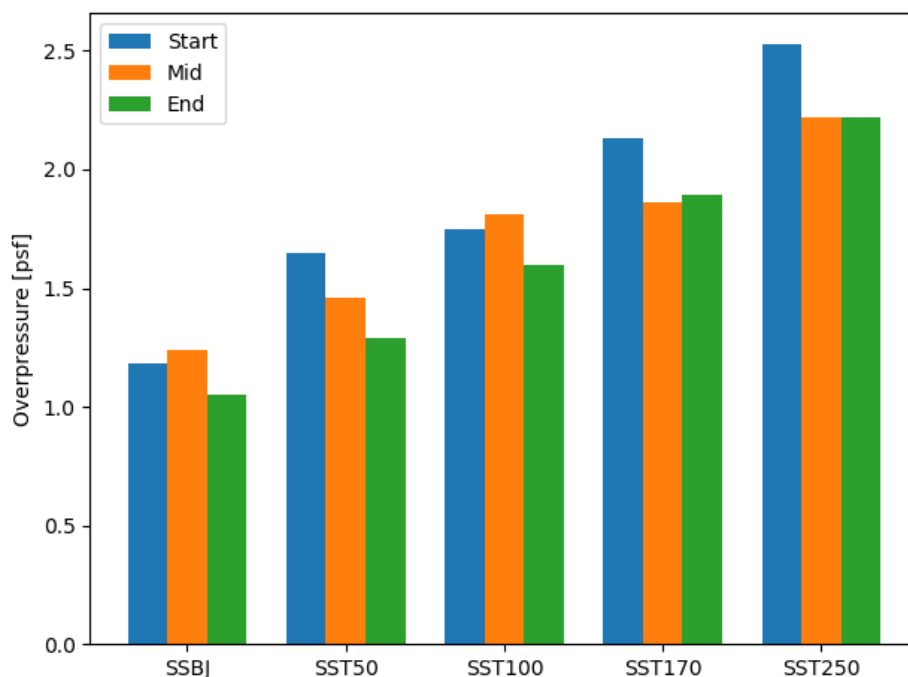


Figure 9.9: Non-optimised boom overpressure during cruise

As can be seen boom overpressure increases with increasing aircraft size. As the takeoff weight decreases during cruise the overpressure usually decreases. The reason why this does not always hap-

pen is due to the difference in effective aircraft shape at the various points during cruise. As the weight decreases, the wing lift decreases as well. The equivalent area due to lift accounts for a large portion of the maximum effective area. Any change in the maximum effective area results in a change in the slope of the area distribution curve, indicating a larger change in effective area, resulting in a stronger or weaker boom. This is indicated in Figure 9.10 for the SSBJ from Figure 9.9. The exact reason why this only happens at certain aircraft could not be found, but most likely it is a combination of relative weight change during cruise and aerodynamic efficiency. Additionally, some aircraft have a sufficiently large tailplane assembly that the maximum effective area is located at the tail. This has a large influence on the calculated shape parameter and the resulting overpressure. This may be an unwanted effect of the way the equivalent area is calculated, since no large aircraft with a tailplane were mentioned in the report.

Aircraft weight has a large influence on the boom loudness. The boom strength at the end of cruise decreases by 0.13 to 0.36 psf, which is 8.5% to 22% lower than the boom strength at the start of cruise.

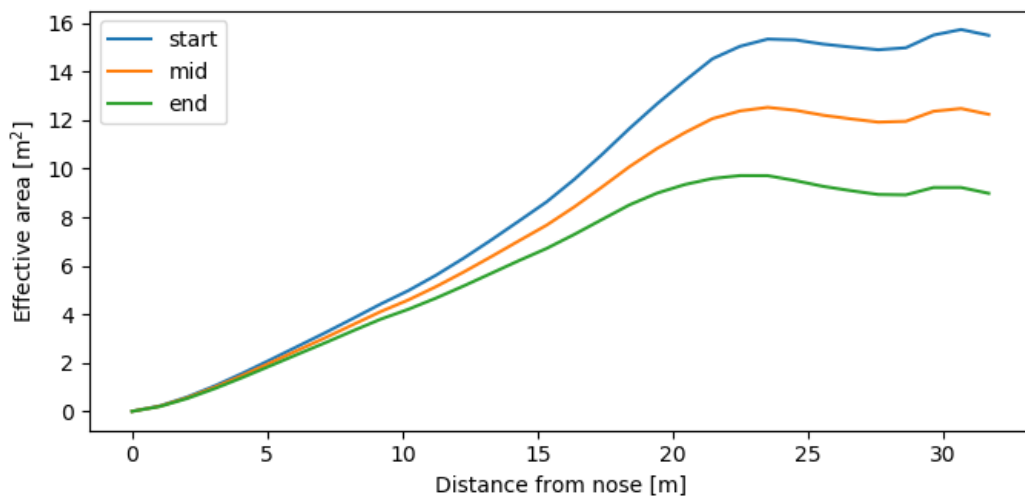


Figure 9.10: Effective area distribution for the SSBJ

Figure 9.9 also shows that at least some improvement over Concorde can be made. The SST100 aircraft has a maximum overpressure of 1.81 psf, which is 20% lower than Concorde's overpressure. The main reasons for this are the technological improvements that are expected to be made compared to Concorde, which allow for a lower takeoff mass. For the SST100 that is 126,000 kg while Concorde had a maximum takeoff mass of 185,000 kg.

Figure 9.11 shows each aircraft's overpressure according to the minimum overpressure method on top of the graph of Figure 9.9. In this figure it can be seen that the minimum boom strength always increases with weight and always decreases between the begin and end of cruise flight.

The effect of optimising an aircraft to decrease the sonic boom loudness is clearly visible. The sonic boom overpressure at the start of cruise decreases with around 68% for all aircraft, except the SSBJ where the reduction is 57%. This shows that there is much room for optimisation and that the boom loudness of these aircraft may be reduced to acceptable levels. More about the acceptability of sonic booms can be found in section 9.3.2.

While the relative difference between the Carlson and Seebass methods is fairly constant, the overpressure difference grows when the aircraft size is increased. A reason for this may be that a large aircraft can be reshaped better than a small aircraft, given a certain length and weight. This can be visualised with the non-optimised effective area distribution for the SSBJ and the SST100 (Figure 9.12). As can be seen the curve of the SST250 is below the SSBJ. The SSBJ has an improved effective area development due to the more gradual increase. That means that the SST250 can be improved more than the SSBJ, indicating a larger difference between the non-optimised and optimised predictions.

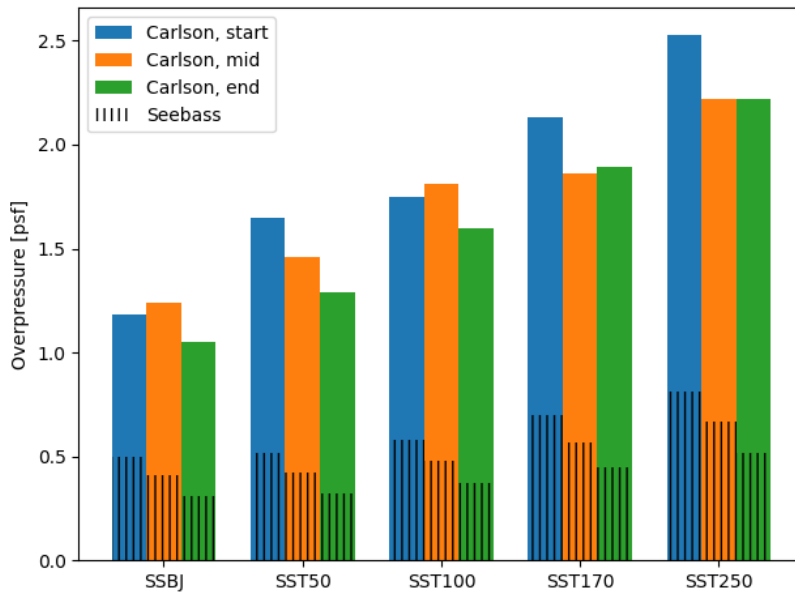


Figure 9.11: Theoretical minimum boom overpressure during cruise overlaid on the Carlson method results

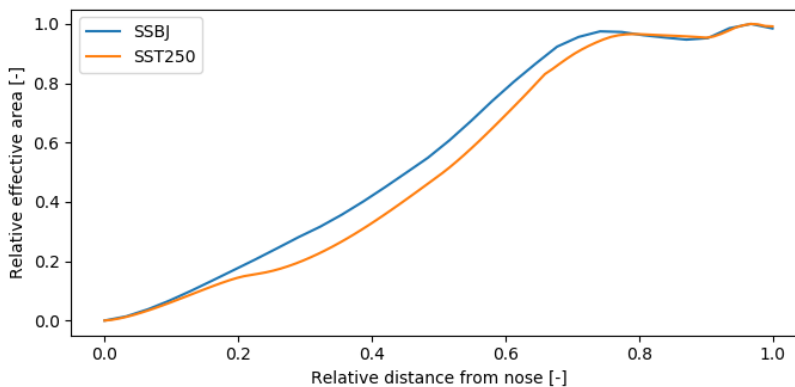


Figure 9.12: Relative effective area (maximum = 1) vs. relative distance from nose of SSBJ and SST50

What the figure also shows is that the boom strength at the cruise start grows faster than the boom strength at the end of cruise when the aircraft size increases. This happens since the overpressure depends on the square root of weight, while height influences the overpressure more directly.

This also indicates the importance of climbing during cruise. A cruise climb method was not included in the design program since no way could be found to calculate all parameters for a stepwise or continuous climb during cruise [5]. A higher end-of-cruise altitude would decrease the boom loudness. If the cruise altitude of the SST250 would be raised by 1,000 m, the boom overpressure at the end of cruise would be 16% lower. Therefore, climbing during cruise not only increases fuel efficiency, but also decreases the sonic boom loudness.

It is also interesting to investigate the influence of the input parameters on boom overpressure. For this the Seebass method is applied for a range of altitudes, Mach numbers, weights and aircraft lengths. As reference, the SSBJ is used with a weight of 40,460 kg and a length of 31.4 m. The baseline cruise altitude is 16 km and the default Mach number is 1.8. The results can be found in Figures 9.13-9.16.

These graphs show useful trends regarding the sonic boom strength of SSBJs. Figure 9.13 shows that the overpressure decreases with increasing altitude until 10 km. As opposed to the SST250 mentioned before, higher cruise altitudes barely change the boom overpressure for SSBJs. The slight increase in

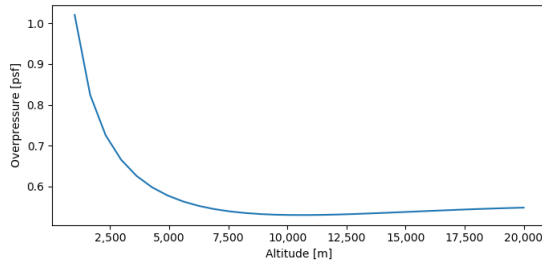


Figure 9.13: Overpressure variation with altitude

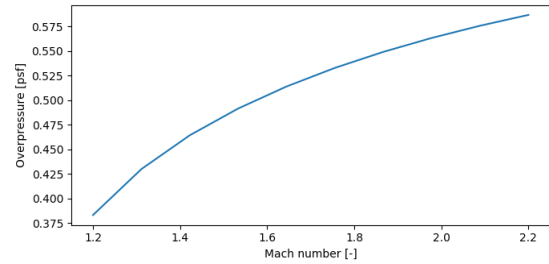


Figure 9.14: Overpressure variation with Mach number

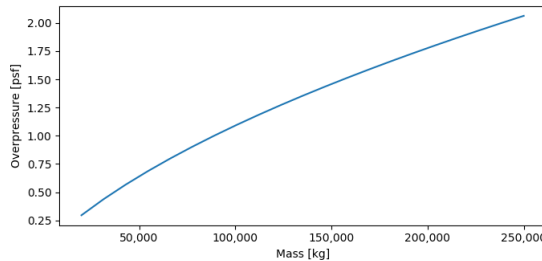


Figure 9.15: Overpressure variation with cruise mass

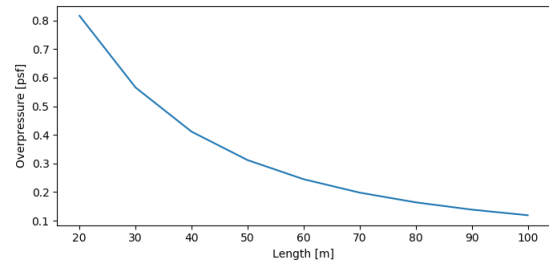


Figure 9.16: Overpressure variation with aircraft length

overpressure above 10 km is caused by the different temperature gradient according to the ISA [111]. The overpressure increases with Mach number, but the differences are small. Between  $M=1.2$  and  $M=2.2$  the overpressure increases by less than 0.2 psf. This indicates that for an optimised SSBJ the boom strength does not need to be a factor in deciding the ideal cruise Mach number.

The strongest effect on overpressure is shown by the aircraft mass. The relation between mass and minimum overpressure is almost linear such that a doubling in mass results in double the overpressure. Figure 9.15 also shows the reason why a SSBJ will be much more realistic to operate than a larger supersonic airliner. The larger weight will make the boom much stronger and it is unlikely that such strong booms can be suppressed to an acceptable level, as explained below in section 9.3.2.

Aircraft length also has a strong influence on boom overpressure. As can be seen in Figure 9.16 a theoretical point exists where the boom can be reduced so much that it either is inaudible or that no boom can be measured on ground at all [104]. This figure also shows the importance of fuselage slenderness, since a more slender fuselage will be longer for the same capacity, therefore increasing length. However, this is not an easy achievement, as Figure 9.17 shows. Here the relationships found between number of passengers, fuselage length and aircraft weight in earlier chapters were used to find the relationship between number of passengers and boom overpressure.

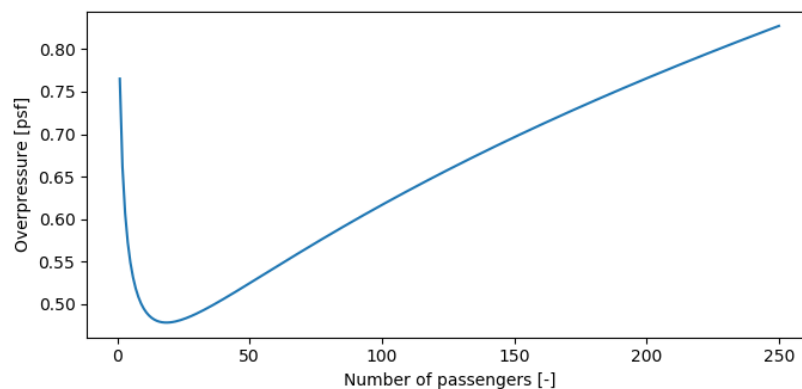


Figure 9.17: Minimum boom strength variation with number of passengers

As can be seen, the overpressure drops steeply for low passenger numbers, after which it keeps growing for passenger numbers above 20. The initial drop is caused by lengthening the fuselage which can be done without changing the total weight much. However, when passenger numbers increase the fuselage will become wider, reducing the slenderness and increasing the effect of weight on the overpressure. This is the reason why the overpressure keeps growing for passenger numbers above 20.

### Limitations

This study however is limited since the method used is only suitable for flat-top sonic boom signatures. While this is a feasible way of reducing the boom loudness, it is not the only way. As explained before a ramped signature as shown in the bottom of Figure 9.5 also decreases sonic boom loudness, but a method to compare the loudness of different boom signatures is not available for the low-fidelity designs created here.

Another limitation which could have consequences for the noise on ground is the so-called focal boom. Flight tests and measurements have shown that during transonic acceleration a large focused boom is generated. The acceleration causes acoustical rays to curve due to the accumulating Mach cones. These acoustical rays then combine into a single, much stronger boom [112] (Figure 9.18). This boom can be up to five times stronger than the cruise boom [113]. The focal boom happens at a flight phase that is so much different to the design cruise conditions (weight is higher while Mach number and altitude are lower). Therefore, shaping the aircraft for low-boom cruise does not necessarily help the aircraft to achieve a shaped sonic boom, as was demonstrated by the F-5SSBD [114]. However, numerical analysis indicates that designing aircraft for low boom does help in strongly reducing the focus boom loudness [115].

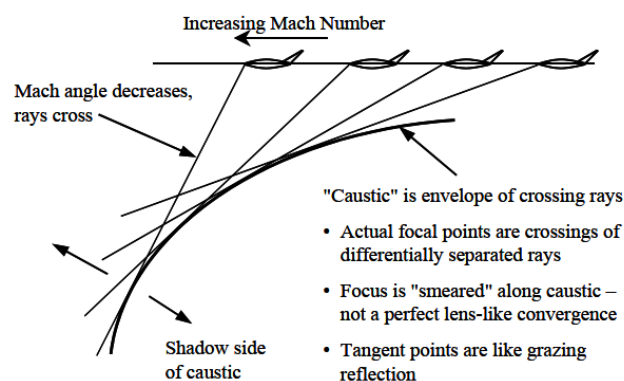


Figure 9.18: Acoustic rays forming a focus boom during transonic acceleration [114]

To find the actually achievable boom strength is not straightforward. CFD, computational aeroacoustics (CAA) and multidisciplinary design, analysis and optimization (MDAO) are usually employed to find an optimal low-boom design solution. These were not used in this thesis, since its goal was to predict a bandwidth of sonic boom loudnesses that are likely to be present on future supersonic aircraft, rather than finding the optimal solution. Therefore, it is likely that any supersonic business jet will produce boom overpressures that are closer to the Seebass and George minimum than the result of the Carlson method.

Besides this, the aircraft designed in this thesis were not designed for low-boom cruise. Designing a low-boom aircraft with exactly the same set of requirements as a high-boom aircraft has major influences. Aronstein and Schueler designed a SSBJs both with and without boom constraint. The result was that the low-boom SSBJ which had an initial overpressure of 0.4 psf was about 25% longer and had an 18% higher MTOW [109]. Welge performed a similar analysis, where a boom loudness reduction from 91 PLdB to 85 PLdB resulted in a 10% increase in fuel burn, 10% reduction in range and an unknown weight increase which would increase the fuel and range penalties while reducing the boom advantage.

It can be concluded that overpressures of 0.5 psf and lower can be achieved by small supersonic aircraft. However, this is likely to result in fuel burn penalties which may render the aircraft not economically viable.

### 9.3.2. Acceptability of boom loudness

The debate on what boom loudness is acceptable for people on ground can in some way be compared to the acceptability of airport community noise. However, in 1973, before the start of Concorde operations, the FAA decided to ban all supersonic flights over the United States to prohibit sonic booms over populated areas<sup>7</sup>. This indicates that there was some awareness that sonic booms of any loudness would be unacceptable by the public. This seems to contradict FAA reports where the effects of sonic booms on people and buildings was investigated. The influence of sonic booms with an overpressure of 1.0 psf on sleep was found to be "functionally not significant" [116]. A study into startle effects of sonic booms concluded that "booms of perhaps 50 N/m<sup>2</sup> [around 1.0 psf] or less might be close to the threshold level for indoor startle effects" [117].

This corresponds to the opinions of scientists from that time that 1.0 psf N-wave booms were the strongest acceptable booms for civil flight. Parker [118] compiled a table with N-wave peak overpressures and the associated phenomena (Table 9.2) which also says booms with an overpressure of 1.0 psf are tolerable.

Table 9.2: Sonic boom noise phenomena

Overpressure [psf]	Resulting physiological reaction	Associated physical phenomena
0.1 to 0.3	Not objectionable	Barely audible explosion
0.3 to 1.0	Tolerable	Distant explosion or thunder
1.0 to 3.0	Objectionable	Close range thunder, some window damage
3.0 to 10.0		Damage to large plate-glass windows
10.0 to 30.0		Definite damage to small barracks-type windows

A criterion proposed by the U.S. Environmental Protection Agency in 1974 recommended that the sonic boom peak overpressure should not be higher than  $0.75/\sqrt{N}$  psf, where  $N$  is the number of sonic booms experienced per day. This relation is shown in Figure 9.19 where it can be seen that the limit overpressure drops to below 0.5 psf when 3 sonic booms per day are experienced.

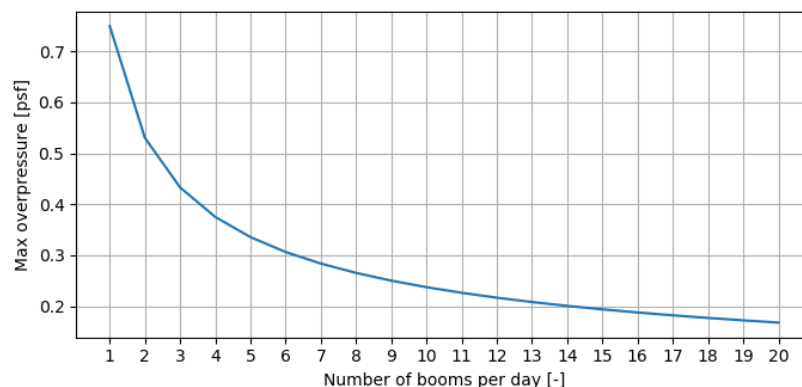


Figure 9.19: Limit boom overpressure suggested by the U.S. Environmental Protection Agency

<sup>7</sup><https://www.nytimes.com/1973/03/28/archives/supersonic-civilianflights-over-us-are-outlawed.html>. Accessed 14 September 2020

More recently the metric for boom strength has shifted from overpressure to loudness. Due to the findings regarding boom shaping it was realised that not only the overpressure plays a role in the boom loudness, but also the pressure rise time. By using a loudness scale in decibel both factors can be taken into account.

For this reason it is impossible to accurately compare sonic boom overpressure and their loudness. Besides this, there is no consensus for which loudness measure represents human perceived loudness of sonic booms in the most accurate way. Among the measures that are considered for describing sonic boom loudness are PNL, weighted Sound Exposure Levels (SELs) and hybrid methods combining multiple weighted SELs [119].

Which sonic booms currently would be considered acceptable is still unknown. Tests will have to prove what noise level will be acceptable for a majority of the public. The NASA X-59 Quiet SuperSonic Technology aircraft (QueSST) is expected to have a maximum overpressure of around 0.4 psf and a loudness of around 75 PLdB [107]. This is comparable to the sound of a car door slam across the street or distant thunder [107]. Due to the expected low noise, the X-59 sonic boom is called a thump by NASA. NASA set a maximum of 85 PLdB for an N+2 SST carrying 35 to 70 passengers [93]. These results are supported by calculations and simulations. The question remains whether these can be reflected in reality. Therefore, the results of the flight tests of the X-59 and the Boom XB-1 are eagerly awaited.

If it turns out to be impossible to reduce the boom to barely audible levels, then there is no future for supersonic aircraft. A strong sonic boom will not only be heard directly below the flight path, but the so-called boom carpet could be as wide as 75 km [112]. The audibility of the boom varies within the carpet, so not all people within the boom carpet would hear the boom, but it is indicative of the potentially large impact even a single supersonic flight has.



# 10

## Conclusion

This thesis was written to fulfil a request from the ICAO CAEP to discuss the acceptability of future supersonic transport aircraft. The goal of this thesis was twofold: to develop a design program for supersonic aircraft and to evaluate the noise production of these aircraft. Therefore two research questions were formulated:

- *Is it possible to create a low-fidelity conceptual SST design using a KBE-like tool?*
- *What will the noise levels of various generated SST concepts be, compared to subsonic aircraft?*

The answer to the first question is that an SST design program has been successfully created. Several separate modules have been built which all had deviations of less than 10% from reality. These modules were connected, resulting in a valid aircraft design with weight overestimations of less than 10%. This is acceptable for a low-fidelity tool.

The answer to the second question is less straightforward. For the airport noise prediction it was found that no publicly available tools could be used. Therefore, this prediction is mostly based on literature. The most contributing factors to supersonic aircraft noise during landing or takeoff compared to subsonic aircraft were found to be the longer landing gear legs and the lower bypass ratio of the engines. The other physical differences like the different wing shape barely contribute to the total noise.

No definitive conclusion could be reached on whether new supersonic aircraft can keep up with the new regulations. Any new noise reduction measures that will be introduced to supersonic aircraft will also find its way to subsonic aircraft. Major noise reduction from advanced supersonic engines is not expected for the near future. The only realistic solution found was to fly a different approach or departure path. This is currently not allowed by regulators, but the FAA recently released a Notice of Proposed Rulemaking intending to relax the noise regulations for light supersonic aircraft and allows for deviations from the standard flight path. This may allow for enough regulatory room for aircraft up to 50 seats.

However, an analysis was performed with Concorde as baseline and introducing various noise reduction measures which indicated that such an improved aircraft would not be able to meet Chapter 4 limits by at least 5 dB. The new ICAO Chapter 14 limits which apply from 2021 will be 7 dB lower while the proposed limit by the FAA lies between the Chapter 4 and Chapter 14 limits. It is unlikely that smaller or larger aircraft will have a much different margin to the noise limits.

The sonic boom analysis showed that a future non-optimised 100-seat aircraft will have a lower boom overpressure than Concorde had. The overpressure variations found with flight parameters were as expected. However, these methods are limited since only a few specific boom signature shapes could be investigated. Optimising an aircraft for low sonic boom can induce weight penalties of up to 20%.

While low-boom flight seems to be possible, it is unknown whether these limitations will allow for profitable flight. In case of multiple supersonic overflights the maximum acceptable sonic boom may need

to become lower than 0.4 psf or 75 PLdB. Sonic booms that have this low energy require either a long aircraft or a low Mach number, both of which make supersonic flight less practical.

In conclusion this thesis gives a little more insight on the noise problems associated with supersonic flight, their origins and possible (partial) solutions. For definitive answers more research is needed with more advanced tools and flight tests. Whether supersonic aircraft noise will be acceptable in the near future is doubtful.

## Recommendations

The research covered in this thesis was aimed at building a design program for the automated conceptual design of supersonic airliners and predicting the noise these aircraft generate. While the design program was successfully built and noise and climate modules were added, many things can be improved to obtain more accurate results. Besides the recommendations Den Boer gave [5], possible improvements that can be made on the subjects investigated in this thesis are written below.

Regarding the aircraft design the following recommendations can be made:

- The design should have an option for having three engines. The current program only allows for either two or four engines. Having three engines may be optimal for aircraft in the 30-100 passenger range.
- The design cruise should be described and analysed in more detail. This would result in a more accurate analysis of the cruise fuel requirement and a better sonic boom prediction
- The engine design method could be optimised in multiple ways. The method by Bos could be evaluated further to implement this in the program. Furthermore, if an automatic way could be found for using and adapting compressor maps these could be combined with software like GSP or GasTurb. It is unsure whether this added complexity would result in higher accuracy for the design point calculation, but it is likely to improve the off-design accuracy.
- The wing design method could be optimised numerically in order to get an optimal wing design. The current design only uses 'best practice' methods and no actual lift/drag optimisation. This will likely improve the aerodynamic performance of the design.
- The fuselage design method assumes a circular fuselage. A differently shaped fuselage may provide more room for passengers and a more optimised volume usage.
- Currently the empennage design has very little influence on the design. To improve this, stability analyses should be performed. Den Boer already has already explained other reasons why having a stability analysis would be beneficial [5].
- The fuselage and wing design and positioning should depend more on the desired area distribution and lift distribution for an optimal low-boom design. Only then the sonic boom loudness can be estimated reliably, taking into account all performance penalties of a typical low-boom design. Such optimisations will likely require the involvement of CFD and CAA.
- Designing the landing gear would help making an accurate design. The weight estimation, landing drag estimation and the noise prediction will all benefit from this.

For the noise analysis the following improvements are suggested:

- Make the aircraft design so detailed that a reliable airport noise estimation using ANOPP or similar programs can be made. This would mainly require a more detailed engine performance analysis, but a landing gear design would be required as well. Improved access to these programs would also be helpful.
- Find a more accurate sonic boom prediction method. While this may not be possible for a low-fidelity conceptual design, a more detailed fuselage volume utilisation and its associated effective

area distribution would result in a better approximation. As Carlson's method only seemed applicable for N-shaped signatures a different method for this would be required as well. Besides this, a more accurate area distribution can also be used for a boom loudness prediction by using methods like those from May [120] or Bolander [121].

# Bibliography

- [1] Candel, S. Concorde and the Future of Supersonic Transport. *Journal of Propulsion and Power*, 20(1):59–68, 2004. ISSN 0748-4658. doi: 10.2514/1.9180.
- [2] Liebhardt, B., Gollnick, V., and Luetjens, K. Estimation of the Market Potential for Supersonic Airliners via Analysis of the Global Premium Ticket Market. In *11th AIAA Aviation Technology, Integration, and Operations (ATIO) Conference*, 2011. doi: 10.2514/6.2011-6806.
- [3] Liebhardt, B., Lütjens, K., Tracy, R. R., and Haas, A. O. Exploring the Prospect of Small Supersonic Airliners - A Business Case Study Based on the Aerion AS2 Jet. In *17th AIAA Aviation Technology, Integration, and Operations Conference*, 2017. doi: 10.2514/6.2017-3588.
- [4] Fahey, D. W., Keim, E. R., Boering, K. A., Brock, C. A., Wilson, J. C., Jonsson, H. H., Anthony, S., Hanisco, T. F., Wennberg, P. O., Miake-Lye, R. C., Salawitch, R. J., Louisnard, N., Woodbridge, E. L., Gao, R. S., Donnelly, S. G., Wamsley, R. C., Del Negro, L. A., Solomon, S., Daube, B. C., Wofsy, S. C., Webster, C. R., May, R. D., Kelly, K. K., Loewenstein, M., Podolske, J. R., and Chan, K. R. Emission Measurements of the Concorde Supersonic Aircraft in the Lower Stratosphere. *Science*, 270(5233):70–74, 1995. ISSN 0036-8075. doi: 10.1126/science.270.5233.70.
- [5] den Boer, M. P. *Assessing the Performance and Climate Effects of Future Supersonic Transport*. Thesis, Delft University of Technology, Faculty of Aerospace Engineering, 2019.
- [6] Torenbeek, E. *Synthesis of Subsonic Airplane design*. Springer Science & Business Media, 1982. ISBN 90-247-2724-3.
- [7] Anderson, John D., J. *Aircraft performance and design*. WCB/McGraw-Hill, Boston, 1999. ISBN 9780070019713.
- [8] Roskam, J. *Airplane Design Part I: Preliminary Sizing of Airplanes*. Airplane Design. DARcorporation, Lawrence, Kansas, 1985. ISBN 188488542X.
- [9] Elmendorp, R., Vos, R., and La Rocca, G. A conceptual design and analysis method for conventional and unconventional airplanes. In *ICAS 2014: Proceedings of the 29th Congress of the International Council of the Aeronautical Sciences, St. Petersburg, Russia, 7-12 September 2014*. International Council of Aeronautical Sciences, 2014.
- [10] Botero, E. M., Wendorff, A., MacDonald, T., Variyar, A., Vegh, J. M., Lukaczyk, T. W., Alonso, J. J., Orra, T. H., and Ilario da Silva, C. R. SUAVE: An Open-Source Environment for Conceptual Vehicle Design and Optimization. In *54th AIAA Aerospace Sciences Meeting*, 2016. doi: 10.2514/6.2016-1275.
- [11] MacDonald, T., Botero, E., Vegh, J. M., Variyar, A., Alonso, J. J., Orra, T. H., and Ilario da Silva, C. R. SUAVE: An Open-Source Environment Enabling Unconventional Vehicle Designs through Higher Fidelity. In *55th AIAA Aerospace Sciences Meeting*. American Institute of Aeronautics and Astronautics, 2017. doi: 10.2514/6.2017-0234.
- [12] EASA. *Certification Specifications and Acceptable Means of Compliance for Large Aeroplanes CS-25*. July 2019.
- [13] Torenbeek, E. *Advanced Aircraft Design : Conceptual Design, Technology and Optimization of Subsonic Civil Airplanes*. Wiley, 2013. ISBN 1299560725 9781299560727 9781118568088 1118568087 9781118568118 1118568117.
- [14] Raymer, D. P. *Aircraft Design: A Conceptual Approach*. American Institute of Aeronautics and Astronautics, Inc., 2018. ISBN 978-1-62410-490-9. doi: 10.2514/4.104909.
- [15] Howe, D. and Rorie, G. *Aircraft Conceptual Design Synthesis*. Professional Engineering Publishing, London, UK, 2000. ISBN 9781860583018. doi: 10.1002/9781118903094.
- [16] Papamoschou, D. and Debiasi, M. Conceptual Development of Quiet Turbofan Engines for Supersonic Aircraft. *Journal of Propulsion and Power*, 19(2):161–169, 2003. ISSN 0748-4658. doi: 10.2514/2.6103.
- [17] Rolls-Royce. *The Jet Engine*. John Wiley & Sons Ltd, 5th edition, 2005. ISBN 9781119065999.

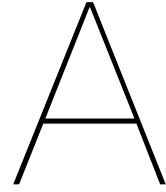
- [18] Leylekian, L., Lebrun, M., and Lempereur, P. An Overview of Aircraft Noise Reduction Technologies. *Aerospace Lab Journal*, 7, 2014. doi: 10.12762/2014.AL07-01.
- [19] Mattingly, J. D., Boyer, K. M., Haven, B. A., Heiser, W. H., and Pratt, D. T. *Aircraft Engine Design*. AIAA Education Series. AIAA, 3rd edition, 2019. ISBN 9781624105173.
- [20] Walsh, P. P. and Fletcher, P. *Gas Turbine Performance*. Blackwell Science, 2nd edition, 2004. ISBN 0-632-06434-X.
- [21] van Buijtenen, J., Visser, W. P. J., Shakariyants, S., and Montella, F. *Gas Turbines, Propulsion and Power, AE2-203*. Delft, 1st edition, 2011.
- [22] Edwards, J. T. Reference Jet Fuels for Combustion Testing. In *55th AIAA Aerospace Sciences Meeting*, 2017. doi: 10.2514/6.2017-0146.
- [23] Yin, F. *Modeling and Characteristics of a Novel Multi-Fuel Hybrid Engine for Future Aircraft*. Thesis, Delft University of Technology, 2016.
- [24] Zukoski, E. E. Afterburners. In Oates, G., editor, *The Aerothermodynamics of Aircraft Gas Turbine Engines*, AFAPL-TR-78-52, 1978. Air Force Aero Propulsion Laboratory.
- [25] Marshall, R. L., Canuel, G. E., and Sullivan, D. J. Combustion in Advanced Gas Turbine Systems. In Smith, I. E., editor, *International Propulsion Symposium*. Pergamon Press, 1968. ISBN 1483186369.
- [26] Isaac, J., Ramesh, N., Krishnakumar, V., Rajashekar, C., Shyamsundar, S., Haran, A., and Sundararajan, V. A Methodology for Afterburner Evaluation. In *3rd National Conference on Air Breathing Engines and Aerospace Propulsion*, 1996.
- [27] Mattingly, J. D., Heiser, W. H., and Pratt, D. T. *Aircraft Engine Design*. American Institute of Aeronautics & Astronautics, Reston, VA, 2nd edition, 2002. ISBN 160086144X.
- [28] Jenkinson, L. R., Simpkin, P., and Rhodes, D. *Civil Jet Aircraft Design*. Arnold, 1999. ISBN 0 340 74152 X.
- [29] Kurzke, J. and Halliwell, I. *Propulsion and Power: An Exploration of Gas Turbine Performance Modeling*. Springer, 2018. ISBN 978-3-319-75977-7. doi: 10.1007/978-3-319-75979-1.
- [30] Visser, W. P. J. and Broomhead, M. J. GSP, a Generic Object-Oriented Gas Turbine Simulation Environment. In *ASME Turbo Expo 2000: Power for Land, Sea, and Air*. American Society of Mechanical Engineers, 2000. doi: 10.1115/2000-GT-0002.
- [31] Kurzke, J. Advanced User-Friendly Gas Turbine Performance Calculations on a Personal Computer. In *ASME 1995 International Gas Turbine and Aeroengine Congress and Exposition*, 1995. doi: 10.1115/95-gt-147.
- [32] Kurzke, J. How to Create a Performance Model of a Gas Turbine From a Limited Amount of Information. In *ASME Turbo Expo 2005: Power for Land, Sea, and Air*, pages 145–153, 2005. doi: 10.1115/GT2005-68536.
- [33] Mirza-Baig, F. S. and Saravanamuttoo, H. I. H. Off-Design Performance Prediction of Turbofans Using Gasdynamics. In *ASME 1991 International Gas Turbine and Aeroengine Congress and Exposition*. American Society of Mechanical Engineers, 1991. doi: 10.1115/91-GT-389.
- [34] Bos, D. A flexible method for the off-design analysis of SST powerplant installations suitable for global optimization. *Aircraft Design*, 1(1):13–24, 1998. doi: 10.1016/S1369-8869(98)00003-2.
- [35] Silberhorn, D. and Schaupp, D. Conceptual Design and Analysis of a High-Efficient Low-Emission Supersonic Aircraft HELESA. Report, Institute of Aircraft Design, University Stuttgart, 2017.
- [36] Fenbert, J. W., Ozoroski, L. P., Geiselhart, K. A., Shields, E. W., and McElroy, M. O. Concept Development of a Mach 2.4 High-Speed Civil Transport. Report TP-1999-209694, NASA, 1999.
- [37] Lowrie, B. W. and Portejoie, E. Two Variable Engine Cycle Concepts for Second Generation Supersonic Transport. *SAE Transactions*, pages 1718–1722, 1990. ISSN 0096-736X. doi: 10.4271/901892.
- [38] Agosta, R., Bilbija, D., Deutsch, M., Gallant, D., Rose, D., Shreve, G., Smario, D., and Suffredini, B. The Edge supersonic transport. Report CR-192074, NASA, 1992.
- [39] Stoney, W. E. J. Transonic drag measurements of eight body-nose shapes. Report RM L53K17, NACA, 1954.
- [40] Seiff, A. and Sandahl, C. A. The Effect of Nose Shape on the Drag of Bodies of Revolution at

- Zero Angle of Attack. Report RM A51J25, NACA, 1951.
- [41] Wallskog, H. A. and Hart, R. G. Investigation of the Drag of Blunt-nosed Bodies of Revolution in Free Flight at Mach Numbers from 0.6 to 2.3. Report RM L53D14a, NACA, 1953.
- [42] Hoerner, S. F. *Fluid-Dynamic Drag*. Hoerner Fluid Dynamics, USA, 1965.
- [43] Kramer, L. J., Williams, S., Arthur, T., Bailey, R., Shelton, K., Severance, K., and Kibler, K. Initial Flight Testing of an eXternal Vision System (XVS) for the Low Boom Flight Demonstrator (LBFD). In *2018 Flight Testing Conference*, Atlanta, GA, 2018. doi: 10.2514/6.2018-3411.
- [44] Wells, D. P., Horvath, B. L., and McCullers, L. A. The Flight Optimization System Weights Estimation Method. Report TM-2017-219627-Vol. I, NASA, 2017.
- [45] Roskam, J. *Aircraft Design Part II: Preliminary Configuration Design and Integration of the Propulsion System*. Airplane Design. DARcorporation, 1985. ISBN 1884885438.
- [46] Whitford, R. *Design for Air Combat*. Jane's, 1987. ISBN 9780710604262.
- [47] Jones, R. T. The oblique wing—aircraft design for transonic and low supersonic speeds. *Acta Astronautica*, 4(1):99–109, 1977. ISSN 0094-5765. doi: 10.1016/0094-5765(77)90035-2.
- [48] Galloway, T., Gelhausen, P., Moore, M., and Waters, M. Oblique wing supersonic transport concepts. In *Guidance, Navigation and Control Conference*, 1992. doi: 10.2514/6.1992-4230.
- [49] Van der Velden, A. J. M. and Kroo, I. The Aerodynamic Design of the Oblique Flying Wing Supersonic Transport. Report CR 177552, NASA, 1990.
- [50] Leyman, C. S. A review of the technical development of Concorde. *Progress in Aerospace Sciences*, 23(3):185–238, 1986. ISSN 0376-0421. doi: 10.1016/0376-0421(86)90007-2.
- [51] Matsushima, K., Iwamiya, T., and Nakahashi, K. Wing design for supersonic transports using integral equation method. *Engineering Analysis with Boundary Elements*, 28(3):247–255, 2004. ISSN 0955-7997. doi: 10.1016/S0955-7997(03)00055-9.
- [52] Jones, R. T. Wing plan forms for high-speed flight. Report TN 1033, NACA, 1946.
- [53] Turner, H. Fuel Management for Concorde: A brief account of the fuel system and the fuel pumps developed for the aircraft. *Aircraft Engineering and Aerospace Technology*, 43(3):36–39, 1971. doi: 10.1108/eb034746.
- [54] Hoak, D. E. and Finck, R. D. USAF Stability and Control DATCOM. Report, Air Force Flight Dynamics Laboratory, 1978.
- [55] Polhamus, E. C. Charts for predicting the subsonic vortex-lift characteristics of arrow, delta, and diamond wings. Report TN D-6243, NASA, 1971.
- [56] Torenbeek, E., Jesse, E., and Laban, M. Conceptual Design and Analysis of a Mach 1.6 Airliner. In *10th AIAA/ISSMO Multidisciplinary Analysis and Optimization Conference*, Multidisciplinary Analysis Optimization Conferences. American Institute of Aeronautics and Astronautics, 2004. doi: 10.2514/6.2004-4541.
- [57] Williams, J. E. and Vukelich, S. R. The USAF Stability and Control Digital DATCOM. Report TR-79-3032, USAF, 1979.
- [58] Snow, R. M. and Bonney, E. A. Aerodynamic Characteristics of Wings at Supersonic Speeds. Report 55, The Johns Hopkins University Applied Physics Laboratory, 1947.
- [59] Roskam, J. *Aircraft Design Part V: Component weight estimation*. Airplane Design. DARcorporation, 1985. ISBN 1884885500.
- [60] Nicolai, L. and Carichner, G. *Fundamentals of Aircraft and Airship Design*. American Institute of Aeronautics and Astronautics, 2010. ISBN 9781600867514.
- [61] Kroo, I. and Shevell, R. *Aircraft Design: Synthesis and Analysis*. Desktop Aeronautics, 2001. Digital version 0.99.
- [62] Maglieri, D. J. Compilation and Review of Supersonic Business Jet Studies from 1963 through 1995. Report CR-2011-217144, NASA, 2011.
- [63] ICAO. *Annex 16 to the Convention on International Civil Aviation: Environmental Protection: Volume I - Aircraft Noise*. International Civil Aviation Organization, Quebec, 2017.
- [64] Ruijgrok, G. J. J. *Elements of aviation acoustics*. VSSD, Delft, 2nd edition, 2009. ISBN 9789065622037.
- [65] Filippone, A. Aircraft noise prediction. *Progress in Aerospace Sciences*, 68:27–63, 2014. ISSN 0376-0421. doi: 10.1016/j.paerosci.2014.02.001.
- [66] Farassat, F. and Casper, J. H. Towards an Airframe Noise Prediction Methodology: Survey

- of Current Approaches. In *44th AIAA Aerospace Sciences Meeting and Exhibit*, 2006. doi: 10.2514/6.2006-210.
- [67] Crighton, D. G. Aircraft Noise. In Hubbard, H. H., editor, *Aeroacoustics of Flight Vehicles: Theory and Practice*, volume 1: Noise Sources, Hampton, VA, 1991.
- [68] Crighton, D. G. Radiation from vortex filament motion near a half plane. *Journal of Fluid Mechanics*, 51(2):357–362, 1972. ISSN 0022-1120. doi: 10.1017/S0022112072001235.
- [69] Lighthill, M. J. and Newman, M. H. A. On sound generated aerodynamically I. General theory. *Proceedings of the Royal Society of London. Series A. Mathematical and Physical Sciences*, 211 (1107):564–587, 1952. doi: 10.1098/rspa.1952.0060.
- [70] Lighthill, M. J. On sound generated aerodynamically II. Turbulence as a source of sound. *Proceedings of the Royal Society of London. Series A. Mathematical and Physical Sciences*, 222 (1148):1–32, 1954. doi: 10.1098/rspa.1954.0049.
- [71] Goldstein, M. E. A generalized acoustic analogy. *Journal of Fluid Mechanics*, 488:315–333, 2003. ISSN 0022-1120. doi: 10.1017/S0022112003004890.
- [72] Bertsch, L., Simons, D. G., and Snellen, M. Aircraft Noise: The major sources, modelling capabilities, and reduction possibilities. Report IB 224-2015 A 110, DLR, 2015.
- [73] Raney, J. P. Development of a new computer system for aircraft noise prediction. In *2nd Aeroacoustics Conference*, 1975. doi: 10.2514/6.1975-536.
- [74] Lopes, L. and Burley, C. Design of the Next Generation Aircraft Noise Prediction Program: ANOPP2. In *17th AIAA/CEAS Aeroacoustics Conference (32nd AIAA Aeroacoustics Conference)*, 2011. doi: 10.2514/6.2011-2854.
- [75] Malbéqui, P., Rozenberg, Y., and Bulté, J. Aircraft noise prediction in the IESTA program. In *3rd European Conference for Aero-Space Sciences*, 2009.
- [76] Brunet, M., Malbéqui, P., and Ghedhaifi, W. A novel approach to air transport system environmental impact evaluation through physical modelling and simulation. In *26th International Congress of the Aeronautical Sciences (ICAS'08)*, 2008.
- [77] Zellmann, C., Wunderli, J. M., and Schäffer, B. SonAIR-Data acquisition for a next generation aircraft noise simulation model. In *42nd International Congress and Exposition on Noise Control Engineering*, pages 842–850, 2013.
- [78] Bertsch, E.-L. *Noise Prediction within Conceptual Aircraft Design*. Thesis, TU Braunschweig / DLR, 2013.
- [79] Bertsch, L., Dobrzynski, W., and Guérin, S. Tool Development for Low-Noise Aircraft Design. *Journal of Aircraft*, 47(2):694–699, 2010. ISSN 0021-8669. doi: 10.2514/1.43188.
- [80] Zorumski, W. E. Aircraft noise prediction program theoretical manual, part 2. Report TM-83199-PT-2, NASA, 1982.
- [81] Smith, M., Lowrie, B., Brooks, J., and Bushell, K. Future Supersonic Transport Noise - Lessons from the Past. In *24th Joint Propulsion Conference*, 1988. doi: 10.2514/6.1988-2989.
- [82] Ffowcs Williams, J. E. and Hall, L. H. Aerodynamic sound generation by turbulent flow in the vicinity of a scattering half plane. *Journal of Fluid Mechanics*, 40(4):657–670, 1970. ISSN 0022-1120. doi: 10.1017/S0022112070000368.
- [83] Dobrzynski, W. Almost 40 Years of Airframe Noise Research: What Did We Achieve? *Journal of Aircraft*, 47(2):353–367, 2010. doi: 10.2514/1.44457.
- [84] Fink, M. R. Noise Component Method for Airframe Noise. *Journal of Aircraft*, 16(10):659–665, 1979. doi: 10.2514/3.58586.
- [85] Astley, R., Agarwal, A., Joseph, P., Self, R., Smith, M., Sugimoto, R., and Tester, B. Predicting and reducing aircraft noise. In *14th International Congress on Sound and Vibration (12/07/07)*, 2007.
- [86] Simons, D. G., Snellen, M., Merino-Martinez, R., and Malgoezar, A. Noise breakdown of landing aircraft using a microphone array and an airframe noise model. In *INTER-NOISE and NOISE-CON Congress and Conference Proceedings*, volume 255, pages 2725–2736. Institute of Noise Control Engineering, 2017. ISBN 0736-2935.
- [87] Guo, Y. A model for slat noise generation. In *3rd AIAA/CEAS Aeroacoustics Conference*, 1997. doi: 10.2514/6.1997-1647.
- [88] Guo, Y. P., Yamamoto, K. J., and Stoker, R. W. Experimental Study on Aircraft Landing Gear

- Noise. *Journal of Aircraft*, 43(2):306–317, 2006. doi: 10.2514/1.11085.
- [89] Antoine, N. E. and Kroo, I. M. Aircraft Optimization for Minimal Environmental Impact. *Journal of Aircraft*, 41(4):790–797, 2004. doi: 10.2514/1.71.
- [90] Strang, W. J. and McKinlay, R. M. Concorde in service. *The Aeronautical Journal*, 83(818): 39–52, 1979. ISSN 0001-9240. doi: 10.1017/S0001924000095427.
- [91] Lockard, D. P. and Lilley, G. M. The Airframe Noise Reduction Challenge. Report TM-2004-213013, NASA, 2004.
- [92] Huff, D. L., Henderson, B. S., Berton, J. J., and Seidel, J. A. Perceived Noise Analysis for Offset Jets Applied to Commercial Supersonic Aircraft. In *54th AIAA Aerospace Sciences Meeting*, 2016. doi: 10.2514/6.2016-1635.
- [93] Morgenstern, J., Buonanno, M., Yao, J., Murugappan, M., Paliath, U., Cheung, L., Malcevic, I., Ramakrishnan, K., Pastouchenko, N., and Wood, T. Advanced Concept Studies for Supersonic Commercial Transports Entering Service in the 2018-2020 Period Phase 2. Report CR-2015-218719, NASA, 2015.
- [94] Willis, E. Variable-cycle engines for supersonic cruise aircraft. Report TM X-73463, NASA, 1976.
- [95] Berton, J. J., Haller, W. J., Senick, P. F., Jones, S. M., and Seidel, J. A. A comparative propulsion system analysis for the high-speed civil transport. Report TM-2005-213414, NASA, 2005.
- [96] Berton, J. J., Jones, S. M., Seidel, J. A., and Huff, D. L. Advanced Noise Abatement Procedures for a Supersonic Business Jet. Report TN-43842, NASA, 2017.
- [97] FAA. Noise Certification of Supersonic Airplanes. *Federal Register*, 85(71):20431–20447, April 13 2020.
- [98] Berton, J. J., Huff, D. L., Geiselhart, K., and Seidel, J. Supersonic Technology Concept Aeroplanes for Environmental Studies. In *AIAA Scitech 2020 Forum*, 2020. doi: 10.2514/6.2020-0263.
- [99] Tanner, C. S. Noise measurement of Concorde 02 approach and takeoff at Dallas - Ft. Worth and Dulles International Airports. Report EPA 550/9-74-013, U.S. Environmental Protection Agency. Office of Noise Abatement and Control, 1974.
- [100] ANOTEC Consulting. Background Noise level and noise levels from En Route Aircraft (BA-NOERAC). Report EASA.2008/OP14, EASA, 2009.
- [101] Powell, C. A. FAA/NASA En Route Noise Symposium. Report CP-3067, NASA, 1990.
- [102] Anderson, J. D. *Fundamentals of Aerodynamics*. McGraw-Hill, New York, 6th edition, 2016. ISBN 9781259251344.
- [103] Plotkin, K. J. and Maglieri, D. J. Sonic boom research: History and future. In *33rd AIAA Fluid Dynamics Conference and Exhibit*, 2003. doi: 10.2514/6.2003-3575.
- [104] Seebass, R. and George, A. R. Sonic-Boom Minimization. *The Journal of the Acoustical Society of America*, 51(2):686–694, 1972. ISSN 0001-4966. doi: 10.1121/1.1912902.
- [105] Seebass, R. and Argrow, B. Sonic boom minimization revisited. In *2nd AIAA Theoretical Fluid Mechanics Meeting*, 1998. doi: 10.2514/6.1998-2956.
- [106] Pawlowski, J. W., Graham, D. H., Boccadoro, C. H., Coen, P. G., and Maglieri, D. J. Origins and Overview of the Shaped Sonic Boom Demonstration Program. In *43rd AIAA Aerospace Sciences Meeting & Exhibit*, 2005. doi: 10.2514/6.2005-5.
- [107] Doebler, W. J. and Rathsam, J. How loud is X-59's shaped sonic boom? *Proceedings of Meetings on Acoustics*, 36(1):040005, 2019. doi: 10.1121/2.0001265.
- [108] Carlson, H. W. Simplified sonic-boom prediction. Report TP-1122, NASA, 1978.
- [109] Aronstein, D. C. and Schueler, K. L. Two Supersonic Business Aircraft Conceptual Designs With and Without Sonic Boom Constraint. *Journal of Aircraft*, 42(3):775–786, 2005. ISSN 0021-8669. doi: 10.2514/1.7578.
- [110] Mack, R. J. A Supersonic Business-Jet Concept Designed for Low Sonic Boom. Report TM-2003-212435, NASA, 2003.
- [111] Kane, E. J. and Palmer, T. Y. Meteorological Aspects of the Sonic Boom. Report RD64-160, FAA, 1965.
- [112] Coulouvrat, F. The Challenges of Defining an Acceptable Sonic Boom Overland. In *15th AIAA/CEAS Aeroacoustics Conference (30th AIAA Aeroacoustics Conference)*, Aeroacoustics Conferences. American Institute of Aeronautics and Astronautics, 2009. doi: 10.2514/6.

- 2009-3384.
- [113] Downing, M., Zamot, N., Moss, C., Morin, D., Wolski, E., Chung, S., Plotkin, K., and Maglieri, D. Controlled focused sonic booms from maneuvering aircraft. *The Journal of the Acoustical Society of America*, 104(1):112–121, 1998. doi: 10.1121/1.423261.
- [114] Plotkin, K., Martin, R., Maglieri, D., Haering, E., and Murray, J. Pushover Focus Booms from the Shaped Sonic Boom Demonstrator. In *43rd AIAA Aerospace Sciences Meeting and Exhibit*, 2005. doi: 10.2514/6.2005-11.
- [115] Kanamori, M., Takahashi, T., and Makino, Y. Effect of Low-Boom Waveform on Focus Boom Using Lossy Nonlinear Tricomi Analysis. *AIAA Journal*, 55(6):2029–2042, 2017. doi: 10.2514/1.J055226.
- [116] Collins, W. E. and Iampietro, P. F. Simulated Sonic Booms and Sleep: Effects of Repeated Booms of 1.0 PSF. Report FAA-AM-72-35, FAA Civil Aeromedical Institute, 1972.
- [117] Thackray, R. I., Rylander, R., and Touchstone, R. M. Sonic Boom Startle Effects—Report of a Field Study. Report FAA-AM-73-11, FAA Civil Aeromedical Institute, 1973.
- [118] Parker, M. A. The Sonic Boom Problem: An examination of the overpressures on the ground caused by supersonic aircraft with particular application to Concorde. *Aircraft Engineering and Aerospace Technology*, 40(8):30–38, 1968. ISSN 0002-2667. doi: 10.1108/eb034413.
- [119] Page, J. A. and Loubeau, A. Overall vehicle system noise: sonic boom. *CEAS Aeronautical Journal*, 10(1):335–353, 2019. ISSN 1869-5590. doi: 10.1007/s13272-019-00379-0.
- [120] May, D. N. The loudness of sonic booms heard outdoors as simple functions of overpressure and rise time. *Journal of Sound and Vibration*, 18(1):31–43, 1971. ISSN 0022-460X. doi: 10.1016/0022-460X(71)90628-6.
- [121] Bolander, C. R., Hunsaker, D. F., Shen, H., and Carpenter, F. L. Procedure for the Calculation of the Perceived Loudness of Sonic Booms. In *AIAA Scitech 2019 Forum*, 2019. doi: 10.2514/6.2019-2091.
- [122] Sun, J., Hoekstra, J., and Ellerbroek, J. Aircraft Drag Polar Estimation Based on a Stochastic Hierarchical Model. In *8th SESAR Innovation Days*, 2018. doi: urn:NBN:nl:ui:24-uuid:9977a616-4506-4acb-9d27-b9e27f9ddb8d.
- [123] Obert, E. *Aerodynamic design of transport aircraft*. Ios Press ; Delft University of Technology, Faculty of Aerospace Engineering, Section Design of Aircraft and Rotorcraft, Amsterdam; [Delft], 2009. ISBN 9781586039707 1586039709.
- [124] Mathieu, M. S., Marin, A. M., Stephenson, K. J., Beard, J. E., Castillo, E., Weddle-Weaver, C., Teni, D., and Takahashi, T. T. Preliminary Design of an N+1 Overwater Supersonic Commercial Transport Aircraft. In *55th AIAA Aerospace Sciences Meeting*, 2017. doi: 10.2514/6.2017-1387.
- [125] Mascitti, V. R. A preliminary study of the performance and characteristics of a supersonic executive aircraft. Report TM-74055, NASA, 1977.
- [126] SAE. Aircraft Propulsion System Performance Station Designation. Manual AS755F, SAE International, 2014.
- [127] Bray, D., Lawson, N., and Harding, S. Supersonic business jet aircraft design. In *ICAS 2002*, 2002.
- [128] Whitham, G. B. The flow pattern of a supersonic projectile. *Communications on Pure and Applied Mathematics*, 5(3):301–348, 1952. ISSN 0010-3640. doi: 10.1002/cpa.3160050305.
- [129] Walkden, F. The Shock Pattern of a Wing-Body Combination, Far from the Flight Path. *Aeronautical Quarterly*, 9(2):164–194, 1958. ISSN 0001-9259. doi: 10.1017/S0001925900001372.
- [130] Maglieri, D. J., Bobbitt, P. J., Plotkin, K. J., Shepherd, K. P., Coen, P. G., and Richwine, D. M. Sonic boom: Six decades of research. Report SP-2014-622, NASA, 2014.



# Validation data for design point method

This appendix shows the data used to validate the results of the design point calculation. Most data is obtained from reliable sources, but for some data less reliable references had to be used and sometimes estimations had to be made. The data is shown in Table A.1. The explanation for estimations and assumptions made can be found in the footnotes below the table.

Table A.1: Validation data for design point calculation

Variable	Concorde	NLR	HELESA	SC-13	SSXJET	A320-232
$M_{cr_{sup}}$ [-]	2.02	1.6	1.6	1.3	2.2	
$h_{cr_{sup}}$ [m]	18,300	16,000	15,000	14,000	18,288	
$M_{cr_{sub}}$ [-]	0.95	0.95	0.92	0.95	0.95	0.78
$h_{cr_{sub}}$ [m]	9,000	9,450	13,000	8,840	9,144	12,000
$h_{airport}$ [m]	0 <sup>1</sup>	0 <sup>1</sup>	0 <sup>1</sup>	0 <sup>1</sup>	0 <sup>1</sup>	0 <sup>1</sup>
$s_{TO}$ [m]	3,140	3,048	1,900	2,164	1,981	1,890
$s_{land}$ [m]	2,220	2,000	1,150			1,491
$V_{appr}$ [m/s]	92	80	67	90	77	59 <sup>2</sup>
$A_w$ [-]	1.7	2.8	1.28 <sup>3</sup>	2.7	1.84	9.5
$n_{eng}$ [-]	4	4	2	2	2	2
$\Lambda_{LE,eq}$ [°]	55	62.5	-58 <sup>4</sup>	56.5	67.5	25
$C_{L_{max,clean}}$ [-]	1 <sup>5</sup>	0.6 <sup>6</sup>	0.8 <sup>7</sup>	0.6	0.8	1.5 <sup>8</sup>
$C_{L_{max,land}}$ [-]	1 <sup>9</sup>	1.1 <sup>9</sup>	1.75	1	1	3 <sup>8</sup>
$C_{L_{max,TO}}$ [-]	1 <sup>5</sup>	0.7	1.5	0.8 <sup>10</sup>	0.85	2 <sup>8</sup>
$C_{D_{0,sub}}$ [-]	0.008 <sup>11</sup>	0.006	0.012	0.011	0.017	0.023 <sup>12</sup>
$C_{D_{0,sup}}$ [-]	0.012	0.008	0.016	0.014	0.013	0.023 <sup>12</sup>
$C_{D_{0,lg}}$ [-]	0.01 <sup>13</sup>	0.01 <sup>13</sup>	0.01 <sup>13</sup>	0.01 <sup>13</sup>	0.008	0.017 <sup>12</sup>

<sup>1</sup>Set to zero, because takeoff data was given for sea level

<sup>2</sup>Based on Eurocontrol data

<sup>3</sup>Variable sweep wing. Aspect ratio varies between 3.4 for takeoff and landing ( $\Lambda_{LE} = 20^\circ$ ), 2.02 for subsonic cruise ( $\Lambda_{LE} = 45^\circ$ ) and 1.28 for supersonic cruise ( $\Lambda_{LE} = 58^\circ$ )

<sup>4</sup>Forward sweep, varies between  $-20^\circ$  for takeoff and landing,  $-45^\circ$  for subsonic cruise and  $-58^\circ$  for supersonic cruise

<sup>5</sup>Aircraft has no flaps, so clean, takeoff and landing  $C_L$  should be equal

<sup>6</sup>Based on known lift parameters

<sup>7</sup>Based on average  $C_{L_{max,clean}}$  of supersonic aircraft

<sup>8</sup>Estimate, based on typical airliner numbers

<sup>9</sup>Calculated from landing speed

<sup>10</sup>Average between clean and landing lift coefficient

<sup>11</sup>Based on average difference between supersonic and subsonic  $C_{D_0}$

<sup>12</sup>Based on data from [122]

<sup>13</sup>Based on [8]

Table A.1: Validation data for design point calculation

Variable	Concorde	NLR	HELESA	SC-13	SSXJET	A320-232
$e_{TO}$ [-]	0.90 <sup>14</sup>	0.66 <sup>14</sup>	0.96 <sup>15</sup>	0.77 <sup>14</sup>	0.65 <sup>14</sup>	0.93 <sup>14</sup>
$e_{land}$ [-]	0.95 <sup>16</sup>	0.71 <sup>16</sup>	0.99 <sup>15</sup>	0.82 <sup>16</sup>	0.70 <sup>16</sup>	0.98 <sup>1</sup>
$e_{sub}$ [-]	0.87 <sup>15</sup>	0.63 <sup>15</sup>	0.93 <sup>15</sup>	0.74 <sup>15</sup>	0.62 <sup>15</sup>	0.9 <sup>12</sup>
$e_{appr}$ [-]	0.91 <sup>17</sup>	0.67 <sup>17</sup>	0.96 <sup>17</sup>	0.78 <sup>17</sup>	0.66 <sup>17</sup>	0.94 <sup>17</sup>
$W_{MTO}$ [kg]	185,065	340,000	43,100	140,160	34,360	78,000
$W_{land,max}$ [kg]	111,130	250,000	28,015 <sup>18</sup>	83,379	24,346 <sup>19</sup>	66,000
$W_{sub,start}$ [kg]	165,000 <sup>20</sup>	305,000 <sup>20</sup>	38,500 <sup>20</sup>	125,000 <sup>20</sup>	31,000 <sup>20</sup>	76,000 <sup>12</sup>
$W_{sup,mid}$ [kg]	130,000 <sup>21</sup>	240,000 <sup>21</sup>	30,000 <sup>21</sup>	100,000 <sup>21</sup>	24,000 <sup>21</sup>	
$\eta_{inlet}$ [-]	0.85 <sup>22</sup>	0.9 <sup>22</sup>	0.9 <sup>22</sup>	0.9 <sup>22</sup>	0.9 <sup>22</sup>	0.98 <sup>22</sup>
$BPR$ [-]	0	1.5	2.5	1	0	4.8
$WS_{ref}$ [kg/m <sup>2</sup> ]	5,068	4,276	4,365	4,932	3,907	6,252
$TW_{ref}$ [-]	0.37	0.35	0.45	0.58	0.37	0.31
Source(s)	[122] <sup>23,24</sup>	[56]	[35]	[124]	[125]	<sup>25</sup>

<sup>14</sup>Subsonic  $e$  + 0.03, based on [123]<sup>15</sup>Calculated using an equation from [14]<sup>16</sup>Subsonic  $e$  + 0.05, based on [123]<sup>17</sup>Average of value for subsonic flight and landing<sup>18</sup>Based on the average MTOW/MLW relation of multiple supersonic aircraft:  $MLW = 0.65 \cdot MTOW$ <sup>19</sup>Normal landing weight + 20%<sup>20</sup>Based on mission profile from [5], assumed to be 89% of MTOW<sup>21</sup>Based on mission profile from [5], assumed to be 70% of MTOW<sup>22</sup>Based on [19]<sup>23</sup><http://www.concordesst.com>. Accessed 20 November 2019<sup>24</sup>[https://janes.ihs.com/JAWAInServices/Display/jau\\_0804-jau\\_](https://janes.ihs.com/JAWAInServices/Display/jau_0804-jau_). Accessed 20 December 2019<sup>25</sup><https://janes.ihs.com/JAWADevelopmentProduction/Display/jawa0416-jawa>. Accessed 20 December 2019

# B

## Support data for engine method

This appendix shows data that were used during the creation of the engine module. Section B.1 shows validation data for both the cycle calculations and the design method. Section B.2 explains the station numbering used in the program and this report.

### B.1. Validation data for engine design

To get a proper basis for engine parameters, a few reference engines were selected and an attempt was made to validate the data from Mattingly [19]. The parameters mentioned there are listed in Table B.1 below.

Table B.1: Component efficiencies and pressure ratios [19]

Component	Type	Variable	1965-1985	1985-2005	2005-2025	2025-2045
Inlet	Subsonic, engines in nacelles	$\frac{P_{0,2}}{P_{0,0 \max}}$	0.95	0.98	0.995	0.998
	Subsonic, engines in airframe		0.93	0.96	0.98	0.985
	Supersonic, engines in airframe		0.90	0.94	0.96	0.97
Compressor		$\eta_{pol_{comp}}$	0.84	0.88	0.90	0.91
Fan		$\eta_{pol_{fan}}$	0.82	0.86	0.89	0.92
Combustor		$\Pi_{cc}$	0.92	0.94	0.95	0.96
		$\eta_{cc}$	0.94	0.99	0.999	0.999
Turbine	uncooled	$\eta_{pol_{turb}}$	0.85	0.89	0.90	0.91
	cooled		0.83	0.87	0.89	0.9
Nozzle	Fixed-area, convergent	$\Pi_{nozzle}$	0.97	0.98	0.995	0.997
	Variable-area, convergent		0.96	0.97	0.98	0.99
	Variable-area, convergent-divergent		0.93	0.95	0.97	0.98
Combustor exit		$T_{0,4_{\max}}$ [K]	1390	1780	2000	2220

Table B.2 shows the data for these engines that were either selected or adapted from the book or taken from data sources like Janes. Using these data, the design point calculation method was run, which resulted in an estimated fuel flow rate required for the specified thrust. This value could then be compared to the real fuel flow rate to say something about the accuracy of the program.

The thrust, fuel data, TIT and certification year, as well as the pressure ratios (except  $\Pi_{cc}$ ) were taken

Table B.2: Engine data for validation of efficiency numbers

Engine	CFM CF6-6D	CFM CF6- 80E1A2	GE GE- 90-85B	GE F-110- GE-100	CFM CF34-1A	CFM CF34-8C1	P&W PW6122A	P&W JT8D-7
BPR	5.9	5.3	8.3	0.76	6.2	4.8	5	1.07
OPR	24.3	32.4	36.9	30.4	21	28	26.1	15.4
$\Pi_{fan}$	1.6	1.6	1.4	1.5	1.5	1.5	1.4	1.9
$\Pi_{LPC}$	2.6	3.4	1.1	1.0	1.6	2.1	1.7	1.3
$\Pi_{HPC}$	6.0	6.0	23.0	20.3	8.5	9.0	11.0	6
$\Pi_{cc}$	0.96	0.96	0.94	0.94	0.92	0.94	0.94	0.92
TIT	1603	1630	1592	1650	1130	1350	1500	1200
$\eta_{intake}$	0.95	0.95	0.98	0.94	0.95	0.98	0.98	0.95
$\eta_{pol_{fan}}$	0.87	0.87	0.86	0.86	0.82	0.86	0.86	0.82
$\eta_{pol_{comp}}$	0.87	0.87	0.88	0.88	0.84	0.88	0.88	0.84
$\eta_{cc}$	0.94	0.97	0.99	0.99	0.94	0.99	0.99	0.94
$\eta_{mech}$	0.99	0.99	0.99	0.99	0.99	0.99	0.99	0.99
$\eta_{pol_{turb}}$	0.9	0.9	0.87	0.87	0.83	0.87	0.87	0.89
$\eta_{nozzle}$	0.97	0.97	0.98	0.95	0.97	0.98	0.98	0.97
$\dot{m}$	593	873.6	1415	122.4	151	200	290	143
year	1970	2003	1995	1986	1982	1999	2004	1964

from Janes<sup>1</sup>. All other data were estimated based on the suggestions by Mattingly. The only deviations from the exact numbers listed in Table B.1 are for interpolating. The pressure ratios for the fan, LPC and HPC were either supplied in the data from Janes or estimated based on the number of compressor stages (as explained in Section 4.1.2). Whether these pressure ratios closely match those of the real components is not really important, as long as the OPR is correct [33]. The temperature and pressure calculated between the compressors and turbines will not match reality in this case, but this does not influence the final result. What does change is the isentropic component efficiency, but the effect of this is on the thrust and sfc is very small, namely less than 1% after  $\Pi_{HPC}$  was halved while the OPR was kept the same.

It was found that the TIT varies greatly among engines having approximately the same certification year, as shown in Figure B.1. They always are below the maximum TIT as specified in equation 4.17 and Table B.1.

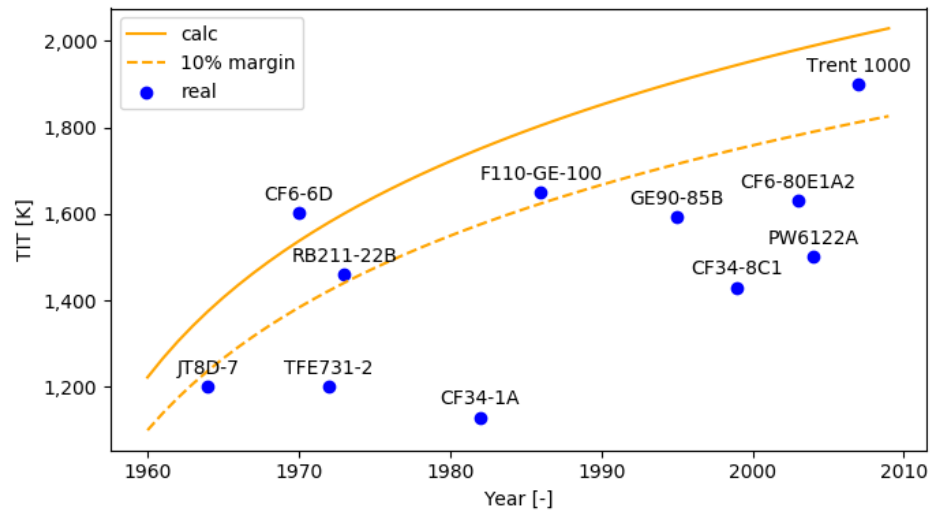


Figure B.1: Maximum TIT trend with certification year

<sup>1</sup><https://janes.ihs.com/AeroEngines/Reference>. Accessed 8 February 2019

This equation therefore does describe a 'maximum' but it does not suit well as a guideline for a random engine design. However this can be explained by taking the development process of engines into account. For instance, the CFM CF6-80E1A2 is developed from the CF6-6D and has seen little changes to the combustion chamber. Therefore the TIT does not change much. For engines that are closer to a 'clean sheet' design in time or development have a TIT closer to the maximum value described by the equation. Examples of this are the Trent 1000 and CF6-6D engines. In addition to the relatively low effect the TIT has on the takeoff weight (see Appendix D) the conclusion is that the method gives a sufficient approximation of the TIT for newly designed engines (like those envisioned for this aircraft design), but a more detailed method is necessary for a more exact approximation.

The results of the validation are shown in Table B.3. As can be seen, both the thrust and sfc match almost every time within 10% without adapting the TIT or component efficiencies. This shows that these numbers are a realistic prediction of turbofan performance for this design stage. Therefore they can also be used for the modelling of the engines for this supersonic aircraft.

Table B.3: Thrust validation data

Engine	Thrust [N]			sfc [kg/(N*s)]		
	real	calc	deviation [%]	real	calc	deviation [%]
CF6-6D	178,000	183,229	2.85	9.86	10.40	5.22
CF6-80E1A2	292,700	277,618	-5.43	9.40	9.99	5.89
GE90-85B	376,800	355,766	-5.91	8.30	7.61	-9.13
F110-GE-100	78,060	74,527	-4.74	18.13	19.47	6.89
CF34-8C1	56,380	57,701	2.29	10.47	9.30	-12.60
PW6122A	100,240	97,385	-2.93	10.20	10.15	-0.47
JT8D-7	62,280	54,767	-13.72	16.13	16.67	3.25

## B.2. Station numbering

Many different station numberings are used worldwide to distinguish engine components in an orderly way. Because this easily causes confusion, the Society of Automotive Engineers (SAE) created a standard for gas turbine nomenclature, AS 755 [126]. This numbering system is used in this report and the accompanying code as well. The most important sections are shown below.

### B.2.1. Primary station numbering

The primary numbers include the core components of the engine.

amb	Ambient conditions
0	Ram conditions in free stream
1	Engine intake front flange
2	First compressor/fan front face
3	Last compressor exit
4	Combustor exit plane
5	Last turbine exit
6	Front face of mixer
7	Propelling nozzle inlet
8	Propelling nozzle throat
9	Propelling nozzle or exhaust diffuser exit plane

### B.2.2. Secondary station numbering

The secondary numbers are suffixes to the primary numbers. The numbers used in this thesis are listed below. A picture with the most important numbers can be found in Figure B.2.

13	Fan exit, bypass flow
16	Cold mixer inlet (only if mixer present)
18	Cold propelling nozzle throat
21	Fan exit, core flow
23	First compressor exit
25	Second compressor front face
45	Second turbine front
65	Mixer outlet

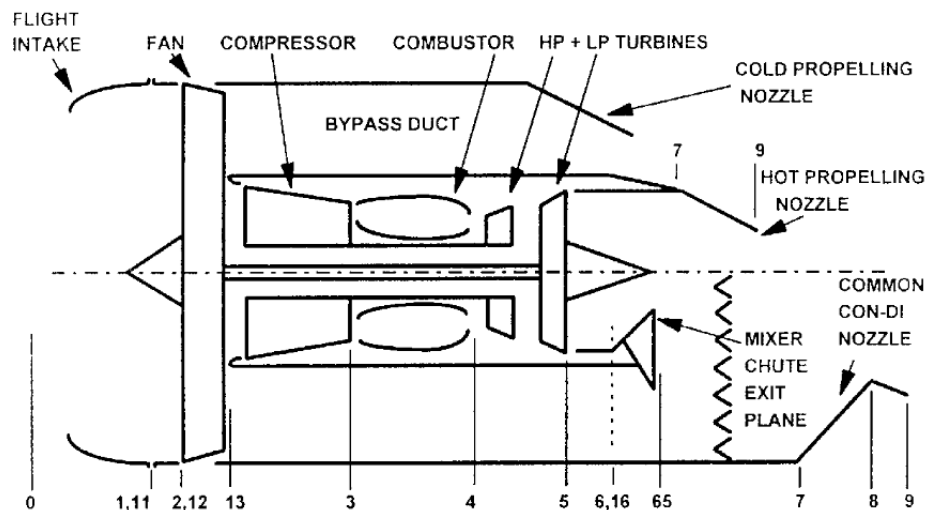


Figure B.2: Station numbering for mixed and unmixed turbofan [20]

The station number in the method by Mirza-Baig for the off-design calculations [33] uses a different station numbering. For clarity, this numbering is used throughout the (separate) offdesign program after which the data is converted to the standard numbering. For completeness, this numbering method is listed here as well (also see Figure B.3).

- amb Ambient conditions
- 0 Ram conditions in free stream
- 1 Engine intake front flange
- 2 First compressor/fan front face
- 3 First compressor/fan exit
- 4 Last compressor exit
- 5 Combustor exit plane
- 6 Front face of second turbine
- 7 Last turbine exit
- e Propelling nozzle throat

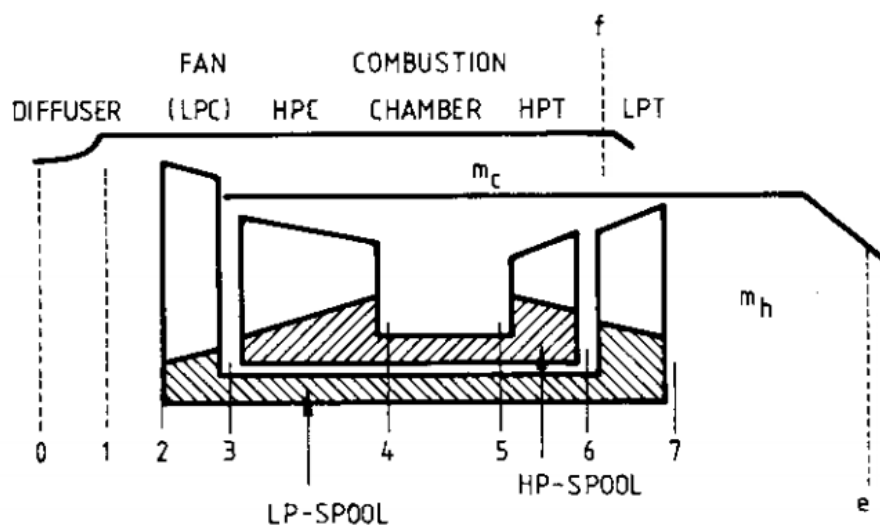
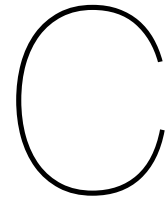


Figure B.3: Station numbering for turbofan [33]





# Geometric data

The goal of this appendix is to give more insight on the source data used for the geometry calculations and decisions taken in Chapter 5.

## C.1. Aircraft configuration

For information about seat data and the number of galleys, lavatories and closets, the website SeatGuru<sup>1</sup> was consulted. A 'random' selection of airlines was made having varying passenger comfort levels and using varying long haul aircraft. The result is visible in Table C.1.

The number of galleys and lavatories may be off by 1 or 2 since the real situation may differ from the website because multiple galley icons may be used for what actually can be considered a single galley. For the seat layouts all seat types were divided into either business, premium economy or economy class, even though actual names may differ or multiple class types are combined into a single class, usually business class. For example, Air France A380s have four classes: besides the normal business class there is a 'La Première' with suites. Those are disregarded in this table as they can not be seen as normal seats and are considered to be too much a premium product which may not be useful on supersonic flights. The aircraft codes in the table are the ICAO codes combined with the additions used by the SeatGuru website to distinguish between layout variants in a single aircraft type.

Table C.1: Seat dimensions and number of galleys, lavatories and closets

Air France	A343	275	Bus	61	21.5	4	7	1
			Prem	38	19			
			Econ	32	18			
	A359	324	Bus	74	21	6	9	4
			Prem	37	18.8			
			Econ	31	17			
	A388	516	Bus	55	24	9	14	
			Prem	38	19			
			Econ	32	17.5			
	B772 v1	309	Bus	79	21	4	8	2
			Prem	38	19			
			Econ	32	17			
	B772 v2	280	Bus	61	21.5	6	7	
			Prem	38	19			
			Econ	32	17			

<sup>1</sup><https://www.seatguru.com>. Accessed 10 October 2019

Table C.1: Seat dimensions and number of galleys, lavatories and closets (continued)

Airline	Aircraft	Passengers	Class	Pitch [in]	Width [in]	Galleys	Lavatories	Closets
	B772 v3	312	Bus	61	21	10	8	4
			Prem	38	19			
			Econ	32	17			
	B772 v4	312	Bus	61	21	8	7	5
	B77W 3cl	381	Bus	61	21.5	5	9	
			Prem	38	19			
			Econ	32	17			
	B789	276	Bus	42	21	11	8	
			Prem	40	19			
			Econ	31	17			
KLM	A333	292	Bus	60	20.25	10	8	2
			Prem	35	17.5			
			Econ	31	17.5			
	B789	294	Bus	42	20.25	9	6	2
	B77W	408	Bus	63	20	12	7	1
			Prem	34	17.5			
			Econ	31	17.5			
	B772	316	Bus	63	20	7	6	
			Prem	35	17.5			
			Econ	31	17.5			
Icelandair	B763	259	Bus	40	20.5	6	5	
			Econ	31-33	17.6			
	B752 v1	183	Bus	40	20.5	4	3	2
	Econ	33	19					
B752 v2	171	Bus	40	20.5	4	3		
Econ	33	19						
Delta Air Lines	A332	234	Bus	80	21	8	6	4
			Prem	35	18			
			Econ	31-32	18			
	A333	293	Bus	80	21	8	8	4
	A359	306	Bus	76-81	22-24	10	8	
			Prem	38	18.5			
			Econ	31-32	18			
	B772 3cl	291	Bus	77-78	22-24	9	7	2
			Prem	38	19			
			Econ	31-32	18.5			
Qatar	A359	283	Bus	80	22	11	8	

Table C.1: Seat dimensions and number of galleys, lavatories and closets (continued)

Airline	Aircraft	Passengers	Class	Pitch [in]	Width [in]	Galleys	Lavatories	Closets
Airways			Econ	31-32	18			
	B788	254	Bus Econ	80 31	22 17.2	7	9	
	B77W v1	358	Bus Econ	78 31-33	21.8 17	17	10	
Singapore Airlines	B78X	337	Bus Econ	60 32	30 17.5	10	7	
	B773	284	Bus Prem Econ	71 60 32	35 24.5 19	8	11	
	B77W	278	Bus Prem Econ	71 51 32	35 30 19	12	11	
	A333	285	Bus Econ	60 32	24.5 19	9	8	
Etihad Airways	B78X	299	Bus Econ	73 31-32	22 17.1	12	9	7

Based on this data a trend for the number of galleys, lavatories or closets could not be found in relation to the number of passengers (Table C.2). Therefore the method as described in FLOPS [44] was used for this calculation.

Table C.2: Number of galleys, lavatories and closets related to number of passengers

	pax/galley	pax/lavatory	pax/closet
Average	40.1	41.2	141.4
Standard deviation	14.8	9.2	97.2

Seat dimensions however are more homogeneous. The seat pitch for economy class varies between 31 and 33 inch, and the width varies between 17 and 19 inch. Premium economy and business class seats have more variation, which may be related to a combination of the comfort level and the flight distance. Airlines that offer a more premium experience like Singapore Airlines or Qatar Airways have larger business seats than airlines like Icelandair who have a less premium brand and fly on average on shorter routes. This same trend can be seen when larger, long haul aircraft are compared to smaller short haul aircraft.

Since supersonic aircraft fly faster than subsonic aircraft the flight time is reduced and therefore it is estimated that there will be less need for extra comfort like lie-flat seats. This will greatly reduce the dimensions for business class seats.

In the end the decision was made to use economy seats that are comparable to the large variant of current economy seats, with a pitch of 32 inch and a width of 17.5 inch. Premium economy seats, which will only be considered for aircraft with 21 to 130 seats, will have a seat pitch of 38 inch and a width of 19.5 inch. Business class seats which will be used exclusively on the aircraft variants with 20 or less seats and as business class on the large aircraft with more than 130 seats will have a pitch of 42 inch and a width of 21.5 inch.

## C.2. Supersonic aircraft length and slenderness

Data from several supersonic aircraft that have existed and many concept studies were compiled in Table C.3.

Table C.3: Various data from several supersonic aircraft

Name	Year <sup>2</sup>	Mach	Passen- gers	Length [m]	Cabin diameter [m]	Slender- ness	Source
U-1	1963	3	4	12.2	1.22	10	[62]
I-1	1965	2	12	25.5	1.55	16.5	[62]
U-2	1967	2.2	10	27.3	1.83	14.9	[62]
U-3	1967	2	9	25.9	1.46	17.7	[62]
N-1	1977	2.2	8	32.6	1.74	18.7	[62]
N-2	1977	2.4	0	28.5	1.37	20.8	[62]
N-3	1980	2.7	8-10	29.3	1.65	17.8	[62]
I-3	1981	2.1	8	30.5	1.83	16.7	[62]
N-5	1981	2.7	8	31.4	1.77	17.7	[62]
N-6	1983	2.3	8	31.4	1.46	21.5	[62]
N-7	1984	2	8	32.6	1.62	20.1	[62]
N-8	1986	2	8	31.4	1.74	18.0	[62]
I-4	1987	2	-	31.4	1.74	18.0	[62]
I-5	1988	1.5	8	38.1	1.83	20.8	[62]
U-6	1993	2.2	7	32.6	1.89	17.2	[62]
I-8	1995	1.8	8-10	27.7	1.83	15.1	[62]
Tu-144	1968	2.3	100-150	67.05	3.3	20.3	3,4
Concorde	1969	2.02	88	62.1	2.63	23.6	5
SSXJET	1977	2.2	6-8	31.39	1.52	20.6	[125]
Edge	1992	2.4	250?	94.49	4.01	23.5	[38]
NASA HSCT	1999	2.4	250	91.44	3.66	25	[36]
Cranfield SSBJ	2002	1.6	19	41.8	2.2	19	[127]
NASA low-boom SSBJ	2003	2	10	40.39	1.93	20.9	[110]
NLR M1.6	2004	1.6	250	89	4.25	20.9	[56]
HELESA	2017	1.6	18	41	1.86	22	[35]
N+1 Overwater	2017	1.3	128	53.34	2.01	26.6	[124]
Aerion AS2	2021	1.4		51.82	2.29	22.6	6
Boom Overture	2023	2.2	55	51.82	2.19	23.6	7

<sup>2</sup>Report date for concept studies, (planned) first flight date for existing/planned aircraft

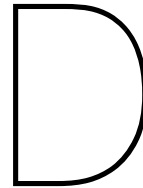
<sup>3</sup>[https://janes.ihs.com/JAWAInServices/Display/jau\\_9046-jau\\_](https://janes.ihs.com/JAWAInServices/Display/jau_9046-jau_). Accessed 20 December 2019

<sup>4</sup><http://tu144sst.com/techspecs/accomodation.html>. Accessed 20 December 2019

<sup>5</sup>[https://janes.ihs.com/JAWAInServices/Display/jau\\_0804-jau\\_](https://janes.ihs.com/JAWAInServices/Display/jau_0804-jau_). Accessed 20 December 2019

<sup>6</sup><https://janes.ihs.com/JAWADevelopmentProduction/Display/jawaa070-jawa>. Accessed 20 December 2019

<sup>7</sup><https://boomsupersonic.com/overture>. Accessed 20 December 2019



# Program inputs

The aircraft design program uses an Excel document where all the input parameters are listed. The user can see and change these parameters and save the document before running the program. These parameters are divided in two tabs: main (primary) inputs and secondary inputs. They are divided in several categories and for each value minimum and maximum values are listed. Section D.1 lists the main inputs, Section D.2 lists the secondary inputs and in Section D.3 is defined why which input parameters were used in the sensitivity analysis in Chapter 7.

## D.1. Main inputs

The main inputs tab contains the most important input parameters that are likely to be changed every single run. They contain run parameters (Table D.1), key design parameters (Table D.2), airport constraints, performance first guesses, initial guesses for the maximum lift coefficient and parameters for the climate effect analysis.

### D.1.1. Run parameters

The run parameters are used to define file names of the program output. They are listed in Table D.1.

Table D.1: Main input run parameters

Name	Unit	Description
folder_name	[-]	Name of output folder and PDF file
aircraft_name	[-]	Aircraft name

### D.1.2. Key design parameters

These parameters are considered the most important of the aircraft design and represent the mission definition along with some geometry constraints. The number of pilots and flight attendants depends on the number of passengers. The parameters for subsonic cruise range are included for the possibility that the cruise segment may not be flown completely at supersonic speeds. The list of these parameters can be found in Table D.2.

Table D.2: Main input design parameters

Name	Unit	Description
Payload_weight	[kg]	Payload weight (optional)
n_pax	[-]	Number of passengers
n_pilot	[-]	Number of pilots
n_attendants	[-]	Number of flight attendants
R_mission	[NM]	Mission range (between takeoff and landing)
R_sub1_fraction	[-] or [NM]	Subsonic cruise range before supersonic cruise (fraction of total cruise distance or absolute distance)
R_sub2_fraction	[-] or [NM]	Subsonic cruise range after supersonic cruise (fraction of total cruise distance or absolute distance)
load_factor	[-]	Load factor at design point
M_cr_sup	[-]	Supersonic cruise Mach number
h_cr_sup	[m]	Supersonic cruise altitude
M_cr_sub	[-]	Subsonic cruise Mach number
h_cr_sub	[m]	Cruise altitude for first subsonic cruise, contingency and diversion segments
h_cr_sub2	[m]	Cruise altitude for second subsonic cruise segment
n_eng	[-]	Number of engines
w_AR	[-]	Wing aspect ratio

### D.1.3. Performance first guess parameters

The Class I weight analysis requires the lift-drag ratio and sfc to be known for certain mission segments (see Table D.3). Therefore a first guess for these numbers is required. Apart from making sure the program can iterate to a valid solution, these values have no effect on the model outcome.

Table D.3: First guesses for performance parameters

Name	Unit	Description
LD_sup	[-]	Supersonic L/D ratio
cj_sup	[1/hr]	Supersonic sfc
LD_sub	[-]	Subsonic L/D ratio
cj_sub	[1/hr]	Subsonic sfc
LD_loiter	[-]	Loiter L/D ratio
cj_loiter	[1/hr]	Loiter sfc
user_cj	[Boolean]	Whether these input values are final or whether they can be changed by the program

### D.1.4. Airport constraints

The airport constraints contain the runway length limits, airport altitude and stall speed, as shown in Table D.4.

Table D.4: Airport constraint inputs

Name	Unit	Description
h_airport	[m]	Airport elevation above sea level
takeoff_dist	[m]	Takeoff distance
V_stall	[m/s]	Sea level clean stall speed
landing_dist	[m]	Landing distance

### D.1.5. Maximum lift coefficients first guess

The maximum lift coefficients are required for modules that are run before the aerodynamics module. Therefore an estimation is required for these values for the initial run. Additionally, a switch for the use of leading edge high-lift devices is included (see Table D.5).

Table D.5: First guess for maximum lift coefficients

Name	Unit	Description
CLmax_clean	[-]	Maximum clean lift coefficient
CLmax_land	[-]	Maximum landing lift coefficient
CLmax_TO	[-]	Maximum takeoff lift coefficient
TE_inb_HLD_type	[-]	Inboard HLD type to be used
TE_outb_HLD_type	[-]	Outboard HLD type to be used
allow_LE_HLD	[Boolean]	Boolean to indicate whether LE HLDs can be included if needed

### D.1.6. Climate parameters

The final set of main input variables is that of the climate module. These define a set of reference data against which the program results will be compared.

Table D.6: Parameters for climate analysis

Name	Unit	Description
EI_reference_engine	string	Reference engine in the emissions databank
engine_UID	string	Reference engine ID in the emissions databank
use_SST_engine_data	boolean	Boolean indicating whether the fuel flow for the reference engine should be scaled using SST fuel flow and OPR/T_TO
custom_engine_LTO	boolean	Boolean to indicate whether the custom engine LTO data from "custom_LTO_data"-tab should be used
use_sub_LTO_regulations	boolean	Boolean to indicate whether subsonic LTO regulatory values should be used
use_sub_LTO_definition	boolean	Boolean to indicate whether subsonic LTO regulatory values should be used
n_aircraft2050	[-]	Number of SST aircraft in service in 2050
n_flights_ac	[-]	Number of flights per aircraft in 2050
sup_ac_productivity	[-]	Factor indicating how much more productive a supersonic aircraft is than a subsonic one
sub_ac1	string	ID for the first subsonic aircraft used for global climate impact comparison
sub_ac2	string	ID for the second subsonic aircraft used for global climate impact comparison

## D.2. Secondary inputs

The secondary inputs contain all kinds of module-specific inputs. They are separated by module as can be seen below.

### D.2.1. Run parameters

The secondary run parameters are shown in Table D.7. This section contains more general parameters, like the main file storage location, the maximum number of iterations and options for intermediate data storage and display.

Table D.7: Secondary run inputs

Name	Unit	Description
desktop_location	string	Main location to store outputs
store_folder	string	Storage folder for the outputs
parapy_patch_folder	string	ParaPy patch folder
max_iter	[-]	Maximum number of iterations by the full program
weight_conv_limit	[%]	Iteration weight convergence criterion
n_stable_iter	[-]	Number of times that the weight has to be within the convergence limit
inter_storage	boolean	Intermediate storage option
plot_each_gust_scenario	boolean	Gust diagram option
C1_print_overview	boolean	Print Class I intermediate weight overviews
include_envelope_PDF	boolean	Include flight envelope
include_environment_PDF	boolean	Include environmental impact data
show_convergence	boolean	Show the takeoff weight convergence
clear_results_folder	boolean	Clean up the results folder at the start of the run
store_values_excel	boolean	Store final values in Excel sheet
excel_name	string	Excel sheet name
excel_sheet_name	string	Sheet name
excel_column_ID	string	Indicate column number to write values to

### D.2.2. Passenger data

The passenger input data only consists of passenger and luggage weight data and is shown in Table D.8.

Table D.8: Passenger input data

Name	Unit	Description
l_pax	[-]	Fraction of passengers with extra (belly) luggage
m_pax	[kg]	Passenger weight (including carry-on)
m_luggage	[kg]	Luggage weight

### D.2.3. Class I inputs

The class I data holds parameters for defining mission segment lengths and conditions (Table D.9).

Table D.9: Inputs for class I weight estimation

Name	Unit	Description
sf_climb_descent	[-]	Climb and descent distance safety factor
t_cont	[min]	Contingency flight time
R_div	[NM]	Divergence distance
t_loiter	[min]	Loiter time
V_hold_loiter	[kts]	Loiter holding speed
t_finalres	[min]	Final reserve time
V_hold_final	[kts]	Final reserve holding speed
sub_climb_dist_fraction	[-]	Subsonic climb/descent distance fraction
max_fuel_harmonic_ratio	[-]	Maximum fuel-to-harmonic fuel ratio

### D.2.4. Aerodynamics inputs

The aerodynamics inputs contain parameters defining various angles of attack and wing and high-lift device parameters. They are shown in Table D.10.

Table D.10: Inputs for aerodynamics module

Name	Unit	Description
alpha_max_04	[deg]	Angle of attack for Mach 0.4 CLmax calculation
alpha_max_sub	[deg]	Angle of attack for subsonic cruise CLmax calculation
alpha_max_sup	[deg]	Angle of attack for supersonic cruise CLmax calculation
h_hold_loiter	[m]	Altitude for loiter segment
M_hold_loiter	[-]	Mach number for loiter segment
h_hold_final	[m]	Altitude for final reserve segment
M_hold_final	[-]	Mach number for final reserve segment
M_takeoff	[-]	Takeoff Mach number
w_incid	[deg]	Wing incidence
w_twist	[deg]	Wing twist for digital DATCOM
h_M14	[m]	Altitude for Mach 1.4 used in digital DATCOM setup
induced_method	string	Induced drag method ('kroo' or 'scholz' method)
e_theo	[-]	Theoretical span efficiency factor used for Kroo method
ss_drag_method	string	Supersonic drag method to be used (NLR or Raymer)
E_WD	[-]	Wave drag efficiency factor for Raymer method to correct for not being a SH-body
alpha_max_clean	[deg]	Angle of attack for maximum clean lift coefficient at sea-level (M=0.25)
alpha_TO	[deg]	Angle of attack for takeoff CLmax calculations
alpha_land	[deg]	Angle of attack for landing CLmax calculations
flap_fuse_margin	[m]	Margin from fuselage to flap start
slat_fuse_margin	[m]	Slat/LE flap margin to fuselage
outer_flap_limit	[-]	Outer limiting span fraction for flap
kink_flap_margin	[m]	Flap margin around wing kink
outer_slat_limit	[-]	Outer limiting fraction for slat/LE flap
inner_flap_hinge_c_frac	[-]	Inner flap hinge line fraction of chord
inner_flap_c_frac	[-]	Inner flap chord length
outer_flap_c_frac	[-]	Outer flap hinge line fraction of chord
flap_defl_TO	[deg]	Takeoff TE flap deflection angle
flap_defl_land	[deg]	Landing TE flap deflection angle
TO_HLD_lift_fraction	[-]	Takeoff lift increment fraction
slice_dist	[m]	Slice distance for cross-sectional area distribution in ParaPy

### D.2.5. Airfoil inputs

The airfoil inputs are grouped separately and contain the airfoil names and thicknesses (Table D.11).

Table D.11: Airfoil data

Name	Unit	Description
w_af_root	string	Wing root airfoil (used only at root, w_airfoil used at kink and tip)
w_af_kink	string	Wing kink airfoil (used only at kink)
w_af_tip	string	Wing tip airfoil (used only at tip)
w_dih_inb	[deg]	Inboard section dihedral angle
w_dih_outb	[deg]	Outboard section dihedral angle
w_airfoil	string	Airfoil designation to be used by digital DATCOM (either 4-series, e.g. "0012" or 64A/65A-series, e.g. 64A103)
w_xc_max_t	[-]	Location of maximum thickness for wing airfoil
w_tc_avg	[-]	Wing average thickness-to-chord ratio
emp_airfoil	string	Airfoil designation for empennage used for fuel volume calculations and ParaPy
emp_xc_max_t	[-]	Maximum thickness location along chord for empennage airfoil
emp_tc_avg	[-]	Empennage average thickness-to-chord ratio
CD0_LG	[-]	Landing gear drag coefficient

### D.2.6. Class II inputs

The input data for the class II weight estimation contains switches and weight penalties for various aircraft components. Additionally, parameters for the random technology development factors are included here. The parameters are listed in Table D.12.

Table D.12: Inputs for class II weight estimation

Name	Unit	Description
W_uav	[kg]	Uninstalled avionics weight
long_short_range	[-]	Long or short range aircraft
press_hydr	[psi]	Hydraulic system pressure
var_sweep_pen	[-]	Variable sweep penalty
spoiler_present	boolean	Spoilers present
HT_included	boolean	Horizontal tail inclusion switch
rudder_ratio	[-]	Rudder area to VT area ratio
move_nose	boolean	Movable nose switch
include_APU	boolean	Include APU switch
emp_C2_method	string	Empennage weight method
K_PIV	[-]	Wing variable sweep structural factor
overhead_frac	[-]	Fraction of luggage stored overhead
weight_growth	[-]	Component weight growth factor
ECS_penalty	[-]	Environment control system weight penalty
hydr_penalty	[-]	Hydraulics weight penalty
ht_penalty	[-]	Horizontal tail weight penalty
vt_penalty	[-]	Vertical tail weight penalty
random_tech	boolean	Random technology development factors switch
ssd_addition	[-]	Number of SSDs added or subtracted from average
n_random	[-]	Number of random technology draws
alpha_rand_dist	[-]	Alpha (or a) value for beta distribution
beta_rand_dist	[-]	Beta (or b) value for beta distribution

### D.2.7. Geometry inputs

The geometry inputs contain data for the sizing of the fuselage, wing and empennage (Table D.13).

Table D.13: Inputs for geometry module

Name	Unit	Description
aisle_width	[m]	Aisle width
nose_slenderness	[-]	Slenderness ratio for nose
tail_slenderness	[-]	Slenderness ratio for tail
fus_added_height	[m]	Additional fuselage height
fuse_upsweep_angle	[deg]	Fuselage upsweep angle
cabin_length_factor	[-]	Extra cabin length factor
w_kink_frac	[-]	Kink location
w_sweep_LE_eff	[deg]	Effective sweep angle
w_MAC_pos	[-]	Mean aerodynamic chord position
w_taper	[-]	Average taper ratio
w_front_spar_loc	[-]	Front spar location wing
ht_AR	[-]	Horizontal tail aspect ratio
ht_sweep_LE	[deg]	Horizontal tail leading edge sweep angle
ht_taper	[-]	Horizontal tail taper ratio
ht_front_spar_loc	[-]	Horizontal tail front spar location
ht_rear_spar_loc	[-]	Horizontal tail rear spar location
ht_rs	[-]	Horizontal tail box ratio
vt_volume	[-]	Vertical tail volume coefficient
vt_AR	[-]	Vertical tail aspect ratio
vt_sweep_LE	[deg]	Vertical tail leading edge sweep angle
vt_taper	[-]	Vertical tail taper ratio
vt_rs	[-]	Vertical tail box ratio

### D.2.8. Engine inputs

The engine inputs are used for the cycle calculations and contain various component efficiencies and other parameters defining the engine performance (Table D.14).

Table D.14: Inputs for engine module

Name	Unit	Description
rho_fuel	[kg/m <sup>3</sup> ]	Fuel density
LHVf	[J/kg]	Lower heating value for fuel
eta_intake	[-]	Intake efficiency
bypass	[-]	Engine bypass ratio
OPR	[-]	Overall engine pressure ratio
eta_pol_fan	[-]	Fan polytropic efficiency
eta_pol_comp	[-]	Compressor polytropic efficiency
eta_CC	[-]	Combustion chamber efficiency
CC_PR	[-]	Combustion chamber pressure ratio
eta_mech	[-]	Mechanical efficiency
eta_pol_turb	[-]	Turbine polytropic efficiency
eta_noz	[-]	Nozzle efficiency
mixer	boolean	Use mixer
eng_spanw_pos	[-]	Engine position fraction (span)
sup_SFC_scale	[-]	Supersonic SFC scaling factor
eta_prop	[-]	Engine propulsive efficiency
TITmax	[K]	Maximum turbine inlet temperature
engineyear	[-]	Engine construction year

### D.3. Parameter selection for sensitivity analysis

From the main inputs only the key design parameters and airport constraints have any influence on the aircraft design. Therefore the other inputs will not be considered for the sensitivity analysis. For the secondary inputs this is a bit different, since all parameters at least have some influence in the design process, but it is unknown whether their influence is larger or smaller. To find out for what variables a more in-depth sensitivity analysis is required, each relevant parameter was changed by 20% and the resulting change in MTOW was evaluated.

The relevant parameters are those that do influence the final result and are not considered constant by default. Parameters like passenger weights and fuel properties are constants and therefore will not be included in the sensitivity analysis. Run parameters and initial guesses will also not be considered for the sensitivity analysis. All other numerical parameters were both increased and decreased by 20% from the default value and the resulting MTOW was compared to the original MTOW. Any booleans representing design choices also were evaluated. Engine data was not changed by 20% but the minimum and maximum values dictated by the theoretical maximums from Appendix B were chosen. The resulting data can be found in Table D.15. Empty cells represent runs that did not result in a feasible design because the MTOW would become too large or were otherwise infeasible.

A variable was considered interesting for a more in-depth sensitivity analysis if any of the resulting changes was more than 10%. Most variables fall outside this category, except the following:

- Number of passengers
- Mission range
- Supersonic cruise Mach number
- Supersonic cruise altitude
- Number of engines
- Stall speed
- Maximum clean angle of attack
- Weight growth factor
- Factor for additional cabin length
- Wing leading edge sweep angle
- Combustion chamber efficiency
- Supersonic sfc scaling factor

From this list the maximum clean angle of attack, cabin length factor and weight growth factor will not be included in the sensitivity analysis. The choice for angle of attack is already treated in the co-report [5]. The cabin length factor is not a value that should be changed and is mainly included for lengthening the fuselage in case there is not enough room to store the fuel. The wing growth factor and its effects are already described in [5].

Table D.15: Results of 20% change in input value on takeoff mass

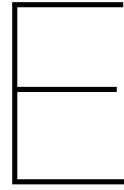
n_pax	80	120	94,031	143,618	<b>-25</b>	<b>14</b>
n_pilot	2	4	126,133	130,304	0.0	3.3
n_attendants	3	15	125,673	130,933	-0.4	3.8
R_mission	3,680	5,520	104,670	154,503	<b>-17</b>	<b>22</b>
R_sub1_fraction	0	0.2	126,133	124,708	0.0	-1.1
R_sub2_fraction	0	0.2	126,133	123,075	0.0	-2.4
load_factor	0.64	0.96		131,933		4.6
M_cr_sup	1.28	1.92	149,084	147,543	<b>18</b>	<b>17</b>
h_cr_sup	12,800	19,200	152,049	129,122	<b>21</b>	2.4
M_cr_sub	0.85	0.95	119,659	126,133	-5.1	0.0
h_cr_sub	8,160	12,240	126,158	128,910	0.0	2.2
h_cr_sub2	9,200	13,800	127,157	129,868	0.8	3.0
n_eng	2	4	145,920	126,133	<b>16</b>	0.0
w_AR	1.68	2.52	141,330	121,394	<b>12</b>	-3.8
h_airport	0	300	126,133	126,205	0.0	0.1

Table D.15: Results of 20% change in input value on takeoff mass (continued)

	r1	r2	MTOW_r1	MTOW_r2	diff_r1	diff_r2
takeoff_dist	2,240	3,360	129,202	125,479	2.4	-0.5
V_stall	64.8	97.2	183,822	130,612	<b>46</b>	3.6
landing_dist	1,680	2,520	126,133	126,133	0.0	0.0
sf_climb_descent	0.8	1.2	128,769	123,655	2.1	-2.0
t_cont	24	36	124,931	127,451	-1.0	1.0
R_div	200	300	125,041	127,319	-0.9	0.9
t_loiter	24	36	124,619	127,741	-1.2	1.3
V_hold_loiter	224	336	126,133	126,133	0.0	0.0
t_finalres	24	36	124,765	127,592	-1.1	1.2
V_hold_final	184	276	126,133	126,133	0.0	0.0
sub_climb_dist_fraction	0.28	0.42	126,133	126,133	0.0	0.0
max_fuel_harmonic_ratio	0.8712	1.3068	125,532	126,309	-0.5	0.1
alpha_max_04	16	24	126,133	126,133	0.0	0.0
alpha_max_sub	16	24	126,133	126,133	0.0	0.0
alpha_max_sup	11.2	16.8	126,133	126,133	0.0	0.0
h_hold_loiter	5,200	7,800	125,511	126,991	-0.5	0.7
M_hold_loiter	0.36656	0.54984	128,728	125,170	2.1	-0.8
h_hold_final	365.6	548.4	126,109	126,158	0.0	0.0
M_hold_final	0.2796	0.4194	127,856	125,732	1.4	-0.3
M_takeoff	0.24	0.36	126,198	126,042	0.1	-0.1
w_incid	-2	2		126,133		0.0
w_twist	-2	2		126,133		0.0
h_M14	10,800	16,200	126,133	126,133	0.0	0.0
e_theo	0.64	0.96	134,459	122,702	6.6	-2.7
E_WD	1.36	2.04	126,133	126,133	0.0	0.0
alpha_max_clean	16	24	143,452	125,652	<b>14</b>	-0.4
alpha_TO	8	12	126,133	126,844	0.0	0.6
alpha_land	10	14	126,133		0.0	
flap_fuse_margin	0.08	0.12	126,133	126,133	0.0	0.0
slat_fuse_margin	1.2	1.8	126,133	126,133	0.0	0.0
outer_flap_limit	0.68	1	126,133	126,893	0.0	0.6
kink_flap_margin	0.04	0.06	126,133	126,133	0.0	0.0
outer_slat_limit	0.64	0.96	126,133	126,133	0.0	0.0
inner_flap_hinge_c_frac	0.8	1	126,133	126,133	0.0	0.0
inner_flap_c_frac	0.6	0.9	126,325	126,035	0.2	-0.1
outer_flap_c_frac	0.6	0.9	126,133	126,133	0.0	0.0
flap_defl_TO	16	24	126,133	126,138	0.0	0.0
flap_defl_land	32	48	126,133	126,133	0.0	0.0
TO_HLD_lift_fraction	0.576	0.864	126,133	126,133	0.0	0.0
slice_dist	0.8	1.2	126,133	126,133	0.0	0.0
w_xc_max_t	0.32	0.48	126,063	126,243	-0.1	0.1
w_tc_avg	0.0224	0.0336	122,173	131,508	-3.1	4.3
emp_xc_max_t	0.24	0.36	126,138	126,106	0.0	0.0
emp_tc_avg	0.024	0.036	125,529	126,840	-0.5	0.6
CD0_LG	0.016	0.024	126,133	126,159	0.0	0.0
W_uav	376	564	126,103	126,158	0.0	0.0
press_hydr	4,000	6,000	126,400	125,929	0.2	-0.2
var_sweep_pen	0	1	126,133	126,264	0.0	0.1
spoiler_present	True	False	125,237	124,579	-0.7	-1.2
HT_included	True	False	126,133		0.0	
rudder_ratio	0.248	0.372	126,133	126,133	0.0	0.0
move_nose	True	False	126,133	126,133	0.0	0.0

Table D.15: Results of 20% change in input value on takeoff mass (continued)

	r1	r2	MTOW_r1	MTOW_r2	diff_r1	diff_r2
include_APU	True	False	126,133	124,782	0.0	-1.1
K_PIV	1	1.175	126,133	127,965	0.0	1.5
overhead_frac	0.32	0.48	126,133	126,133	0.0	0.0
weight_growth	0.84	1.26	95,746	178,571	<b>-24</b>	<b>42</b>
ECS_penalty	1	1.5	124,797	127,458	-1.1	1.1
hydr_penalty	0.96	1.44	125,450	126,793	-0.5	0.5
ht_penalty	0.96	1.44	125,514	126,734	-0.5	0.5
vt_penalty	0.96	1.44	125,734	126,504	-0.3	0.3
aisle_width	0.4064	0.6096	121,426	131,093	-3.7	3.9
nose_slenderness	4	6	126,742	127,033	0.5	0.7
tail_slenderness	5.6	8.4	124,156	129,123	-1.6	2.4
fus_added_height	0.216	0.324	125,749	126,493	-0.3	0.3
fuse_upsweep_angle	3.2	4.8	125,560	126,867	-0.5	0.6
cabin_length_factor	0.8	1.2	102,361	134,259	<b>-19</b>	6.4
w_kink_frac	0.304	0.456	127,512	125,174	1.1	-0.8
w_sweep_LE_eff	54.4	81.6	165,019		<b>31</b>	
w_MAC_pos	0.424	0.636	125,074	127,709	-0.8	1.2
w_taper	0.112	0.168	125,796	126,491	-0.3	0.3
w_front_spar_loc	0.096	0.144	126,133	126,133	0.0	0.0
ht_AR	1.6	2.4	125,883	126,378	-0.2	0.2
ht_sweep_LE	32	48	126,159	126,090	0.0	0.0
ht_taper	0.24	0.36	125,902	126,362	-0.2	0.2
ht_front_spar_loc	0.16	0.24	126,133	126,133	0.0	0.0
ht_rear_spar_loc	0.6	0.9	126,133	126,133	0.0	0.0
ht_rs	0.56	0.84	125,742	126,574	-0.3	0.4
vt_volume	0.064	0.096	125,118	127,131	-0.8	0.8
vt_AR	0.8	1.2	126,037	126,217	-0.1	0.1
vt_sweep_LE	48	72	126,209	125,948	0.1	-0.1
vt_taper	0.12	0.18	126,078	126,187	0.0	0.0
vt_rs	0.56	0.84	125,941	126,368	-0.2	0.2
eta_pol_fan	0.72	0.99	125,096	127,145	-0.8	0.8
eta_pol_comp	0.728	0.99	126,442	126,115	0.2	0.0
eta_CC	0.796	0.99	154,352	126,133	<b>22</b>	0.0
CC_PR	0.76	0.99	126,694	125,423	0.4	-0.6
eta_mech	0.796	0.99	130,068	126,522	3.1	0.3
eta_pol_turb	0.744	0.99	130,344	124,322	3.3	-1.4
eta_noz	0.776	0.99	130,685	123,662	3.6	-2.0
eng_spanw_pos	0.28	0.42	126,065	126,197	-0.1	0.1
sup_SFC_scale	0.992	1.488	106,996	150,649	<b>-15</b>	<b>19</b>
eta_prop	0.512	0.768	126,133	126,133	0.0	0.0
TITmax	1,300	2,200		134,590		6.7
engineyear	1990	2010	117,021	126,133	-7.2	0.0



## Sonic boom and aircraft shaping

The shape of the aircraft has a large influence on the sonic boom signature shape. The far field N-wave was first described theoretically by Whitham [128]. He presented a theory based on ballistic shock waves, already known from weaponry. This theory included a source function, which became known as the Whitham F-function, shown in equation E.1.

$$F(x) = \frac{1}{2\pi} \int_0^x \frac{A''(\xi)}{\sqrt{x-\xi}} d\xi \quad (\text{E.1})$$

where  $x$  is a position on the aircraft's longitudinal axis and  $A$  is the cross-sectional area at  $x$ . The integral is evaluated with the variable  $\xi$ .

The Whitham F-function mentioned above was modified by Walkden for use with wing-body combinations [129], changing  $A$  to the effective area: the cross-sectional area normal to the aircraft's longitudinal axis combined with the equivalent area due to lift. Additionally, he added a dependence on the direction of the lift component  $\theta$ , as shown in equation E.2.

$$A_e x, \theta = A_v(x, \theta) + \frac{\beta}{2q_\infty} \int_0^x L(x, \theta) dx \quad (\text{E.2})$$

The second derivative  $A_e''$  should then be inserted in equation E.1 at the position of  $A''$ .  $\theta$  is the roll angle of the lift vector,  $A_v$  is the cross-sectional area distribution and  $L$  is the spanwise lift per unit of length.  $\beta = \sqrt{M^2 - 1}$  and  $q_\infty$  is the free-stream dynamic pressure.

Later additional refinements were added, like atmospheric propagation [103]. This helped refining the solutions, but the key factor in boom strength still is the shape of the aircraft. The dependence on  $A_e''$  shows that fuselage smoothness is important. This pleads for a smooth and slender fuselage without obstructions like a cockpit.

Furthermore, special attention is needed for the placement of the wing and aircraft interior. An example of this is shown by Aronstein and Schueler in their design of a low-boom and a high-boom SSBJ. The low-boom design is longer and has more unused space, resulting in a smoother area distribution (Figure E.1). Combined with reshaping the wings, this results in a better distribution of the effective cross-sectional area as shown in Figure E.2.

Besides this type of aerodynamic shaping there are a number of exotic concepts that use heat or mass addition. This is done by changing the air stream or by heating the air around or in front of the aircraft. These concepts usually turned out to be too impractical for further research [130] and go beyond the scope of this thesis.

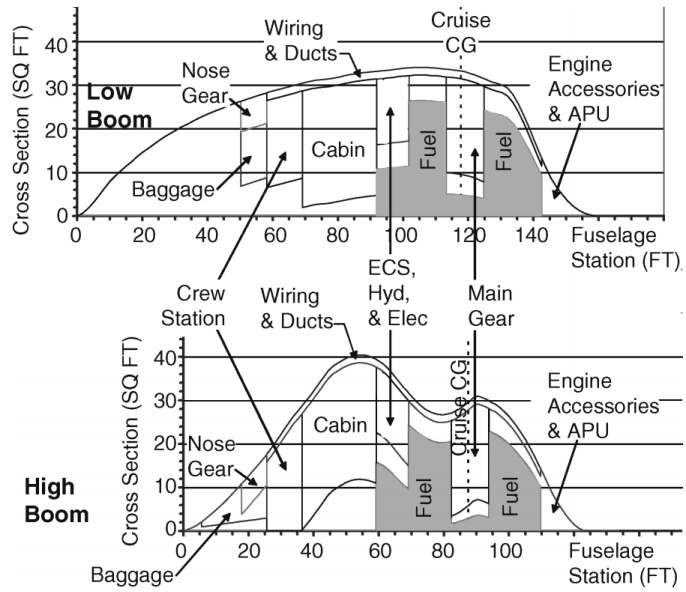


Figure E.1: Internal arrangements of low-boom and high-boom designs [109]

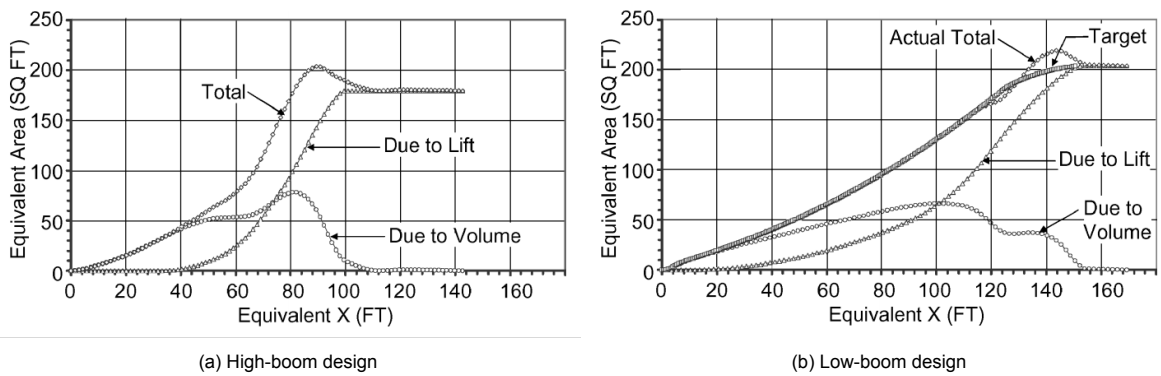


Figure E.2: Effective area distribution for low-boom and high-boom SSBJ designs [109]